**People's Democratic Republic of Algeria**
**Ministry of Higher Education and Scientific Research**
**Ferhat Abbas-Setif1 University**
**Faculty of Sciences**
**Department of Physics**

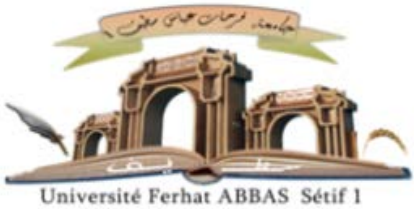


Thesis Submitted for the Degree of Doctor 3rd Cycle LMD of Physics in Radiophysics and Biomedical Imaging

# Title:

## *Contribution of Magnetic Resonance Imaging (MRI) in Glioblastoma radiotherapy treatment planning and dose calculation*

Presented by: **TOUABTI Khalil Mohamed Mokhtar**

Board of Examiners:

| | | |
|---|---|---|
| **Prof. AZIZI Hacene** | University of Setif1 | President |
| **Prof. KHARFI Fayçal** | University of Setif1 | Thesis Director |
| **Dr. OUNOUGHI Nabil** | University of Jijel | Examiner |
| **Dr. BELKHIAT Djamel Eddine Chouaib** | University of Setif1 | Examiner |

**-January 14, 2021-**

# Dedication

I dedicate my work and this final success of long years of research to my wonderful parents Nazli and Abdelmalek who always believed in me, and supported all my life, to whom I owe all and without whom I would not be the man of today

To the most wonderful and extraordinary of the wives, my source of happiness and inspiration, Nadine, who encouraged and supported me all these years in good and bad times.

To my second parents Slim and Fazilé whom I love

To my wonderful sister Manel to whom I wish all the happiness in the world

To my wonderful brothers and sisters, source of my happiness

To all my family

To my in-laws for their encouragement, their support

To all my friends

# Acknowledgment

Firstly, I would like to express my sincere gratitude to my advisor Prof. Fayçal Kharfi for the continuous support of my doctoral study and related research, for his patience, motivation, and immense knowledge. His guidance helped me in all the time of research and writing of this thesis. More than a thesis director, Prof. KHARFI was an important pillar for all these years both in professional and personal life. I could not have imagined having a better advisor and mentor for my doctoral study and a real model for my Career.

Besides my advisor, I would like to thank my thesis committee: Prof. H. Azizi, Dr. N. Ounoughi, and Dr. D.C.E. Belkhiat, for their insightful comments and questions.

My sincere thanks also go to Dr. S.A. Merouane, Dr. H. Boukebous, Dr. S. Khoudri, Pr. K. Bouadaou and Dr. K. Benkahila from the fighting against cancer centre of Setif, who provided me an opportunity to join their team, and who gave me access to the radiotherapy facilities and planning systems. Without they precious support it would not be possible to conduct this research.

I would also like to extend my thanks to the professional and administrative staff of the radiotherapy service of the cancer-fighting centre of Setif.
Special thanks to the teaching staff of the faculty of sciences of Ferhat Abbas-Setif1 University for providing me the necessary fundamental knowledge.

Finally, I wish to thank everyone who supported me.

# CONTENT

**Chapter II: Image Registration and Data Fusion in Radiotherapy: Evaluation Metrics**

**Chapter III: Emerging role of MRI in external radiotherapy treatment planning**

## Chapter IV: MRI Contribution in Glioblastoma radiotherapy treatment planning and delivered dose conformity

# LIST OF FIGURES

## Chapter I



## Chapter II

## Chapter III



## Chapter IV

# LIST OF TABLES

## Chapter II



## Chapter III



## Chapter IV

# LIST OF ABREVIATIONS

RT: Radiotherapy

3DCRT: three Dimension Conformational Radiotherapy

IMRT: Intensity Modulation Radiotherapy

VMAT: Volumetric Arc Therapy

SBRT: Stereotaxic Radiotherapy

IGRT: Image-guided radiotherapy

CT: Computed Tomography

MRI: Magnetic Resonance Imaging

PET: Positron Emission Tomography

SPECT: Single Positron Emission Computed Tomography

GTV: Gross Tumor Volume

CTV: Clinical Target Volume

PTV: Planning Target Volume

OAR: Organ at Risk

# INTRODUCTION

# Introduction

External radiotherapy is a cancer treatment technique using high-energy rays produced by a linear accelerator and directed precisely from outside the body towards the tumour. This type of external beam radiation therapy is the most common way to treat many types of cancer. In order to minimize possible damage to adjacent tissues, combinations of one or more beams are considered with different entrance angles to the body. Generally, prescribed dose is delivered during many sessions that can be extended for several weeks.

The discoveries of X-rays by W.K. Rœntgen in 1895 and of radioactivity by H. Becquerel in 1896 are at the origin of radiotherapy. Following these discoveries, the effects of ionizing radiation on living matter were observed and their potential for treating certain tumours was quickly exploited. During more than one century, radiotherapy has undergone quite considerable technical and fundamental development from trial and error, through rationalization, to end-up with the digitization and the complete inclusion of imaging techniques in the treatment planning. Indeed, the development of Treatment Planning Systems (TPS) in the 90s made it possible to carry out a three-dimensional calculation of the dose and therefore to treatment planning with very high accuracy according to the specific anatomy of any patient and dose constraints not to be exceeded on certain organs at risks (OARs).

The major challenge for the radiotherapist is to identify, as precisely as possible, the tumour and its possible microscopic extensions in order to irradiate it, while sparing the neighboring healthy organs. Technological developments over the past 30 years have completely changed the daily clinical practice of radiotherapy and have brought about a complete change in the therapeutic paradigm. Starting from a large, poorly targeted irradiation, we have come to an increasingly personalized and extremely targeted treatment. These advances are the direct consequences of the integration, in radiotherapy, of medical imaging. This integration, in particular computed tomography (CT), has gone beyond the diagnostic stage to intervene directly in the dose calculation and the therapeutic monitoring of the disease during and after treatment. Unfortunately, CT, which remains the only technique on which the dose calculation is based in radiotherapy, due its direct relation with electron density of different tissues, could not alone cover all the other aspects relating to the precise delineation of organs and structures necessary in radiotherapy planning.

Due to its exceptional soft tissue visualization abilities and its wide range of contrasting images, magnetic resonance imaging (MRI) has become a powerful tool for more

precisely defining tumour boundaries where CT fails. Indeed, better visualization of the target area and nearby OARs is a key factor in improving target volume delineation. The growing role of MRI can also be attributed to its imaging capabilities, which can provide insight into target characterization as well as response to treatment. MRI is used to guide treatment because it provides a high quality contrasting soft tissue image, which can reduce the degree of toxicity to which at-risk organs and healthy tissue are exposed. New magnetic resonance (MR) systems - Magnetic Resonance Simulators (Sim-RM) and Linear Magnetic Resonance Accelerators (MR-linac) - optimize radiotherapy planning and provide real-time guidance for radiotherapy from high accuracy. Moreover, the integration and the use of MRI for dose calculation and radiotherapy planning instead CT is also under consideration and some ideas such as the generation of synthetic CT images based on MRI images is under intensive investigation.

In this thesis work, it was a question of establishing a synthesis on the contribution of MRI in radiotherapy on the different stages of cancer diagnosis and radiotherapy treatment. As a specific objective, we were interested in the study and quantification of the contribution of MRI in radiotherapy for treatment planning of Glioblastoma. The analysis focused on optimizing the dose to be delivered to the tumour by sparing the organs at risk (OARs). Our research was focused on how CT/MRI image registration and fusion contributes in the improvement of radiotherapy treatment planning of such cancer cases. Thus, contribution was assessed in terms of better optimization of treatment through the conformity of dose distribution according to the cases considered. Several patient cases were considered and appropriate metrics were used for the evaluation of registration and fusion of CT/MRI images. This thesis project was carried out in the radiotherapy service of cancer fighting centre of Setif.

This manuscript is organized into four chapters. The first chapter is reserved to the presentation of external radiotherapy and medical imaging. The second chapter presents medical image registration and data fusion in radiotherapy: Interesting information emerging role of MRI in external radiotherapy treatment planning evaluation metrics are given in the third chapter. Finally, in the fourth chapter, we present results on CT/MRI images registration and fusion and how a well-done work can contribute to the radiotherapy treatment planning optimization in case of Glioblastoma.

# CHAPTER I :

## Radiotherapy and Medical Imaging

# I. Radiotherapy

## I.1 Radiotherapy

Radiation therapy is a method of loco regional cancer treatment, using ionizing radiation for the destruction of cancer cells blocking their ability to multiply. In addition, the aim of irradiation is to destroy all the tumor cells while sparing the healthy peripheral tissues. Radiation therapy can be prescribed as a curative treatment (to destroy the tumor), as an adjuvant treatment (to prepare or complete a surgical intervention or chemotherapy), or as a palliative treatment (to reduce pain and increase life expectancy) [1-3].

A radiotherapy treatment is prepared according to the particular situation of each cases; the patient receives a specific care adapted to his personal case. Depending on the type of tumor and its location, different modes of radiotherapy are used in the clinic and are cited below [2-4]:

**Brachytherapy:** consists of introducing radioactive substances into the body by placing them in a natural hollow space, in the tumor itself or in its immediate vicinity. The radiation is generally isotropic. It is therefore important to study the distribution of sources so that the tumor is well destroyed while minimizing the impact on healthy tissue, which is the aims of optimization in brachytherapy.

**Metabolic radiotherapy**: is mainly used in certain forms of thyroid cancer. In this case, the radioactive substance is administered orally or intravenously and will preferentially bind to cancer cells.

**External radiotherapy:** This technique is the most frequent one. The radiation source is outside the patient. It consists of administering the rays through the skin and tissues to irradiate the entire region affected by the tumor as well as possibly the nearest lymph nodes.

In this chapter, we will focus only on External Radiotherapy and explain its principles and these different stages.

## I.2 External Radiotherapy

### I.2.1 Principle

Radiation therapy is a method of locoregional cancer treatment, using radiation to destroy cancer cells while sparing healthy peripheral tissu. External radiotherapy is today essential in oncology since it is programmed in two thirds of the therapeutic schemes either alone or associated with surgery and / or chemotherapy [3-8].

The radiotherapy protocols are defined mainly according to the type of tumor, its location, its size, its extension and its grade. Thus, the techniques used are different for each case, the total dose is not enough to define a treatment by irradiation, but it is also necessary to take into account the dose by fraction, the total number of fractions (or sessions) and the number of fractions per day or per week .

### I.2.2 Techniques used in External Radiotherapy

In external RT several treatment techniques are used: 3D conformal radiotherapy (3D-CRT), radiotherapy by intensity modulation (IMRT) as well as other techniques such as RT 4D, VMAT (Volumetric Arc Therapy), SBRT (Extracranial radiosurgery), IGRT (Image-guided radiotherapy). In the first case, physicists study ballistics to determine the correct configuration of the beams and obtain the desired dose distribution. Whereas in the second case, physicists indicate to the system objectives and dose constraints so that the system determines the best ballistics, while Cyberknife is an even more advanced technique than the previous two [3-8].

#### I.2.2.1 3D Conformal Radiotherapy

This type of radiotherapy is based on the use of patient's images acquired using a CT scanner in the same position as the one at which the treatment will be carried out. The images acquired are reconstructed in three dimensions (3D-CRT). Powerful computers simulate the treatment by proposing the combination of beams suitable for each location and introducing the doses established by doctors for the proper treatment of the patient (Figure I.1).

These computers with the set of associated programs, called planners, perform complex algorithms to calculate the dosimetric distribution represented three-dimensionally on the computer screens. As a result, the so-called dosimetric report is obtained. This report gives, among others, the parameters for the placement of the treatment units as well as the doses in different risk organs and the Monitor Units (UM) to be given to the equipment for the execution of the treatment (Figure I.2) [3-8].

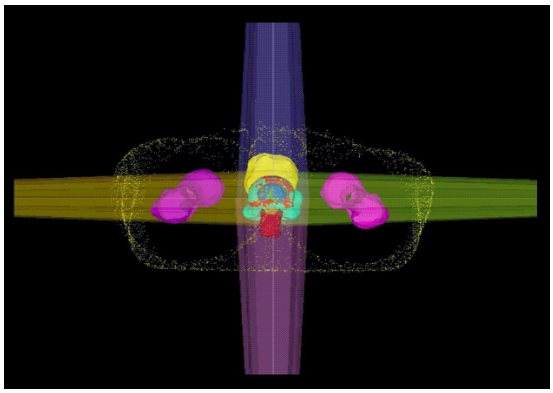

Figure I.1: Ballistic example of four beams on prostate cancer

We talk about direct planning, a representation of the process is presented in Figure I.2 [3-8].

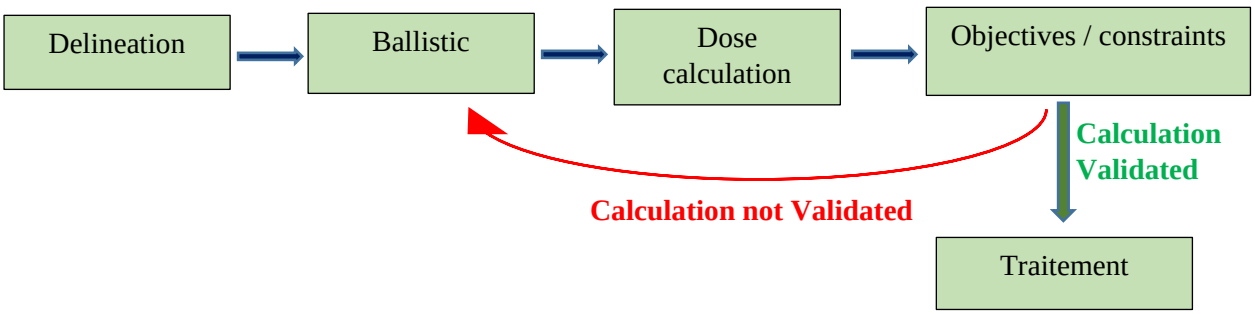


Figure I.2: Process of 3D conformal radiotherapy (3D-CRT)

### I.2.2.2 Fractionated stereotactic radiosurgery

This technique allows the administration of an even higher dose of radiation to brain lesions in very few sessions, thus preserving the structure and function of neighboring healthy cells as much as possible. It is performed by a dose per fraction that cannot cause damage to healthy tissues but accumulates in the diseased tissues, preventing the appearance of sequels or complications. It is applied mainly when the lesion is very close to especially critical structures such as the brain stem, optic nerves, chiasm or pituitary gland.

It is usually used to treat brain and neck tumors but also in the spine, abdomen, liver, lung or prostate for both malignant and benign tumors of small or medium size. In conclusion, it is advisable in the cases of tumors difficult to reach, located in the vicinity of vital organs or key anatomical regions and that are subject to movement within the body.

This treatment of fractionated stereotactic radiosurgery depends on several technological systems. Firstly, the 3D localization images that allow determining the exact coordinates to locate and detect the shape and dimensions of the tumor. In addition, the systems that position and mobilize the patient's body and keep it immobile during surgery must also be used. Furthermore, there is radiation targeting the tumor, which serves to eliminate it.

We also have image-guided radiation therapy (IGRT) to make treatment planning more accurate and precise. Each treatment session is administered using the IMRT technique, which does not only adapt the shape of the irradiation field to the tumor shape with sub-millimetric accuracy but also offers a variable intensity of irradiation beam in each field, adapting to the anatomical characteristics of the tumor and normal structures.

During the treatment, clinician uses thermoplastic masks for the immobilization of the patient to maintain the exact position of the patient for carrying out the treatment. To control this position, an infrared camera system that detects the position changes less than 1 mm and/or exceeding tenths of a second.

In addition, the latest technological improvements ensure fewer side effects, which contributes to better mental and physical health, enabling a better recovery [4-8].

#### I.2.2.3 Intensity Modulated Radiation Therapy

Intensity Modulated Radiation Therapy (IMRT) is a form of high-precision external radiotherapy where the dose of radiation administered by each of the beams is not uniform but modulated in three-dimension shapes to administer a higher dose to the tumor while minimizing the exposure of the surrounding healthy tissue to the radiation.

As IMRT allows the limitation of the dose proportion applied to the healthy tissue to a very low level compared to that applied to the tumor, it is possible to administer higher and more efficient doses of radiation to the tumor with fewer side effects than with conventional radiotherapy techniques. IMRT reduces the toxicity of the treatment.

IMRT is currently used to treat head and neck, prostate, breast, lung and central nervous system tumors. It is also used for breast cancer. In addition, it is used in gynecological, hepatic, lymphoma and sarcoma tumors, as well as some organs and areas close to them. IMRT is also useful for treating childhood tumors [5-9]. A representation of the process is presented in Figure I.3.

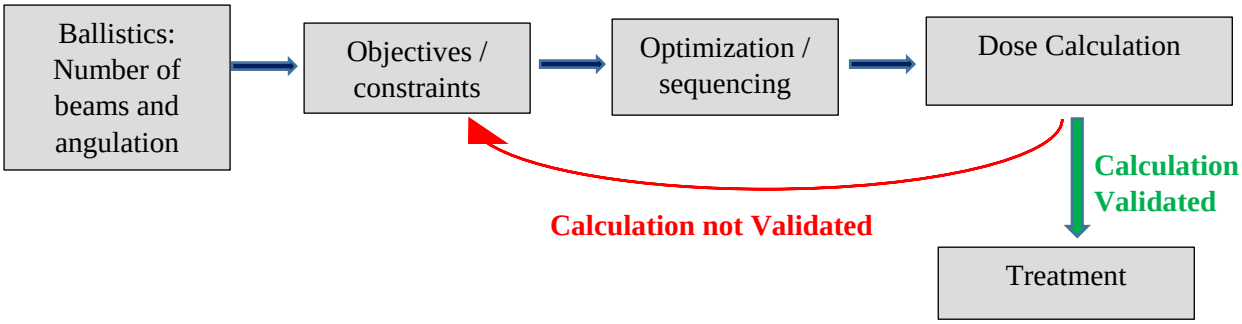


Figure I.3: Process of Intensity Modulated Radiation Therapy (IMRT)

### I.2.3 Stages of radiotherapy treatment

For the planning of a radiotherapeutic treatment, the patient goes through several stages necessary for the good progress and the success of the RT treatment; theses stage are defined below [1-6].

#### I.2.3.1 Anatomical data acquisition

Medical imaging is the essential tool for the acquisition of anatomical data and the location of the geometric limits of tumor volumes and their relationship with neighboring organs, several medical imaging are used to improve diagnostics and RT treatment.

**A/ Computed tomography (CT)**: this is the standard for acquiring anatomical data. The CT necessary slide for the 3D reconstruction as well as the location and contouring of the PTV and OAR, in addition the CT provides the treatment planning system with the electronic density card necessary for the calculation and distribution dose.

**B / MRI magnetic resonance imaging:** offering great tissue power and high resolution, MRI imaging is used to supplement X-rays tomography, facilitates the localization of PTVs, and OARs to the doctor in particular cases such as brain and prostatic tumors.

Other types of imaging such as ultrasound, PET, SPECT are used to improve and complement the information.

#### I.2.3.2 Delineation of treatment volumes and organs at Risk

In an effort to harmonize, the International Commission on Radiation Units and Measurements (ICRU) published three reports from 1978 to 1999 establishing a common language for dose prescription. The purpose of these reports is the use of a common

nomenclature for the definition of interest volumes. These reports have been modified over time to take into account technological developments and the contributions of imagery in the establishment of treatment plans.

The first report N°28 defined three volumes: the target volume to receive the therapeutic dose, the treated volume defined by the volume encompassed by isodose delivering the minimum tumor dose and the irradiated volume defined as the volume receiving a dose considered to be significant for healthy tissue [10]. This report corresponded to conventional radiotherapy practices, based on non-tomographic imaging, with an indirect definition of the target volume from bone markers, treatment plans with dose calculations based on a 2D section or outline.

The use of tomographic imaging in the establishment of treatment plans has motivated the publication of the ICRU 50 report that defines the following volumes [11]:

- Gross Tumor Volume (GTV). It corresponds to the palpable tumor volume, measurable or visualized in imaging.
- The Anatomical Clinical Tumor Volume (Clinical Target Volume, CTV). This volume contains the GTV and any sub-clinical extensions. Its definition is based on clinical and histological knowledge and responds to notions of probability.
- Planning Target Volume (PTV). It includes CTV and additional margins corresponding to organ movements and patient positioning uncertainties.

The ICRU 62 report was drawn up in order to supplement the previous report. The concept of Internal Margin (IM) has appeared [12]. It corresponds to the additional margins to be added to the CTV to compensate for physiological movements and variations in shape of the CTV (respiratory movements, variable filling of the rectum, etc.). The CTV and IM form the Internal Target Volume (ITV). In the ICRU 62 report, the Set-Up Margin (SM) was also defined, which is the margin taking into account the patient's positioning uncertainties. The Figure I.4 below shows the evolution of the definitions of the different volumes in the three successive reports [2-4].

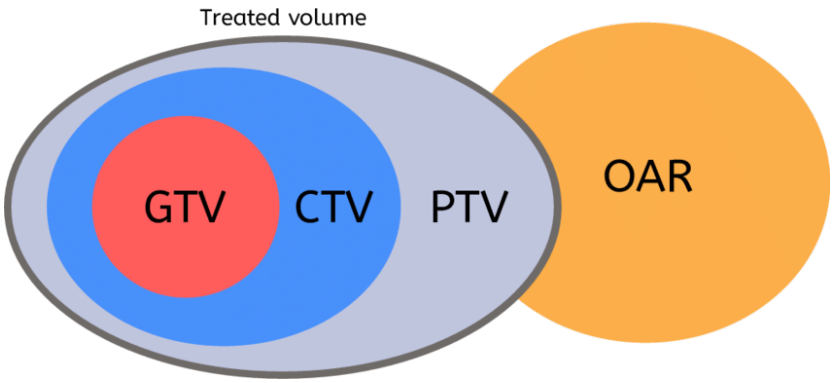


Figure I.4: Main radiotherapy treatment volumes

### I.2.3.3 Simulation

The simulator makes it possible to define and visualize on radiological images the beams of rays adapted to the target volumes. Similar from the radiogenic point of view to radiodiagnostic devices (kV), it differs from it by its mechanical characteristics, which are identical to those of radiotherapy devices, particle accelerators.

The simulator can be used to anticipate or check the ballistics provided by the medical physicist during the "Planimetric study" stage (what is commonly called "virtual simulation") [2-4].

### I.2.3.4 Planimetric and dosimetric study

The "virtual simulation" follows the stage of delineation of PTVs and OARs, this stage is carried out by the medical physicist who studies the appropriate ballistics and calculates the dose using a Treatment Planning System (TPS) (Figure I.5). This particularly critical step leads to the treatment plan and the calculation of the number of monitor units for each irradiation session. However, it is recommended that this calculation be confirmed by a second system, independent of the first, allowing rapid confirmation of the consistency of the results obtained with complex planning software (accreditation criteria) [2-4].

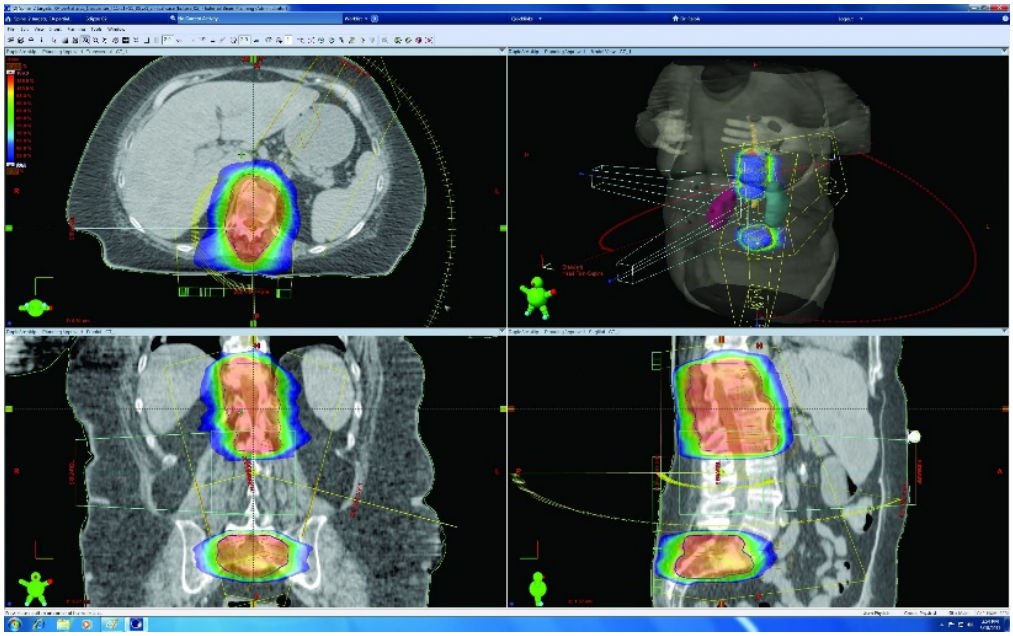

Figure I.5: Definition of target volumes, ICRU report 62 [12]

### I.2.3.5 Organs at risk Protection

During the planimetric study, the primary collimators of the machines define square or rectangular bundles encompassing both tumor volumes, organs at risk and their healthy tissues. Personalized protections are used to limit their irradiation. Their preparation involves all those involved in radiotherapy and requires a technical room with specific equipment. With the new generation of accelerators, protection is provided by an additional multi-blade collimator or integrated into the device consisting of a large series of independent and motorized blades, allowing direct adaptation of the complex shape of the beam with computer control [2-4].

### I.2.3.6 Treatment

The treatment is carried out in bunkers specially designed for RT treatment purposes. Each treatment session lasts approximately 15 to 30 minutes: most of the session is occupied in setting up the patient correctly (lying down on a radiology table); radiation exposures last only about 1 to 2 minutes. The patient will not see or feel the radiation. The treatment itself is painless. There will be no one other than the patient in the room during treatment, but the radiation therapists will observe the patient on a screen and listen through an intercom. They may return to the radiation room from time to time to adjust the position of the device.

The fractionation is generally (4 to 5 sessions per week) for 3 to 7 weeks depending on the case is essential to avoid long-term side effects (sequelae) [2-4].

### I.2.4 R errors and their impact on the patient

Since the start of the use of ionizing radiation, it has been difficult to get around incidents / accidents that have occurred in radiotherapy. With the development of new radiation techniques and their sophistication, total and absolute control of the entire treatment chain is extremely complex and leads irreparably to treatment errors, more or less serious for the patient. Errors can occur at any level, at prescription, dose calculation, radiation, or related to human, computer or Systems [13-14].

#### I.2.4.1 Different sources of errors

Several types of errors can lead to incidents / accidents, whether systematic or random. Their origins have been the problem of many articles in the literature and report a link between error rate and location of the tumor, treatments for sarcomas, leukemias or head and neck being more easily prone to errors. On average, several texts indicate that the errors come mainly from "geometric" factors, relating to the positioning / repositioning of the patient, to the shape of the treatment fields as well as the use of several types of imagery when delineating volumes. . In addition, other research establishes a link between the various origins of the errors and the processing technique used, the more complex techniques involving a greater variety of elements which may fail, or requiring controls not provided for in the protocols issued by learned societies.

Many of these errors are easily detectable before they even have an impact on treatment, thanks to the multiple quality assurance procedures put in place and thanks to the Record and Verify system which traces the stages of personalized patient treatment.

However, errors in the position of the blades or the homogeneity / symmetry of the beam can occur at any time during the irradiation, and can cause discrete but damaging processing errors. Several Examples have shown that the dosimetric impact of a systematic error of one millimeter on the position of the blades of the MLC can lead to a change in the shape of the 95% isodose of almost 8% for complex fields [15, 16].

#### I.2.4.2 Impact of errors and classification of the severity of accidents in radiotherapy

The impact of errors that can occur at any stage in the development or delivery of treatment is usually the same for the patient. This results in the majority of cases by more or less obvious differences between the prescribed dose and the dose delivered to the patient, something that is generally caused by a bad positioning or a bad localization of the target

volumes and the OARs. In case of underdosing or overdosing, the patient will suffer from these differences in dose distribution. A lower dose than that prescribed will limit tumor control and therefore the intrinsic effectiveness of treatment, while too high a dose will increase the risk of complications and the probability of developing radiation-induced cancers. In practice, the International Commission on Radiological Protection (ICRP) considers that an accident must be declared to the high nuclear safety authorities when a difference of 5% on the total delivered dose is observed, in comparison with the prescribed dose. This same commission classifies accidents according to two categories, type A accidents, involving an overdose of 25% or more, directly endangering the patient's life and type B accidents, involving an overdose of 5 to 25% or an under dosage and provided that this type of incident is discovered before the end of treatment and is corrected (otherwise it becomes a type A accident).

A slightly more detailed scale was defined in 2007 by the Nuclear Safety Authority (ASN).The ASN-SFRO scale this time classifies radiotherapy accidents into 7 different levels:

**Level 0:** events with no long-term dosimetric consequence (compensable error during treatment).

**Level 1:** events with no major expected consequence or only likely to cause mild effects.

**Level 2:** incident involving moderate impairment of an organ or function, with a dose greater than the recommended dose.

**Level 3:** severe impairment of an organ or function.

**Level 4:** incidents where the patient's life is endangered and / or disabling consequences for the latter.

**Levels 5 to 7:** the accident results in the death of the patient (s), the level of the accident increasing between 5 and 7 depending on the number of deaths it has caused [15,16].

# II. Medical Imaging

Medical imagery is the graphic reproduction representing information of an anatomical, molecular or metabolic nature of the human body following the use of several exploration signals of various natures such as X-rays, magnetic fields, ultrasound. All these imaging methods are therefore complementary.

## II.1. Roles of medical imaging in radiotherapy

The different medical imaging systems have well-defined roles, which are:

- The diagnosis.

- Treatment planning (surgery, radiotherapy).

- Monitoring the treatment of pathologies.

- Guided interventions in real time: interventional imagery.

- Training / Education [2].

## II.2 Main imaging modalities

### II.2.1 Computed tomography

Computed Tomography (CT), is a radiological technique that generates horizontal, vertical or oblique 2D sections allowing the reconstruction of a 3D volume of the object under examination (Figure I.6). This provides a more detailed view of the interior of the object. This technique is based on the penetration of X-rays (RX) taking into account their properties [14-18].

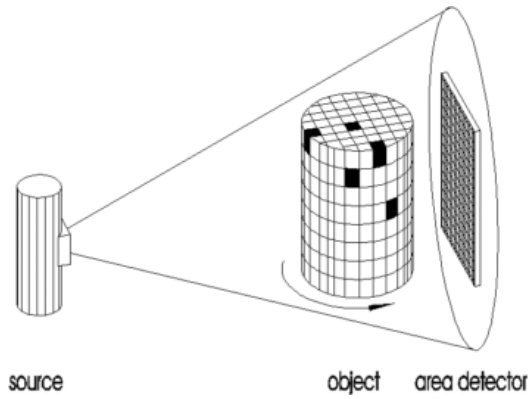


Figure I.6: Principle of computed tomography

### II.2.1.1 Principle of operation

Like conventional radiography, the scanner relies on the more or less significant absorption of X-rays s from the environment traversed (the bones, for example, being much more absorbent than the soft tissues), which scan the patient in different directions in order to get sectional images (Slides). The scanner technique thus allows the precise exploitation of numerous organs. The images obtained are printed on a film to be studied or reconstructed in three dimensions using computer tools connected to the device.

Computed tomography (CT) is based on two essential properties:

• The measurement of the radiological density of the elementary volumes of a section from the absorption of an X-rays beam, which increase the resolution in density of the image of a body section of a factor of 100 compared to what it is in conventional radiology.

• The reconstruction of a sectional image of the human body from the different transverse projections obtained by the system constituting the apparatus [17-21].

### II.2.1.2 Why use Scanner X

Currently, most large hospitals are equipped with scanners, which reveal cancerous tumors of the liver, brain, lung, kidneys and which detect herniated discs. CT can distinguish, for example, cysts, blood masses, fat masses and calcium masses. It has completely revolutionized radiology, in particular in neurology. In addition, the examination is painless and almost harmless to the patient.

### II.2.1.3 X-rays Production

The production and detection of X-rays In an X-rays tube, electrons, emitted by thermionic emission from a cathode consisting of a heated filament and a focusing cup, are accelerated by a high voltage and focused into a beam so that they impinge on a target which forms part of an anode (Figure I.7). These electrons are referred to as projectile electrons. X-rays s are produced by the sudden deceleration of the projectile electrons by the nuclei of the target material or by collision of projectile electrons with electrons in the target atoms. These are referred to as bremsstrahlung X-rays s and characteristic X-rays s respectively. Bremsstrahlung X-rays are emitted when an electron slows down by coulombic interaction with the electrostatic field of a target nucleus. When the electron slows down it loses kinetic energy, which isconverted to electromagnetic radiation, i.e. an accelerated (or decelerated) charge will radiate electromagnetic radiation [17-21].

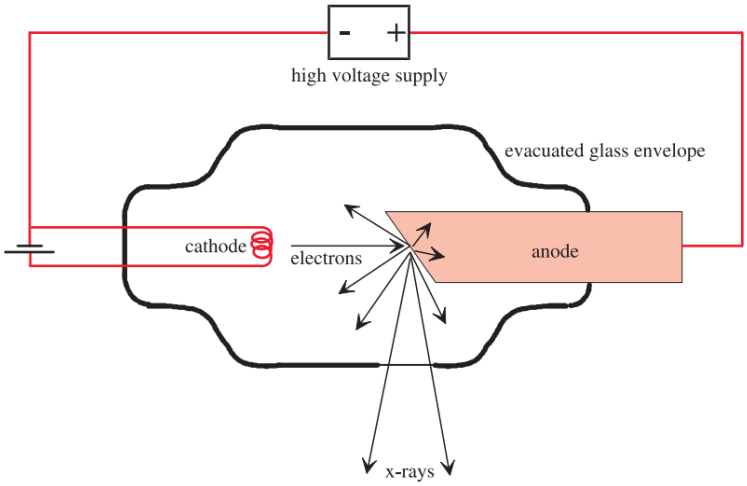


Figure I.7: Schematic diagram of a stationary anode X-ray tube

The amount of energy radiated depends on the closeness of approach of the projectile electron to the target nucleus. Therefore bremsstrahlung X-rays can have a range of energies from 0 up to a maximum equal to the energy of the projectile electrons. Thus the maximum possible X-rays energy (in eV) is numerically equal to the accelerating electric potential, e.g. if the X-rays tube is operated at 50 kV the maximum X-rays energy is 50 keV. Bremsstrahlung radiation is also called white radiation because of the broad continuous spectrum of X-rays energies produced.

Characteristic X-rays arise from vacancies that are created in the electron shells when the target atoms are ionized by the projectile electrons. Electrons from outer shells drop down to fill the vacancy and release their excess energy in the form of X-rays. Characteristic X-rays are monoenergetic. Their energies depend on the binding energies of the electrons in the electron which in turn depend on the type of the atoms in the anode.

Both bremsstrahlung and characteristic X-rays are produced simultaneously. An example spectrum for a tungsten target is shown in Figure I.8. The X-rays tubes used in CT are typically operated at potentials in the range 100 kV to 150 kVs, which in turn depend on the type of the atoms in the anode.

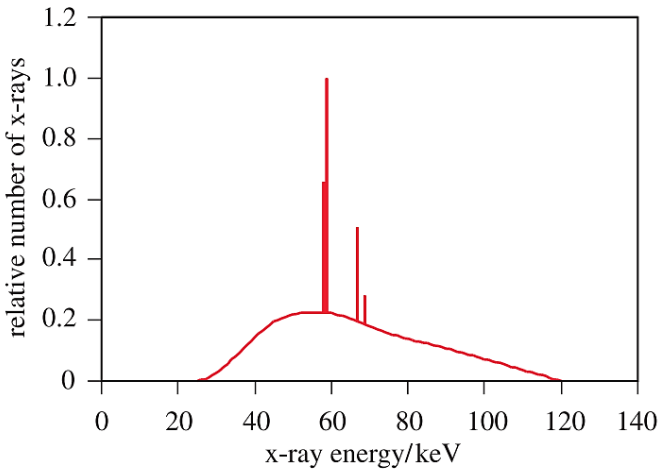


Figure I.8: A typical x-ray spectrum for a CT x-ray tube operated at 120 kV

### II.2.1.4 Basic principle of X-rays Attenuation

When an X-rays beam encounters matter, there is a decrease in its intensity, due to the reduction in the number of photons. Part of the energy lost during the process is absorbed (Ea), while another is diffused and leaves the material in different directions from that of the incident beam (Ed). The explanation of this phenomenon is found in the study of the interactions of photons with electrons when they meet. The law that gives X-rays attenuation is an exponential law; this intensity decreases with the thickness of the crossed environment:

$$I = I_0 . e^{-\mu.x} \quad (I.1)$$

With:

- ✓ Io : The incident Beam of X-rays s penetrating along the x axis of a heterogeneous medium
- ✓ μ: The attenuation coefficient
- ✓ I : The emerging Beam.

The X Scanner is then based on the measurement of different absorption coefficients of the tissues crossed by an X-rays beam. Each tissue has its own absorption coefficient which depends on the density of the tissue and the energy of the ray beam X crossing it, thanks to a multitude of algorithms, transformations, mathematical calculations, the medical image is created [20-24].

### II.2.1.4 Scanning Geometries

The X-rays tube and detector geometry depicted in Figure I.9 is referred to as first generation. Only the very first CT scanners (early 1970s) were of this configuration. Because of the single detector and the combination of both translate and rotate motions, scan times were very long: of the order of a few minutes. Second generation CT scanners (Figure I.10) were developed to decrease scan times. They had a narrow fan-beam of X-rays and a small number of detectors. Multiple projections were acquired simultaneously (one per detector) during each translation and therefore the number of translations required was reduced accordingly [17, 21].

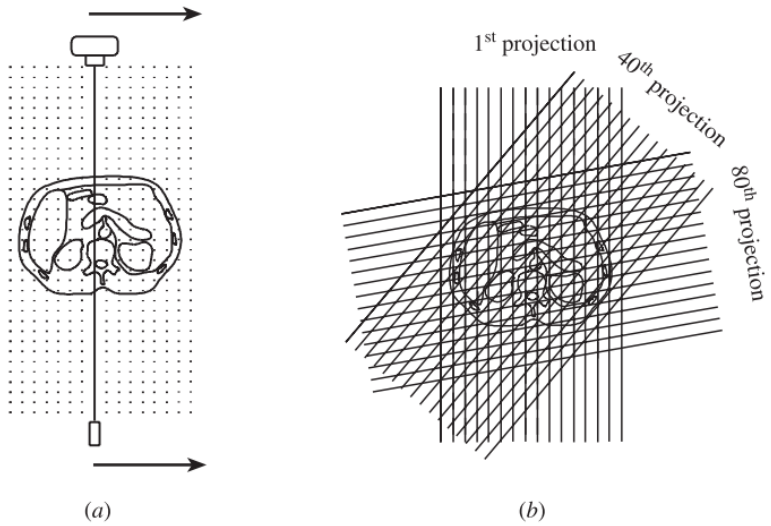


Figure I.9: First Generation of CT scanner

Third generation is that shown in Figure I.11, i.e. the fan beam of X-rays is wide enough to cover the full width of the patient and therefore no translation motion is required. The X-rays tube and detector arc rotate only. The arc of detectors may contain up to 1000 individual detectors.

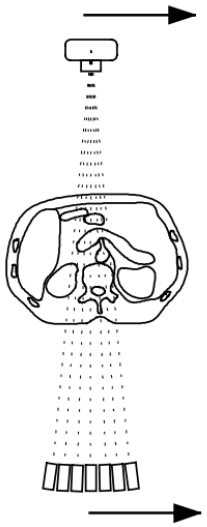

Figure I.10: Second generation CT scanner

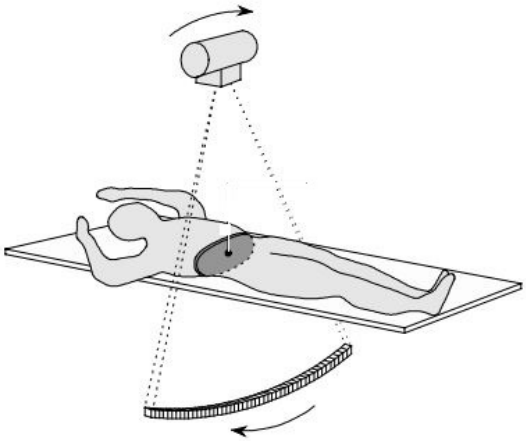

Figure I.11: Third generation CT scanner

In fourth generation, scanners the detectors form a complete ring around the patient and only the X-rays tube has to rotate. These scanners may use up to nearly 5000 individual detectors. A fourth generation CT scanner is depicted in Figure I.12.

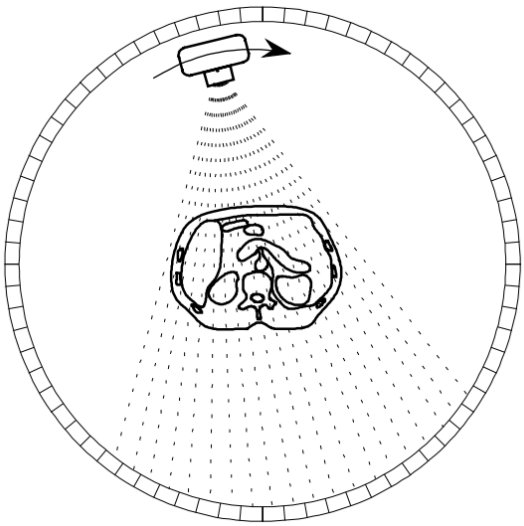

Figure I.12: Fourth generation CT scanner

The fifth generation of CT scanners has eliminated all mechanical motion by using an X-rays tube with an anode that forms a circular arc of about 210◦ around the patient. The scanning motion is achieved by using magnetic fields to sweep the electron beam along the anode. This scanner can acquire a complete set of projection data in as little as 50 ms and is designed specifically for cardiac imaging [17, 21].

### II.2.1.5 Different types of scanner

The equipment is becoming more and more sophisticated and there are now two main types of scanner: spiral (helical) and double tubes.

#### A. Helical computed tomography

In this type of scanner (Figure I.13) the X-rays emission is always continuous. The table move in the circular ring at a fixed speed (given by the pitch parameter: distance per revolution / beam width) by reaching exams that last a few seconds. The first spiral scanners had only a single slice scanner, which allowed only one data acquisition for each position when a rotation of the X-rays tubes was carried out. The appearance of multi-slice scanners has increased the number of cuts per rotation. A scanner is now capable of reaching a total of 320 cuts per rotation. With the latest generation devices, it is possible to perform rotations every 260ms (compared to 500 ms for older devices), the spiral Scanner allowed to have finer cuts and thus allow access to three-dimensional reconstruction small structures (such as the coronary arteries).

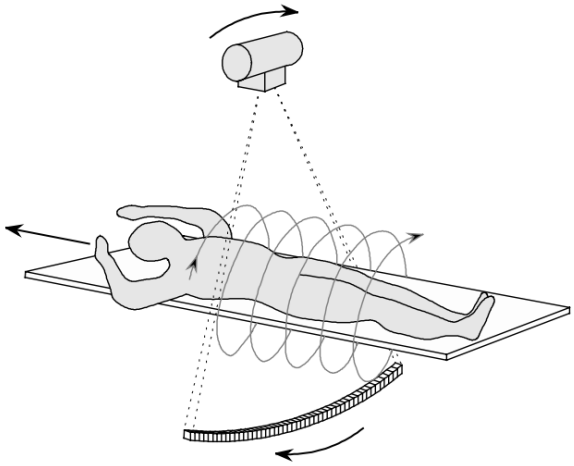

Figure I.13: Principle of acquisition of Helical computed

**B. The double tube scanner**

It is the first dual X-rays source scanner. It is a technology with two X-rays sources which are arranged at 180 angles to each other and which can provide acquisition speed. (a pitch of 3.2) and a time resolution (at 75 ms) twice higher. It is also possible to use the two tubes at different energies (double energy), which opens up new areas of use.

**II.2.1.6 Image Reconstruction**

A mathematic process that generates images from X-rays projection data at many different angles around the patient calls image reconstruction. The fundamental of image reconstruction is to produce and give impact on the quality of image. There are two major methods which are analytical reconstruction and iterative reconstruction. Moreover, analytical reconstruction which is filtered back projection (FBP) is widely used in clinical CT scanners because their efficiency and numerical stability [17, 21].

**A. Analytical reconstruction: filtered back projection**

Figure I.14 (A) shows example of object projection using X-rays source with a projection angle step of 45°. For image tomographic reconstruction, the projections are back-projected through in order to obtain a rough approximation to the original object structure. As a result, the reconstructed tomographic image is apparently blurred as Figure I.14(B). Therefore, ramp filtering is used to remove noise case and eliminate blurring. The combination of back projection and ramp filtering is known as filtered back projection (FBP).

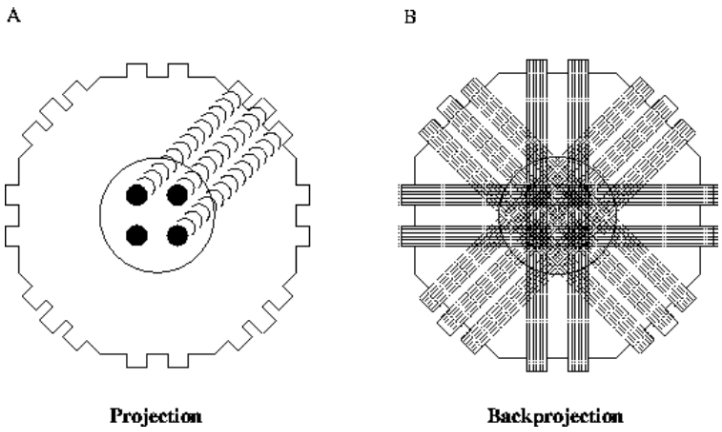


Figure I.14: Illustration of filtered back projection reconstruction

### B. Iterative reconstruction

Iterative reconstruction methods consist of three steps as present in FigureI.15. Artificial raw data are estimated and created from forwarded projection of the volumetric object. Next, all data are being compared to the real measured raw data in order to compute a correction term. The final step is the correction term is back projected onto the volumetric object estimate. The iteration process can be initiated with an empty image estimate or using prior information, for example, a standard FBP reconstruction or a volume of a similar object. In general, the better the prior images match the final images, the faster the process converges towards a stable solution. The iterative process is finished when either a fixed number of iterations is reached, or the update for the current image estimate is considered small enough or when a predefined quality criterion in the image estimate is fulfilled.

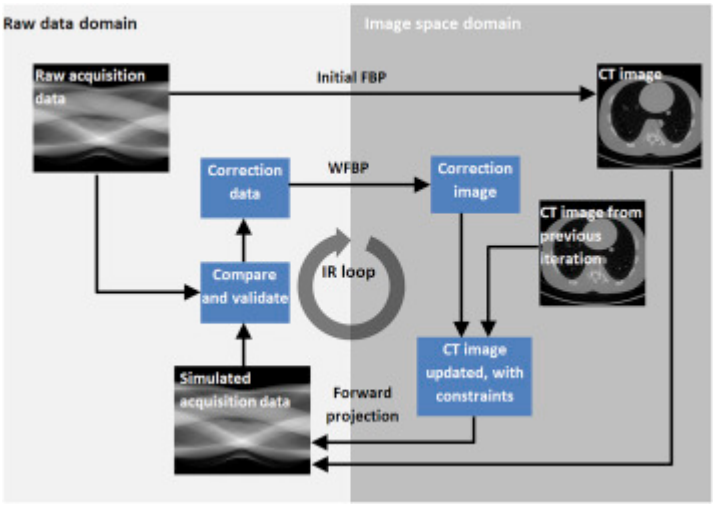


Figure I.15: Schematic view of the iterative reconstruction

### II.2.1.7 Image display

Before the image is displayed, the CT scanner converts the measured attenuation coefficients of the voxels to CT numbers. For a voxel, i, the CT number, $N_i$, of the corresponding pixel is related to the attenuation coefficient, $\mu_i$, of the tissue in the voxel by

$$N_i = 1000\ X\ \frac{\mu_i - \mu_w}{\mu_w} \quad \text{(I.2)}$$

where $\mu_w$ is the attenuation coefficient of water. Expressing the attenuation coefficient relative to that of water dates back to the first clinical CT scanner, the EMI Mark 1 head scanner of 1972. The detectors of this scanner had a low dynamic range. Therefore the patient's head was surrounded by a water bag to reduce the very high X-rays intensity of the unattenuated X-rays beam that would otherwise reach the detectors. The scaling factor of 1000 in equation (I.2) is used so that the CT numbers can be expressed as integers. This reduces computer memory and storage requirements.

From equation (I.2) it can be seen that the CT number of water will be zero, the CT number of air ($\mu \approx 0$ cm−1) will be −1000, and a voxel with tissue having an attenuation coefficient twice that of water (e.g. bone) will have a CT number of +1000. Most soft tissues of the human body lie in the range ±100.

### II.2.2 Magnetic Resonance Imaging

Historically in 1946, two scientists concomitantly and independently describe the phenomenon of nuclear magnetic resonance: Félix Bloch and Edward Purcell succeed in showing that certain nuclei of atoms placed in a magnetic field absorb energy after emission of a radio frequency wave, and then re-emit this energy when they return to their original state. This discovery follows the work of many researchers; it won them the Nobel Prize in Physics in 1952. In the 1930s J. Gorter showed how to measure the nuclear magnetic moment and I.I. Rabi measures it experimentally. This same researcher will observe the phenomenon of nuclear magnetic resonance but will consider that it corresponds to an artefact. In the 1950s, relaxation times were measured on animal tissues removed, then animal experiments began in the following decade. This technique was first used in the fields of chemistry and biochemistry using spectroscopy. In the 1970s Lauterbur, Mansfield and Damadian (the first two obtained the Nobel Prize in medicine in 2003) applied this technique to the medical field with the obtaining

of the first images; their idea was to apply magnetic field gradients in order to obtain a spatial localization of the signal [17-22].

### II.2.2.1 Basic principle

In Magnetic Resonance Imaging (MRI), the magnetism that we measure is from nuclear origin. The magnetic properties are represented by a vector μ called magnetic moment whose length and direction correspond respectively to its intensity and to its direction. The value of the magnetic moment is proportional to a quantity characteristic of the particle in rotation on itself which one calls "spin". Only nuclei with an odd number of protons and neutrons can exhibit detectable magnetism. The nucleus most studied in medical imaging is that of hydrogen, an essential component of water, biological fluids and fats [17-22].

Placed in a natural environment, the magnetic moments of the hydrogen nuclei are randomly oriented and their sum corresponds to a zero magnetization M. These nuclei, when placed in a magnetic field B0 have a precession movement with an angular frequency called the Larmor frequency ($\omega 0 = \gamma B0$). The factor γ, called the gyromagnetic spin constant, is characteristic of the nucleus considered.

The total nuclear magnetization M, describing the sum of the magnetic moments is defined by two components: the "longitudinal" magnetization ML corresponding to the projection of M on the axis parallel to B0, and the transverse magnetization MT corresponding to the projection of M on the xy plane perpendicular to B0. In the presence of a magnetic field B0 the quantum distribution of the proton spins is done according to 2 energy levels, parallel and antiparallel, separated by $\Delta E = \hbar\omega$ with a very slight excess of spins on the low energy or parallel level ( ħ = Planck constant / 2pi).

The phenomenon of resonance is obtained by the transfer of energy between an electromagnetic wave emitted at the Larmor frequency and the system of spins of the nuclei. After the excitation stopped by the radiofrequency wave, the magnetization returns to its equilibrium position parallel to B0 (relaxation). Its evolution over time is characterized by two constants T1 (longitudinal relaxation time) and T2 (transverse relaxation time) which vary according to the tissues and their normal or pathological state.

The transverse component during relaxation describes a spiral in the xy plane. This rotation induces a radio frequency wave, at the origin of the MRI signal (free induction signal or Free Induction Decay). This decrease in transverse magnetization results from a phase shift of the spins in the transverse plane, following two different types of interaction.

The interaction of the spins with each other results in a relaxation phenomenon described by a time T2, "spin-spin" relaxation time. There is an additional spin phase shift due to the heterogeneities of the magnetic field and the magnetic susceptibility effects of the sample. This relaxation is characterized by an additional relaxation time T2 ’and we then consider T2 * the overall relaxation time defined by [17-22]. :

$$\frac{1}{T_2^*} = \frac{1}{T_2'} + \frac{1}{T_2} \quad \text{(II.3)}$$

The equation characterizing transverse relaxation is:

$$M_{xy}(t) = M_{xy} e^{-t/T_2} \quad \text{(II.4)}$$

The regrowth of the longitudinal component is a relaxation phenomenon resulting from the interaction of spins with the network. The equation characterizing this relaxation is:

$$M_0(t) = M_0(1 - e^{-t/T_1}) \quad \text{(II.5)}$$

In which T1 is the "spin-network" relaxation time.

The phenomena of resonance and relaxation do not allow spatial localization. For this it is necessary to superimpose on the main magnetic field B0 field gradients along the three axes of space: $\overrightarrow{G_x}$ , $\overrightarrow{G_y}$ , $\overrightarrow{G_z}$ which disperse the resonance and relaxation frequencies, thus allowing a spatial coding of the radio frequency emission.

**II.2.2.2 Proton and magnetic moment**

Hydrogen nuclei consist of a single proton that carries a positive electrical charge. The proton is constantly spinning and so the positive charge spins around with it. Recalling that a moving electrical charge generates a magnetic field, then protons have their own magnetic fields due to their spin and thus behave like little bar magnets with their own magnetic moment. Magnetic moments are normally randomly orientated. However, when an external magnetic field (B0) is applied they align either with (parallel) or against (antiparallel) to this external field. The preferred state of alignment is the one that requires the least energy: that is, parallel to B0. Accordingly more protons align with B0 than against it. The difference in the number of protons aligning parallel and anti-parallel to B0 is typically very small but ultimately depends on the strength of B0 as well as the temperature of the sample. As a rough estimate, for about

10 million protons aligning parallel to B0, there are approximately 10 000 007 aligning anti-parallel to the external magnetic field (Figure I.16).

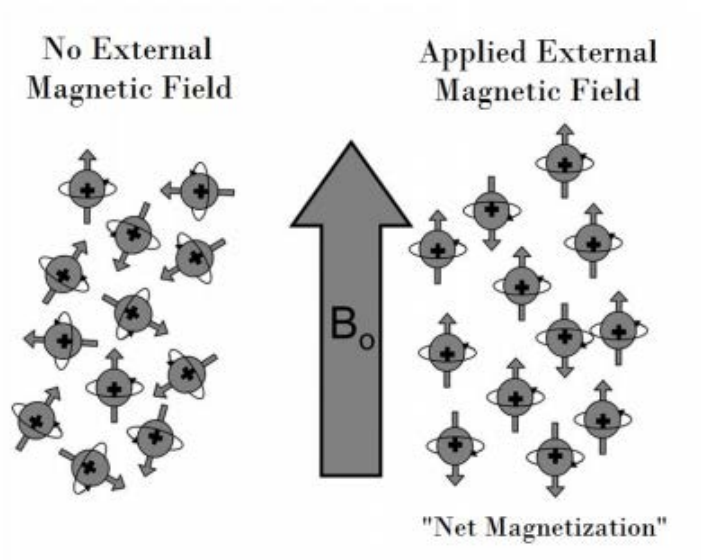


Figure I.16: Alignment of protons due to an external magnetic field process.

### II.2.2.3 Precession

When put in an external static magnetic field, the overall group of protons start to precess. Precession can be likened to the movement of a spinning top, whereby the axis of the top rotates and forms a cone shape. The rate of spin or rather precession of the proton is known as the Larmor frequency. The Larmor frequency depends on the strength of the local static magnetic field B0 in such a way that:

$$f = \gamma \times B0 \qquad \text{(II. 6)}$$

Where, ω is the Larmor frequency in MHz, γ the gyromagnetic ratio in MHz/Tesla and B0 is the strength of the static magnetic field in Tesla.

### II.2.2.4 MRI machine

When we first got into the MRI machine a superconducting magnet creates a near homogeneous magnetic field from one side to the other that determines the strength of the MRI machine. Common systems are the 1T, 1.5T and 3T in strength. There are three sets of gradient magnets in the MRI used to localize locations in 3D space, the z-axis, y-axis and x-axis as shown in Figure I.17.

To select a particular slice of tissue in the body, technologist can turn on the set of electromagnets along the z-axis that create a magnetic gradient from head to toe. By putting in a radio pulse with a certain frequency, he can cause the desired area to resonate. By doing so one can select a specific slice of the body. The local magnetic gradient is homogeneous in that slice, meaning that all of the net magnetic moments will be indistinguishable and spinning together in phase in that slice. To further localise the magnetic moments and their associated signal strength, two more gradient coils are used.

The first gradient is called the phase encoding gradient. Once the phase encoding gradient is turned on, it creates a gradient along the y-axis whereby the resulting magnetic moments at the bottom of the gradient slow down while the ones at the top speed up. The grading is then quickly turned off in order to let the spinning magnetic moments return to their original base frequency. The resulting magnetic moments are spinning at the same rate, yet all have now experienced a phase shift in the y-axis. Meaning that magnetic moments spinning along the x-direction are in phase with each other as they happen to be at the same y-value.

The third gradient is the frequency encoding gradient. This gradient causes the spins to the right to slow down and the ones on the left to speed up i.e. it basically distinguishes between spins along the x-direction. This frequency encoding gradient remains on while the signals are recorded.

After applying this whole process to all the ‘slices’ of the body it can be said that each of the signals received by the receiver coils has a unique phase and frequency which can be localized to unique points in 3D space. Each of these squares or boxes associated with this 3D space is then assigned a grey-scale value corresponding to the local assigned signal. By convention white represents a strong signal while black corresponds to no signal at all. MR images are made up of a series of voxels or volume elements. Each square on the picture corresponds to a volume of tissue on the body. The MR machine is built to measure the NMR signal from each of these small volumes, localize them in 3D space and plot them on a 256 by 256 or 512 by 512 matrix to make a visible picture [17, 22].

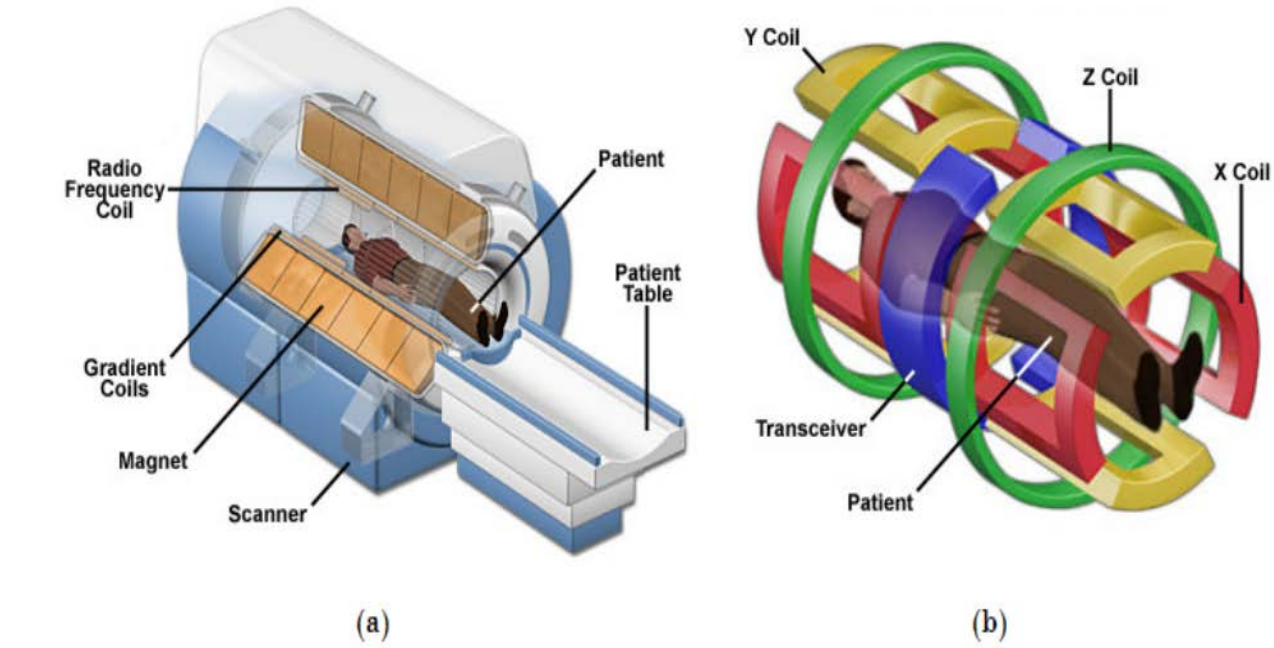


Figure I.17: (a) MRI Scanner Cutaway (b) MRI Scanner Gradient Magnets

### II.2.2.5 The use of MRI Techniques

The radiofrequency energy is affected the nuclei in the human body when it is at the strong magnetic field then it releases at the relaxation period. The image is converted by the emitted energy single which is released from the excited tissue over a short period at 2 relaxations as known as T1 and T2 as explained Before. The contrasts in the images result from different intensities of these emitted signals, which in turn result from different concentrations of the nuclei in different tissues in the body. Therefore, the MRI techniques are used as below:

- T1-weighted imaging (T1-W1). This technique is used low signal intensity from cerebrospinal fluid (CSF) on the brain tissues.
- T2-weighted imaging (T2-W2). This technique is used high signal intensity from cerebrospinal fluid (CSF) on the brain tissues.
- Spin density-weighted imaging. This technique applies when the signal density has similarity to the cerebrospinal fluid.
- Gradient echo imaging. This technique has the highest sensitivity to detect early hemorrhagic changes.

- Diffusion-weighted imaging (DWI). This uses to detect the image which reflects the microscopic random motion of water molecules.
- Perfusion-weighted imaging (PWI). This uses to study the movement of hemodynamic which is blood movement on the brain tissues through MR contrast material.
- Proton density-weighted (PDW) is provided good contrast between gray-bright and white-darker with brain and cerebrospinal fluid.

#### II.2.2.6 Role of MRI in Radiotherapy

Currently, MRI is used in the preparation of conformal external radiotherapy treatment plans only in conjunction with computed tomography. The joint use of these two methods involves image registration (or fusion). A lot of research is currently in progress in order to use the RM images alone for the planning of an RT treatment, more details will be shown on Chapter III.

## III. Linear Accelerator

A medical linear accelerator (Figure I.18) is a system which uses electromagnetic waves of high frequencies, close to 3000 MHz, with the aim of accelerating electrons to energies of the order of 25 MeV through a linear tube. Medical accelerators offer possibilities of treatment in electrons or photons, depending on the patient's situation. The resulting electron beam can either be used, after passing through lead diffusers, to treat superficial lesions, or hit a dense metal target (tungsten) thus producing X-rays s , which can treat deeper tumors. Electrons are emitted from a tungsten plate heated by a spiral filament of an electron gun. They are torn in great numbers then injected into a succession of cavities where very high magnetic fields prevail created by a high frequency wave 3000 MHz so that the electrons become faster and faster as they pass through the cavities. The voltages required to operate these assemblies are produced in pulsed form, which is called a modulator [23].

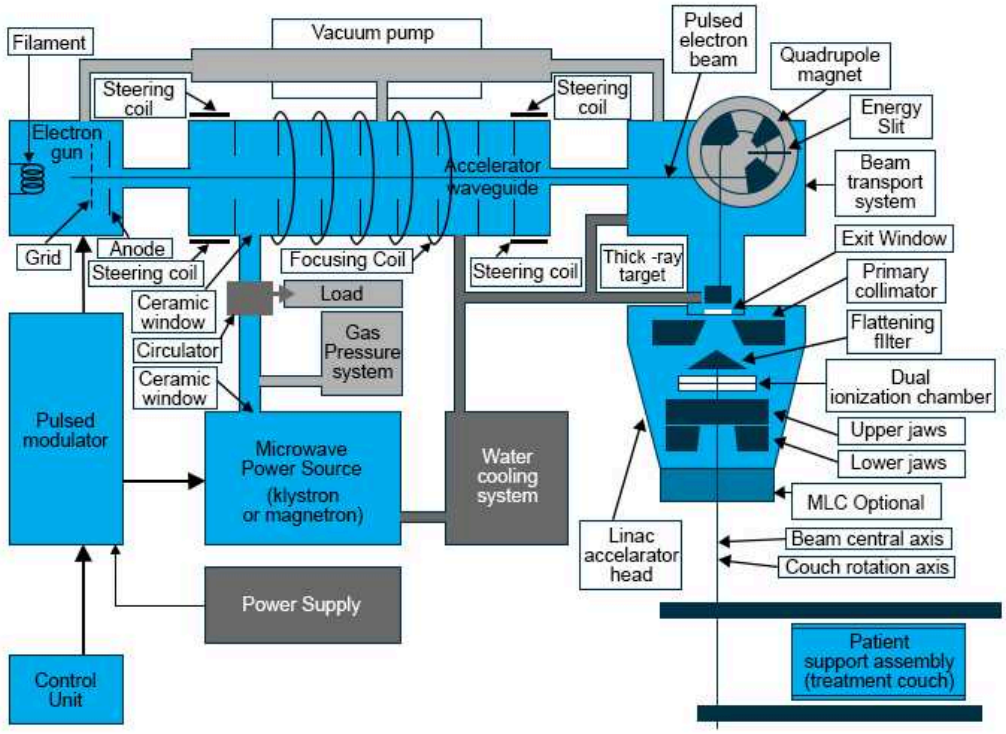


Figure I.18: Linear accelerator components

Once the electrons have accelerated, they are guided by an intense magnetic field towards the target. This tungsten target is interposed in the electron beam to create photons (X-rays s ) with an energy of 6 to 25 MeV [5, 6, 23].

In electron mode as in photon mode, the objective is to produce beams well directed towards the patient and well calibrated in order to meet medical prescription and dosimetry, but the production of radiation is accompanied by multidirectional radiation with good unwanted part. A collimator system directs the useful radiation towards the patient and absorbs the rest. The collimator delimits the beam first thanks to a fixed pyramidal architecture then thanks to two pairs of movable jaws allowing to achieve the desired dimensions for the irradiation.

The movable jaws constitute square or rectangular fields, symmetrical or not, depending on their position relative to the beam axis. The rotation of the collimator expresses in degrees from 0° to 360 ° clockwise. The opening of the collimator is noted X for one side and Y for the other which are respectively declined in X1, X2 for the width and Y1, Y2 for the length of the field which can be reversed according to the manufacturers. This opening determines the dimensions of the irradiation field at the iso-center. For more performance, manufacturers have developed collimators with blades (MLC), focused and controlled allowing to give the fields complex shapes which are adapted to the shape of the tumor and are more precisely the area to be irradiated. The blades are distributed on two opposite sides, they allow to integrate the protections necessary for the treatment [5, 6, 23].

The homogeneity of the beam produced is ensured by an equalizing cone placed on the beam path, Indeed, after the target, the beam comprises in its center more energetic photons therefore more penetrating, which is not satisfactory from a dosimetric point of view. . The presence of the cone in the beam will have a decreasing attenuation of the photons, from the axis towards the edges.

The medical use of accelerators obviously requires controls, especially at the exit of the beams, before they reach the patient. Different devices of dies and adjustments make it possible to define the energy of the electrons at the exit of the beams of treatment (electrons or photons) in order to ensure the quality of the beams. Two flat ionization chambers, placed before the collimator exit, measure the dose, regulate the dose rate, and control the homogeneity and symmetry of the beams. The set of two chambers constitutes what is commonly called a "monitor". They provide instant control of the dose delivered and stop irradiation when the prescribed dose is reached.

The manufacturers offer ergonomic devices (the stand and the treatment table): the stand consists of the arm of the device, which has at one end the accelerating section with the radiogen head, the collimator and the imaging system. The accelerator arm is a rotating structure that rotates around a horizontal axis located a fixed distance of 100 cm from the beam source. The movement of the arm is motorized with an angle of 180° on either side of the axis. The arm rotation parameter is also expressed in degrees from 0° to 360 ° clockwise.

# CHAPTER II:

## Image Registration and Data Fusion in Radiotherapy: Evaluation Metrics

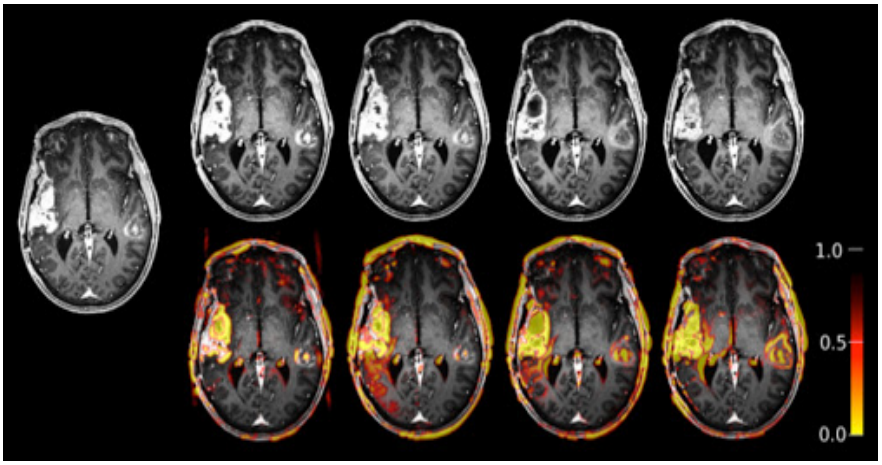

# I. Image

## I.1 What is an image?

Image is a representation of a person or an object through painting, drawing, photography, film, etc. It is also a structured set of information which after being displayed on the screen, has meaning for the human eye. It can be described in the form of a continuous analog function i (x, y), defined in a bounded domain, such that x and y are the spatial coordinates of a point in the image and i is a function of light intensity and color. In this aspect, the image is unusable by the machine, which requires its digitization. [24]

## I.2 Digital image

The digital image is the image whose surface is divided into elements of fixed size called cells or pixels, each having as characteristic a level of gray or colors. Digitizing an image is the conversion of the image from its analog state into a digital image represented by a two-dimensional matrix of digital values f (x, y), where: x, y Cartesian coordinates of a point in the image. F (x, y): intensity level, the value at each point expresses the measurement of light intensity perceived by the sensor [24].

### I.2.1 Characteristics of a digital image

As we have seen, the image is a structured set of information among its characteristics; we can cite the following parameters.

#### I.2.1.1 Pixel

Contraction of "Picture elements": the pixel is the smallest point of the image; it is a numerical value representative of the light intensities. If the bit is the smallest unit of information that a computer can process, the pixel is the smallest element that hardware and software can manipulate in the image. The Smiley, for example, can be displayed as a group of pixels in Figure II.1 [24,25].

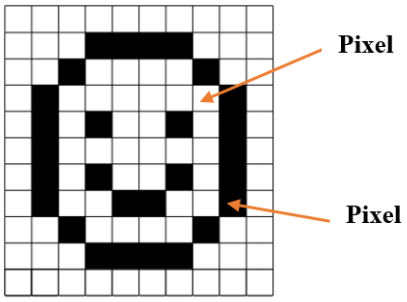


Figure II.1: displayed Smiley as a group of pixels

### I.2.1.2 Image resolution

The resolution of an image corresponds to the level of detail that will be represented on this image. This is the number of pixels per unit length in the image to be scanned. It is in dpi (dots per inch). The higher the number of pixels per unit length, the more information that describes the image and the higher is the resolution as showed on the figure II.2. [24,25]

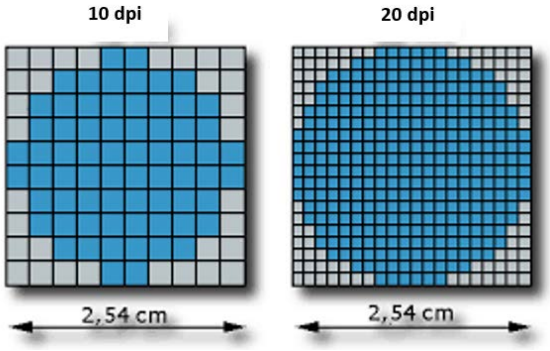


Figure II.2: Differences between 10 dpi and 20 dpi resolution of a geometrical object

### I.2.1.3 Noise in an image

A noise (parasite) in an image is considered as a phenomenon of sudden variation of the intensity of a pixel compared to its neighbors, it comes from the lighting of the optical and electronic devices of the sensor [24,25].

#### I.2.1.4 Edges and textures

The edges represent the border between the objects in the image, or the boundary between two pixels whose gray levels represent a significant difference. The textures describe the structure of these. Contour extraction consists in identifying in the image the points that separate two different textures [25].

### I.2.2 Digital image types

There are three types of images:

- Binary: two colors (background and foreground).
- Monochrome or gray scale: variation of the same shade.
- Full color: true colors [25].

#### I.2.2.1 Binary image

Binary images (Figure II.3) are the simplest. Bi-chromes (whose pixels can only have the values 0 and 1). The 0 corresponds to a black pixel and 1 to a white pixel. The gray level is therefore coded on a single bit [25].

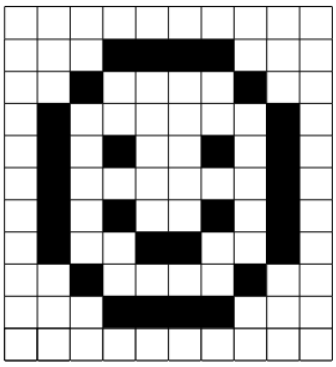

Figure II.3: Binary images (in black and white)

#### I.2.2.2 Grayscale image

The gray level is the value of the light intensity at a point. The pixel color can take values ranging from black to white through a finite number of intermediate levels. Therefore, to represent grayscale images, we can assign each pixel of the image a value corresponding to the amount of light returned. This value can be for example between 0 and 255 (figure II.4) [25].

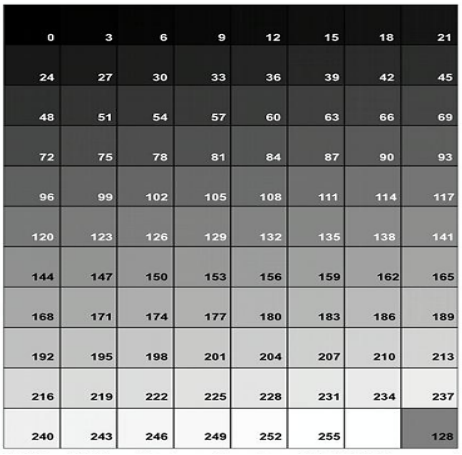


Figure II.4: Gray scale images (monochrome)

### I.2.2.3 Color images

It is obtained by the combination of three so-called primary colors: red, green and blue (RGB) (Figure II.5). Each color is coded as a grayscale image, with values ranging from 0 to 255. For R = G = B = 0 we will have pure black, and for R = G = B = 255 we will have pure white. The representation of color images is therefore done either by an image whose pixel value is a linear combination of the values of the three colors components, or by three distinct images each representing a color component, there are generally two types of images [25]:

- ✓ 24-bit images.
- ✓ Palette images.

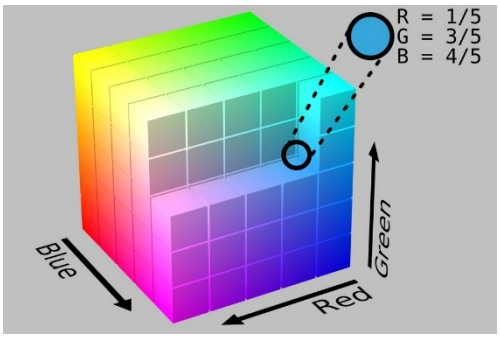


Figure II.5: Polychrome image

### I.2.3 Digital image processing

Image processing can be defined as all the methods and techniques operating on the image in order to extract the most relevant information or simply to provide an image more perceptible to the human eye. In this chapter, we talked about Registration, Fusion and evaluation techniques. Before some basic notions about the image must be understood.

## II. Image registration

The registration of medical images is a geometric process used in medical imaging to align two different images in order to provide additional information necessary to make a diagnosis and plan a treatment [26, 27]. It consists of a set of spatial transformations (translation, rotation, scaling, sampling ...) applied to a target (moving) image so that it is aligned with a reference image (source) (figure II.6). In mathematical terms, image registration is defined as the adequate displacement U (x) that must be applied to an image so that it is in the same space as the second image, while minimizing the cost of the transformation. It is done according to the following general formula:

$$\min f(I1, t(I2)), \text{ with } t \in T \qquad \text{(II.1)}$$

with :

- I1 and I2 images to be registred,
- t: transformation,
-f: criterion of dissimilarity (min) or similarity (max),
- T : set of possible transformations.

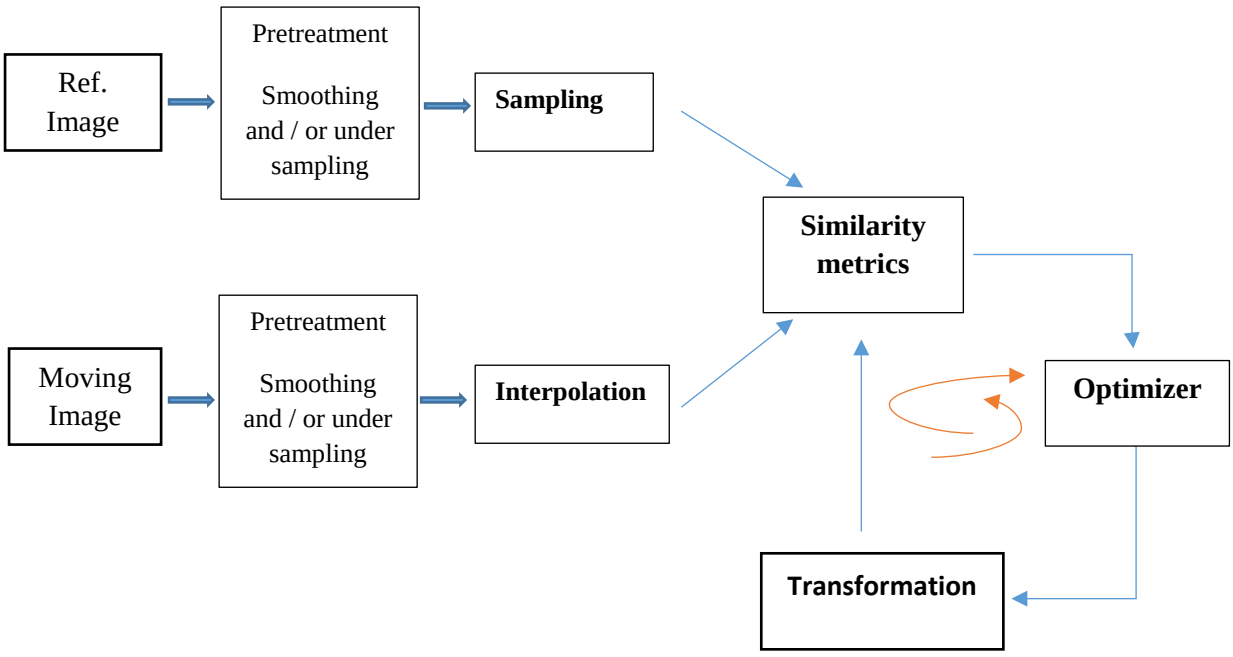


Figure II.6: Scheme representing main image registration steps.

## II.1 Objectives and criteria for image registration

Image registration is an important tool in the field of medical imaging. In many clinical cases, several images of a patient are taken in order to analyze his situation. These images are acquired by different imaging techniques (example: computed tomography, magnetic resonance imaging, nuclear medicine.) Which provide information on the subject's anatomy [27]. The combination of mono- or multimodal information often gives additional clinical information not apparent in the separate images. To perform a registration several parameters need to be taken into account that are summarized in Figure II.6.

## II.2 Registration principle

Two images are involved in the alignment process. The first image is the target image (moving image) IM which is distorted to adapt to the second image, the fixed image IF (x). Fixed and moving images are of different or similar dimensions, but are each defined on their own spatial domain. The transformation is defined as a mapping from the fixed image to the moving image, in order to achieve this alignment, several factors are to be taken into account, to do this, four questions must be asked and understood [28-30] :

- Which information to match?
- Which criterion of similarity to choose?
- Which model of transformation?
- Which optimization strategy?

In the rest of this chapter we will answer the four questions by giving different examples. [26, 31]

### II.2.1 Which information to match?

Information's to match are also called attributes, they are represented by extracted characteristics from the images, this attributes guide the registration and are generally divided into two groups:

- Intrinsic attributes: are the information from the image (gray levels, geometric primitives, shapes, surface, curves, etc.).

- Extrinsic attributes: external markers fixed on the subject.

### II.2.2 Which criterion of similarity to choose?

In mathematics and computer science, similarity is an important criterion for the identification of subgroups in a group of objects. From a mathematical point of view, it is by the differences in distance between two data that we measure their degree of similarity. Several choices for the similarity criterion can be found in the literature. Some common choices are described below [26, 28].

#### II.2.2.1 Mean Squared Displacement

In statistical mechanics, the mean squared displacement (MSD, also mean square displacement, average squared displacement, or mean square fluctuation) is a measure of the deviation of the position of a particle with respect to a reference position over time.

The MSD is defined by the following equation

$$MSD(\mu, I_F, I_M) = \frac{1}{|\Omega_F|} \sum_{xi \in \Omega_F} (I_F\ (\text{xi}) - (T_\mu(x_i)))^2 \qquad \text{(II.2)}$$

With $\Omega_F$ the domain of the fixed image $I_F$, and | $F$ | the number of voxels. Given a transformation T, this measurement can easily be implemented by looping the voxels in the fixed image, taking $I_F\ (x_i)$ and calculating $T_\mu\ (x_i)$ by interpolation, and adding the difference squared to the sum.

#### II.2.2.2 Normalized cross-correlation

In probability and statistics, studying the correlation between two or more random variables or numerical statistics is studying the intensity of the link that can exist between these variables, it is defined by:

$$\text{NCC}(\mu;\ I_F, I_M) = \frac{\sum_{xi \in \Omega_F}(I_F(x_i)-\overline{I_F})(I_M(T_\mu(x_i)-\overline{I_M})}{\sqrt{\sum_{xi \in \Omega_F}(I_F(x_i)-\overline{I_F})^2\ \sum_{xi \in \Omega_F}(I_M(T_\mu(x_i)-\overline{I_M})^2}}\ , \qquad \text{(II.3)}$$

$$\text{with: } \overline{I_F} = \frac{1}{|\Omega_F|}\sum_{xi \in \Omega_F} I_F\ (x_i) \text{ et } \overline{I_M} = \frac{1}{|\Omega_F|}\sum_{xi \in \Omega_F} I_M(T_\mu(x_i)$$

#### II.2.2.3 Mutual information

In probability theory and information theory, the Mutual Information (MI) of two random variables is a measure of the mutual dependence between the two variables. More

specifically, it quantifies the "amount of information" obtained about one random variable through observing the other random variable.

$$MI(\mu, I_F, I_M) = \sum_{m \in L_M} \sum_{f \in L_F} p(f, m, \mu) log_2 \left( \frac{p(f,m,\mu)}{p_F(f) p_M(m,\mu)} \right) \quad \text{(II.4)}$$

Where: $L_F$ and $L_M$ are sets of regularly spaced cubes of intensity, p is the discrete joint probability, and $p_F$ and $p_M$ are the marginal discrete probabilities of the fixed and moving image, obtained by summing p over m and f, respectively.

- MI = 0: the two images are independent.

- More MI increases, more images share Information's (so the two images are better readjusted). There are several other similarity criteria such as: Standard mutual information? Kappa's statistic witch are not defined on this chapter.

### II.2.3 Which model of transformation?

Geometric transformation (or deformation model): is the way witch the image is geometrically modified. The transformation can be local or global; a certain number of parameters represented by μ characterizes it [26, 28].

#### II.2.3.1 Linear Transformation

By definition, linear transformation models affect the whole of space. It's the simplest and most classic method. It combines rotation and translation. In a purely mechanical framework, the objects to be readjusted are rigid, and on the other hand, the images to be readjusted have the same spatial resolution. This transformation preserves the distances between the points of the object. This method is relatively simple to set up, but the domain where it is valid is relatively small. This can be the case in non-destructive testing where the objects do not undergo deformation, and where the images have the same spatial resolution.

The linear transformation are represented by several transformations, which are:

##### II.2.3.1.1 Transformation by Translation

In geometry, a translation is a geometric transformation which corresponds to the idea of dragging an object, without rotation, reversal or deformation of this object. In classical geometry, the notion of translation is very strongly linked to that of vector that the object follows from a point A to a point B (Figure II.7).

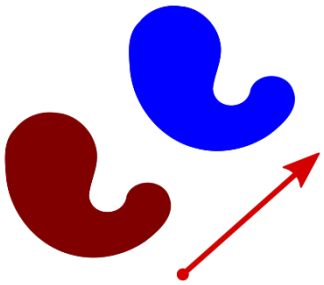

Figure II.7: Transformation of an object by translation

The translation is defined by the following mathematical equation:

$$T_{\mu}(x) = x + t \tag{II.5}$$

With t the translation vector, in this case the transformation parameters are defined as μ = t.

#### II.2.3.1.2 Rigid transformation

In mathematics, a rigid transformation (also called Euclidean transformation) is a geometric transformation, which preserves the Euclidean distance between each pair of points. Rigid transformations include rotations, translations or their combination. (Figure II.8)

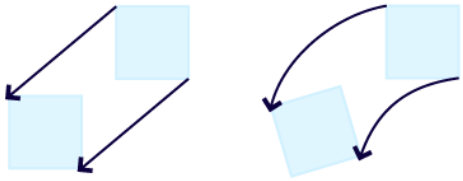

Figure II.8: Rigid transformation of an object by translation

It is defined by the following equation:

$$T_{\mu}(x) = Rx + b \tag{II.6}$$

Where R is the rotation matrix and b the translation vector. Alternatively, a rigid transformation is often written as a pullback transformation, i.e.:

$$h(y) = T^{-1}(y) = R^{-1}(y - b) = R^{*}y + b^{*} \tag{II.7}$$

Where $R^* = R^{-1}$ is a rotation matrix and $b = -R^{-1} b$ is a translation vector.

To simplify things, we will work with the push forward transformation. In 2D, R may be written as:

$$R = \begin{bmatrix} \cos\theta & -\sin\theta \\ \sin\theta & \cos\theta \end{bmatrix} \quad \text{(II.8)}$$

Where θ is the rotation angle about the origin. In 3D, there are three axes of rotation. Thus, one possible parametrization of a rotation matrix is $R = Rz(\gamma)\, Ry(\beta)\, Rx(\alpha)$, where

$$R_x = \begin{bmatrix} 1 & 0 & 0 \\ 0 & \cos\alpha & -\sin\alpha \\ 0 & \sin\alpha & \cos\alpha \end{bmatrix} \quad \text{(II.9)}$$

$$R_y = \begin{bmatrix} \cos\beta & 0 & \sin\beta \\ 0 & 1 & 0 \\ -\sin\beta & 0 & \cos\beta \end{bmatrix} \quad \text{(II.10)}$$

$$R_z = \begin{bmatrix} \cos\gamma & -\sin\gamma & 0 \\ \sin\gamma & \cos\gamma 1 & 0 \\ 0 & 0 & 1 \end{bmatrix} \quad \text{(II.11)}$$

R is rotation matrices along the x, y and z-axis with rotation angles α, β and γ, respectively. Note that the order of rotation (in other words, the order of matrix multiplication) is important. Changing the order rotation gives a different parametrization of the rotation matrix.

Rigid transformations are useful for registering intra-patient data scanned with the same scanner with same spatial settings, since the type of motion introduced for such a dataset usually only involves translation and rotation. Due to the small number of parameters, rigid registration algorithms are extremely fast to compute and are often used for real-time registration. Rigid transformation is customarily used to align the image pair (e.g., alignment of AC-PC points in brain MR image pair) prior

#### II.2.3.1.3 Similarity transformation

A similarity transformation is one or more rigid transformations (reflection, rotation, translation) followed by a dilation. When a figure is transformed by a similarity transformation, an image is created that is similar to the original figure. In other words, two figures are similar

if a similarity transformation will carry the first figure to the second figure [26,28]. In Figure II.9, trapezoid ABCD has been reflected, then rotated, and then dilated with a scale factor of 2. The first three trapezoids are all congruent. The final trapezoid is similar to each of the first three trapezoids.

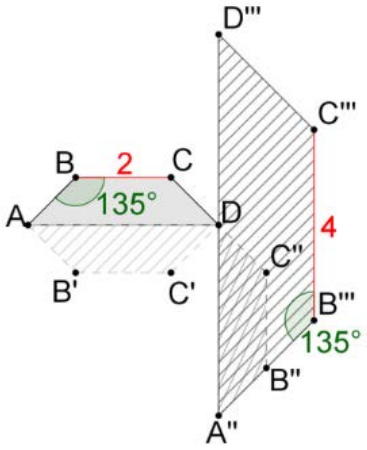


Figure II.9: Similarity transformation with 3 parameters (Reflected, Rotation, Dilatation)

Mathematically it is defined by the following equation:

$$T_x(x) = sR(x - c) + t \tag{II.12}$$

Where s is a scalar relative to scaling and R is the rotation matrix with a center c. the rotation matrix is defined by an angle in 2D which gives a transformation parameters with 4 parameters μ = (s, θz, tx, ty), and with a vector of parameters of 7 in 3D.

#### II.2.3.1.4 Affine transformation

Affine transformation is a linear mapping method that preserves points, straight lines, and planes. Sets of parallel lines remain parallel after an affine transformation.

The affine transformation technique is typically used to correct for geometric distortions or deformations that occur with non-ideal camera angles. For example, satellite imagery uses affine transformations to correct for wide angle lens distortion, panorama stitching, and image registration. Transforming and fusing the images to a large, flat coordinate system is desirable to eliminate distortion. This enables easier interactions and calculations that don't require accounting for image distortion.

Table II.1 and Figure II.10 illustrates the different affine transformations: translation, scale, shear, and rotation.

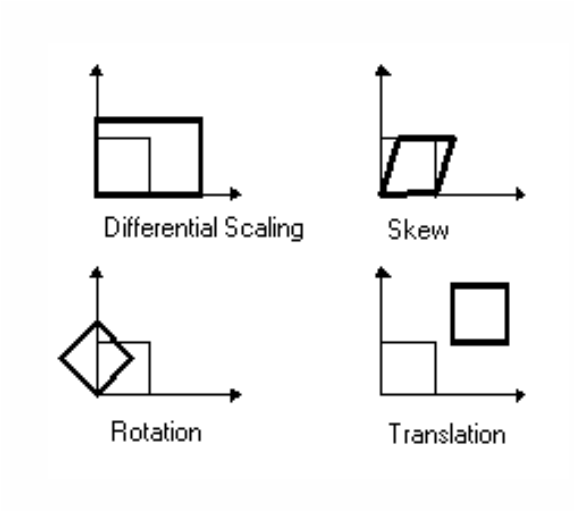


Figure II.10: Parameters of an affine transformation

Table II.1: Parameters of an affine transformation

| Affine Transform | Example | Transformation Matrix | |
|---|---|---|---|
| Translation |  | $\begin{bmatrix} 1 & 0 & 0 \\ 0 & 1 & 0 \\ t_x & t_y & 1 \end{bmatrix}$ | $t_x$ specifies the displacement along the $x$ axis<br>$t_y$ specifies the displacement along the $y$ axis. |
| Scale |  | $\begin{bmatrix} s_x & 0 & 0 \\ 0 & s_y & 0 \\ 0 & 0 & 1 \end{bmatrix}$ | $s_x$ specifies the scale factor along the $x$ axis<br>$s_y$ specifies the scale factor along the $y$ axis. |
| Shear |  | $\begin{bmatrix} 1 & sh_y & 0 \\ sh_x & 1 & 0 \\ 0 & 0 & 1 \end{bmatrix}$ | $sh_x$ specifies the shear factor along the $x$ axis<br>$sh_y$ specifies the shear factor along the $y$ axis. |
| Rotation |  | $\begin{bmatrix} \cos(q) & \sin(q) & 0 \\ -\sin(q) & \cos(q) & 0 \\ 0 & 0 & 1 \end{bmatrix}$ | $q$ specifies the angle of rotation. |

Mathematically it is defined by the following equation:

$$T_x(x) = A(x - c) + t + c \tag{II.13}$$

Where A is an unrestricted matrix, its application on the image can be a translation, rotation, scaling or stretching, The transformation parameter μ is defined by 6 components in 2D, i.e. a21, a22, tx, ty) T. In 3D, this gives a vector of length 12.

### II.2.3.2 Non Linear transformation

The transformation can also be non-linear (Figure II.11). It is then of a higher order, for example thin-plate splines, combinations of B-Splines, etc. In the image processing literature, these transformations can also be called elastic, deformable or even non-rigid [26,32].

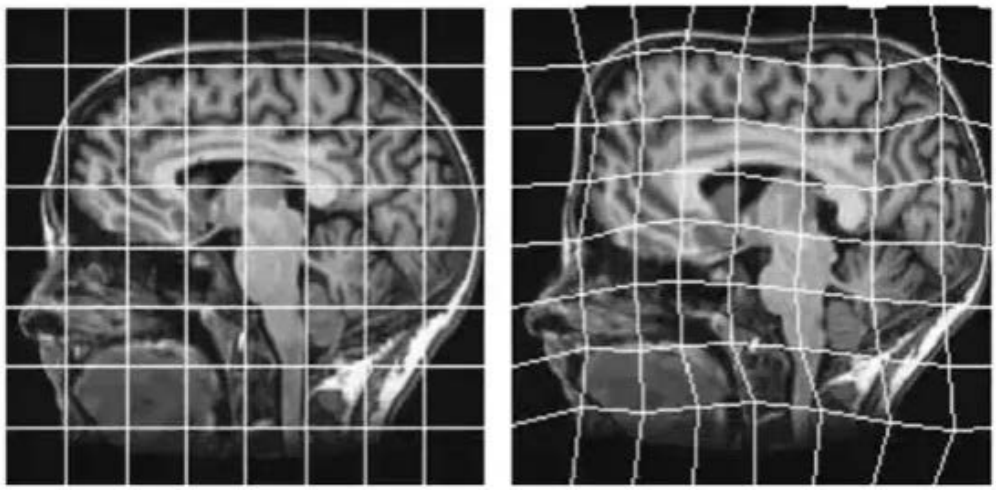

Figure II.11: Non-Rigid transformation of medical Image

Clearly most of the human body does not conform to a rigid or even an affine approximation and much of the most interesting work in registration today involves the development of non-rigid registration techniques for applications ranging from modeling tissue deformations to variability in anatomical structures. Non Rigid registration remains a challenging research problem due to its smoothness requirement and high degree of freedoms in the deformation process. Numerous algorithms have emerged to nonlinearly register medical images to one another. They require a great deal of computation time, which is a major drawback for many clinical applications, accordingly how to improve the precision and how to increase the speed and how to evaluate the registered results need further research. Many algorithms where coded and some of them are shown below:

#### II.2.3.6.1 Spline

One of the most important non linear transformations is the family of splines that have been used in various forms for around 15 years . Many registration techniques using splines are based on the assumption that a set of corresponding points or landmarks can be identified in the source and target images. Spline-based registration algorithms use corresponding control points, in the source and target image and a spline function to define correspondences away from these points. The thin- plat spline has been used extensively to investigate subtle morphometric variation in schizophrenia. Each control point belonging to a thin-plate spline has a global influence on the transformation in that, if its position is perturbed, all other points in the transformed image change. This can be a disadvantage because it limits the ability to model complex and localized deformations and because, as the number of control points increases, the computational cost associated with moving a single point rises steeply. By contrast, B-splines are only defined in the vicinity of each control point; perturbing the position of one control point, only affects the transformation in the neighborhood of the point. Because of this property, B-splines are often referred to as having „„local support"". B-spline based non-rigid registration techniques are popular due to their general applicability, transparency and computational efficiency. Their main disadvantage is that special measures are sometimes required to prevent folding of the deformation field and these measures become more difficult to enforce at finer resolutions. Such problems have not prevented these techniques finding widespread use in the brain, the chest the heart, the liver, the breast, etc [26,32].

#### II.2.3.6.2 Fluid Registration

Registration based on elastic transformations is limited by the fact that highly localized deformations cannot be modeled, since the deformation energy caused by stress increases proportionally with the strength of the deformation. In fluid registration, these constraints are relaxed over time, which enables the modeling of highly localized deformations including corners. This makes fluid registration especially attractive for inter subject registration tasks (including atlas matching) which have to accommodate large deformations and large degrees of variability. At the same time the scope for miss registration increases, as fluid transformations have a vast number of degrees of freedom replacing the elastic model by a viscous fluid model allows large and highly localized deformations. The higher flexibility increases the opportunity for miss registration, generally involving the growth of one region instead of shifting or distorting another.

#### II.2.3.6.3 Demons Algorithms

Researchers proposed another non-rigid technique, the “demons” algorithm which can be thought of as an approximation to fluid registration. The main limitations of the demons algorithm are that it does not provide diffeomorphic transformations. More recently, the “demons” optical flow based non rigid registration algorithm has been used to quantify change in volume of brain structures over time and to quantify the difference in volume of brain structures. It requires a great deal of computation time, which is a major drawback for many clinical applications, accordingly improving the precision ,speed and evaluating the registered results need further research [26,32].

### II.2.4 Which optimization strategy?

The optimization strategy is a method which determine the best transformation depending of a certain cost function. The optimization process change the parameters of the transformation model according to a certain similarity criterion in order to maximize the degree of correspondence. In general, four categories of optimization methods can be distinguished [26,28]:

#### II.2.4.1 Direct methods

These methods are possible when the number of parameters to be estimated is small. The estimation of a rigid or affine transformation between two images from punctual landmarks, by minimizing the sum of the square of the errors on the set of points, admits an analytical solution. As well, the non-rigid registration problem can be formulated by a "least squares" problem.

#### II.2.4.2 Exhaustive methods

They consist of sampling the entire parameter space at regular intervals and choosing the optimal solution. Although they allow access to the minimum value with an accuracy defined by the sampling step, they are, in practice, rarely used because too costly in computation time.

#### II.2.4.3 Iterative numerical methods

These methods are considered when the cost function to be minimized is a non-linear function of the parameters to be optimized. They are based on the calculation of the gradient of the cost function (gradient descent or conjugate gradient descent), this gradient method

therefore consists in using the direction given by the gradient as the direction in which tests will be made to find a point where mutual information is optimum.

#### II.2.4.4 Stochastic methods

These algorithms are the main optimization methods used in the context of registration, which theoretically guarantee convergence towards the minimum value. The use of these methods is mainly restricted to the setting of rigid or affine registration given their low speed of convergence.

## III. Images fusion

Merging information is the step following registration; it consists of combining information from several sources to improve decision-making. To do this, the information must be heterogeneous, that is to say that the sensors must be either of a different nature or of the same nature but used under different conditions, in order to provide additional information [33].

The use of the data must be joint, that is to say that a process leading to a separate decision-making from each dataset, without a global decision, cannot be considered as a merging process. In addition, the purpose of the fusion is to provide decision support.

Technically, Fusion is a method of viewing two images that are already aligned and allows seeing all information of one modality, or to see them at the same time, the choices of transparency of one of the images or on the other, allows the doctor to make a good diagnosis and provides him with the necessary information [33, 34].

### III.1 Historical aspect

The idea of combining images between them arose from the multiplication of imaging methods in many fields of application. First, the purpose of this combination is to match the images, in order to express the coordinates of the different images to be combined in the same repository. This is called the registration or matching phase. This allows you to accurately compare the different images, which are not necessarily taken from the same angle of view. This phase is essential in order to be able to jointly use the information coming from the different images [33, 34].

### III.2 Fusion methods

The Fusion methods of medical image are divided on three aspects, the fusion method based on spatial domain, the fusion method based on transform domain, and the fusion method based on deep learning.

#### III.2.1 Spatial domain

The medical image fusion technology based on spatial domain is the hot topic in early research. Its fusion technology is simple, and the fusion rules can be directly applied to the source image pixels to obtain the merged image. The fusion methods of spatial domain include the high-pass filtering method, the principal component analysis method, the saturation method of hue intensity, the average method, the maximum selection method, the minimum selection method,

and the Brovey method. Due to the spectral distortion and spatial distortion in the fused image of the spatial domain, the heat of research in the spatial domain of the medical image fusion method is gradually decreasing in recent years. Researchers often use spatial domain fusion strategies as a part of the transformation domain to form new research methods.

#### III.2.1.1 Fusion Method Based on IHS Domain

The model proposed by an American scientist Munsell explains the characteristics of the human visual system. It has two characteristics: (1) the intensity component has nothing to do with the color information of the image; (2) hue and saturation components are closely related to the way people perceive color. Therefore, researchers often use this model to solve the color problem in the image fusion process, especially the fusion of PET/SPECT images with color information. Chen [35] combined the IHS model with Log-Gabor transform to propose a new method about the fusion of MRI and PET and decomposed the PET image with IHS to obtain the three basic characteristics of hue (H), saturation (S), and intensity (I). The component intensity represents the brightness of the image, so the intensity components of the MRI and PET images are decomposed by the LogGabor transform consisting of the logarithmic transformation of the Gabor filter to obtain the high-frequency sub-bands and the low-frequency sub-bands. Fusion of high frequency sub-bands comes with maximum selection; fusion of low-frequency sub-bands comes with a new method based on two-level fusion of visibility measurement and weighted average rule. The inverse Log-Gabor transformed component and the original hue and saturation components are inversely HIS to obtain a fused image. It can effectively preserve the structures and details of the source image and reduce the color distortion. This method is superior to the existing IHS+FT method in visual perception. Haddadpour et al. [36] proposed a new fusion method which combining the IHS method with the two-dimensional Hilbert transform. The method [37] introduces the concept of BEMD when merging high- and low-frequency subbands. BEMD is called bidirectional empirical mode decomposition and is extended by empirical mode decomposition. It is widely used in biomedicine field because of its envelope surface. The algorithm has no obvious distortion and is superior to the wavelet algorithms in terms of contrast and color intensity. Its disadvantage is that the information entropy (EN) is relatively low. Figure II.12 shows the framework of the IHS domain fusion method based on the fusion of MRI and PET images. In order to achieve better results, different researchers tend to study the decomposition transform, such as DST and Log-Gabor transform. And they study fusion algorithm about the decomposition transform, such as SR algorithm and maximum selection algorithm.

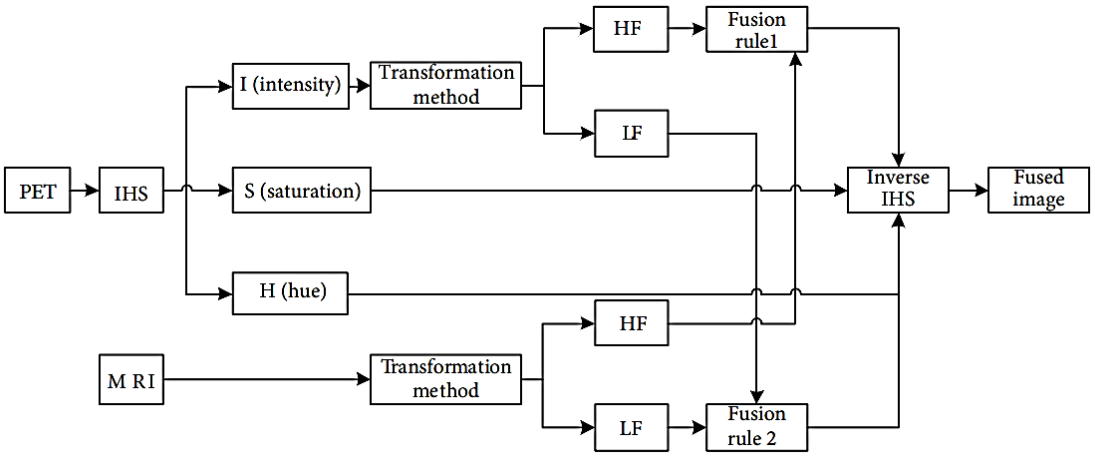


Figure II.12: Fusion Method Based on IHS Domain

### III.2.2 Transform Domain

The medical image fusion methods of the transform domain are mostly based on the multiscale transform (MST) theory, and they are also the hotspots of research in recent years. The MST-based fusion method is generally divided into three steps: decomposition, fusion, and reconstruction. The medical image fusion method based on transform domain is transforming the source image from time domain to frequency domain or other domains to obtain the low-frequency coefficient and high-frequency coefficient. This section focuses on three most commonly used transformations in medical image fusion methods: nonsubsampled contourlet transform, nonsubsampled shearlet transform, and discrete wavelet transform.

#### III.2.2.1 Fusion Based on Nonsubsampled Contourlet Transform (NCT)

The contourlet transform is multiscale which is proposed by Do et al. [38]. It is suitable for constructing multiresolution and multidirectional situations and has advantages in smoothness processing. However, it does not have translation invariance, and it is easy to generate pseudo-Gibbs phenomenon (artifact) near the singular point of the reconstructed image, resulting in image distortion, so it is not the best choice for image fusion method. To this end, many researchers have done more in-depth research. After contourlet transform, Cunha et al. [39] proposed a multiscale decomposition method superior to contourlet transform, which is an improvement of contourlet transform, called nonsubsampled contourlet transform. NSCT has the characteristics of translation invariance and avoiding spectral aliasing. The

structural information of the source image is preserved in the decomposition and reconstruction, and the direction information can be better extracted. Nonsub sampled contourlet transform is one of methods widely used in medical image fusion of transform domain in recent years. Firstly, the source image is decomposed by NSCT to obtain the coarse layer and the detailed layer, and then, The multiscale and multidirectional decompositions are calculated by NSPFB and NSDFB filters to obtain subband images with different scales and directions.

Finally, the image is inverse NSCT to obtain a fused image. A block diagram of the NSCT-based fusion method is shown in Figure II.13.

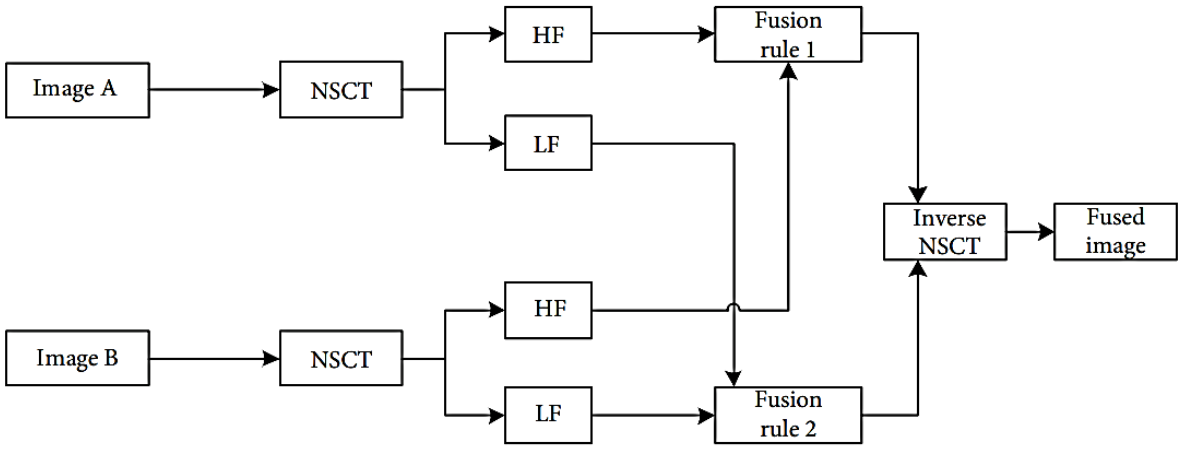


Figure II.13: Fusion based on Nonsubsampled Contourlet Transform (NSCT)

**III.2.2.2 Fusion Method Based on Nonsubsampled Shearlet Transform (NSST) Domain**

In 2005, the tool shearlet proposed by Labate et al. [40] has multiscale, directional, and other characteristic but does not have translation invariance. Until 2007, Easley et al. [41] proposed a nonsubsampled shearlet transform, which solves the problem of translation invariance on the basis of retaining the directivity of shearlets. NSST consists of a Nonsubsampled Laplacian Pyramid (NSLP) and Multiple Shear Filters. The source image is decomposed into high-frequency components and lowfrequency components by NSLP, and then, the direction filter is used to process different subbands and coefficients in different

directions, among which the low-frequency subband is iterative decomposition. Directional filtering is performed using a shear matrix, so it has a strong directivity. As shown in Figure II.14, when the decomposition level is m = 3, the image is decomposed into four subbands with m +1=4, the size of which is the same as that of the source image, thus ensuring the invariance of displacement [42]. Compared with NSCT, NSST has higher sensitivity and lower computational complexity, while overcoming the limitations of components with a certain number of directions.

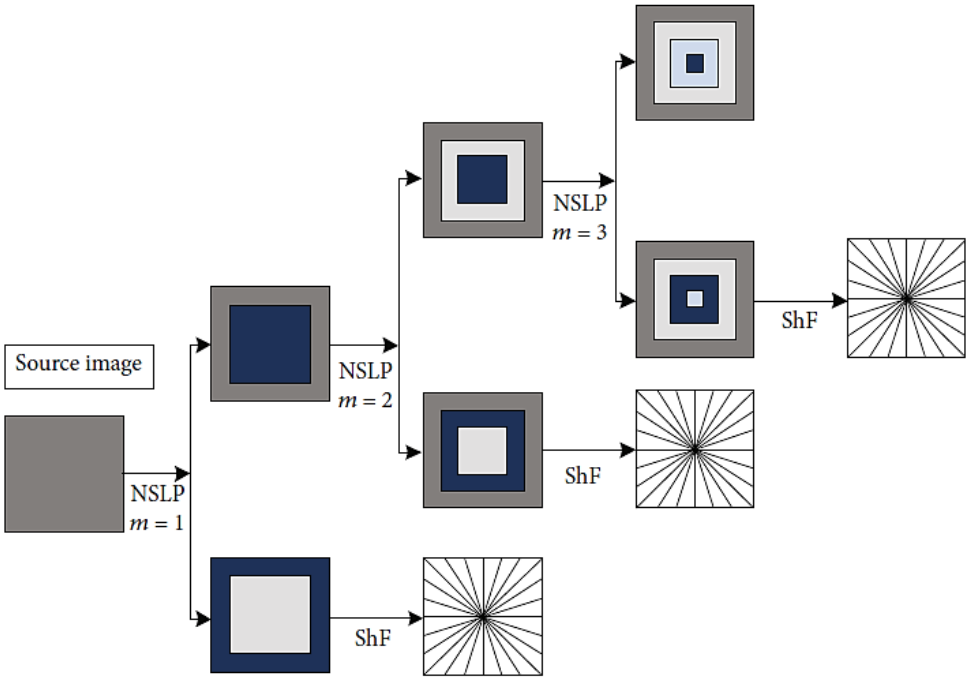


Figure II.14**:** Fusion method based on Nonsubsampled Shearlet Transform (NSST) Domain

### III.2.2.3 Fusion Method Based on Discrete Wavelet Transform (DWT)

Discrete wavelet transform can make different input frequency signals maintaining stable output and has good positioning in the time domain and frequency domain, which helps to preserve the specific information of the image. Therefore, discrete wavelet transform (DWT) is the most widely used transform in the early research of multimodal medical image fusion algorithms. The discrete wavelet transform overcomes the limitations of the principle component analysis and has a good visual and quantitative fusion effect. Most of the DWT-based fusion methods are applied to MRI and PET image fusion [43, 44] but also to others [45]. The source image is preprocessed and enhanced, and the intensity component is extracted from the PET image using the IHS transform, which preserves more anatomical information and reduces color distortion. The DWT transform is performed on the intensity components of MRI and PET to obtain high- and lowfrequency subbands. The high- and low-frequency subbands are, respectively, fused by different fusion rules, and the inverse DWT transform is performed to obtain the fused image [46]. A block diagram based on the DWT fusion method is shown in Figure II.15.

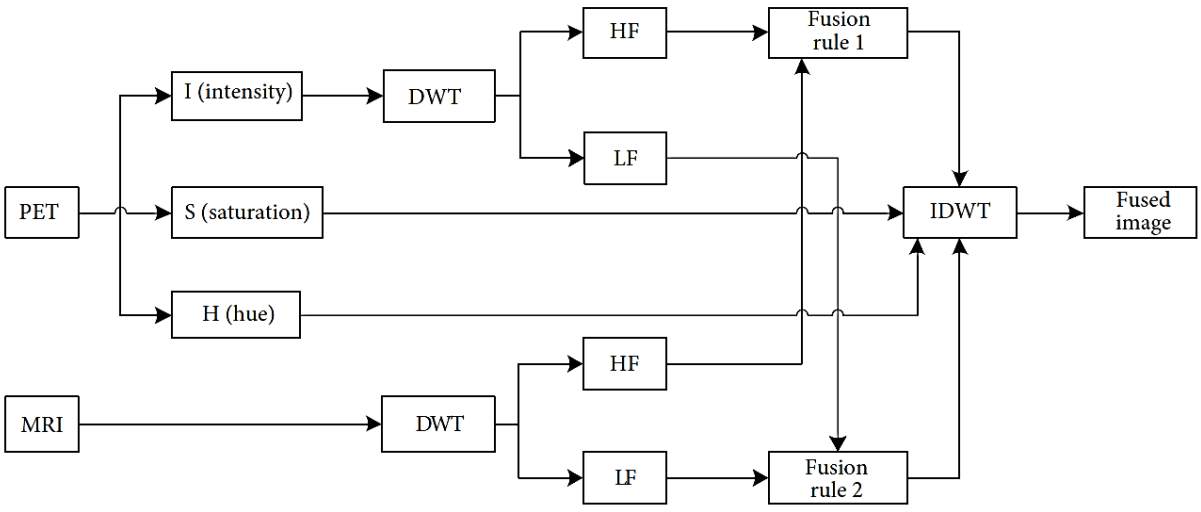


Figure II.15: Fusion method based on Discrete Wavelet Transform (DWT)

### III.2.3 Image Fusion Based on Deep Learning

Deep learning is a new field of medical image fusion research in recent years. Convolutional neural network (CNN) is a typical deep learning model proposed by Krizhevsky et al. [47]. Compared with medical image fusion, deep learning is widely used in the segmentation of medical images and registration of medical images [48-51]. The medical image fusion methods based on spatial domain and transform domain have the defects of activity level measurement (feature extraction) and fusion rules, which need artificial design, and the correlation between them is extremely small. In order to overcome the above problems, Liu et al. [51] applied CNN to image fusion for the first time in 2017, achieving good results relative to the spatial domain and the transform domain. The U-Net network model is widely used in medical image segmentation. From 2D to 3D, its research technology has been relatively mature and has achieved good results in the field of medical image segmentation, but medical image fusion is a new field.

CNN is a multistage feedforward artificial neural network with trainable supervised learning. The convolution operation is multidimensional. In a convolutional network, the first parameter is usually called an input, and the second parameter is called a kernel function, and the output is called a feature map.

#### III.2.3.1 Image Fusion Method Based on Convolutional Neural Network (CNN)

This method uses the Siamese network to generate weight map. The Siamese network [53] is one of the three models for comparing patch similarity in the CNN model. Because its two weight branches are the same, the feature extraction or activity level measurement methods of the source image are the same. This has certain advantages over the models of pseudosiamese and 2-channel, and the ease of training of the siamese model is also the reason why it is favored in fusion applications. After obtaining the weight map, the Gaussian pyramid decomposition is used, and the pyramid transform is used for multiscale decomposition, so that the fusion process is more in line with human visual perception. In addition, the localized similarity-based fusion strategy is used to adaptively adjust the decomposed coefficients. The algorithm combines the common pyramid-based and similarity-based fusion algorithm with the CNN model to produce a superior fusion method. Figure II.16 is a model of the algorithm.

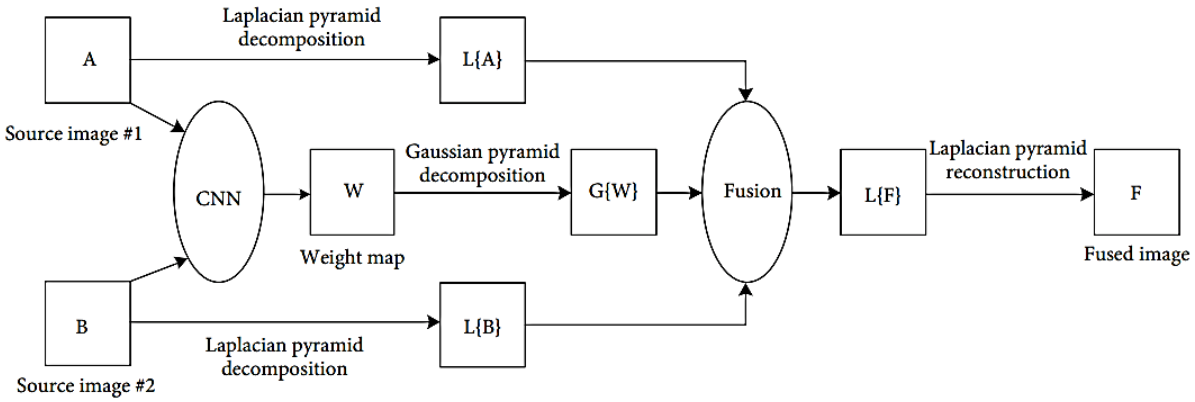


Figure II.16: Image fusion method Based on Convolutional Neural Network (CNN)

### III.2.3.2 Image Fusion Method Based on U-Net

The existing medical image fusion methods neglect the image semantics, do not pay attention to the processing of semantic conflicts, and lose useful semantic information. As a result, the fused image appears blurred boundary, which makes it more difficult for medical workers to parse the fused image. Fan et al. [54] proposed a medical image fusion method based on semantics, which solved the problem of semantic loss of fused images. In this algorithm, two U-Nets are used to construct the FW-Net network model. It is not the first time to combine U-Net with an automatic encoder in medical image research [55]. The left and right structures of FW-Net are the encoder and the decoder. They both follow the structure of U-Net. The encoder is used to extract the semantics of the source image, and the decoder is used to reconstruct the source image. FW-Net can extract the semantics of brightness in the source image and then automatically maps the brightness of different modal images to the same semantic space for image fusion. In order to obtain a smooth and clear image, bilinear interpolation is added to each layer of the encoder and decoder in FW-Net framework. There is no semantic conflict in the fused image, which is superior to other methods in visual effect. This algorithm is only applied to MRI and CT. Other pattern fusion, such as MR and PET fusion and MR and SPECT fusion, will be a research trend in the future. At the same time, the research of U-Net in medical image is not yet mature, so the research of U-Net in medical image fusion is also a focus.

### III.3 Differences between imaging modalities and aims of the fusion

MRI, also known as Magnetic Resonance Imaging, provides information on the soft tissue structure of the brain without functional information. The density of protons in the nervous system, fat, soft tissue, and articular cartilage lesions is large, so the image is particularly clear and does not produce artifacts. It has a high spatial resolution and no radiation damage to the human body, and the advantage of rich information makes it an important position in clinical diagnosis. The density of protons in the bone is very low, so the bone image of MRI is not clear. The CT image is called Computed Tomography imaging. The X-ray is used to scan the human body. The high-density absorption rate of bone tissue relative to soft tissue makes the bone tissue of the CT image particularly clear. The low permeability of X-rays in soft tissue leads to low absorption rate, so CT images show less cartilage information, which represents anatomical information. SPECT is called Single-Photon Emission Computed Tomography, which is a functional image that displays the metabolism of human tissues and organs and the blood flow of arteries and veins. It provides good and malignant information of tumors and is widely used in the diagnosis of various tumor diseases. However, the resolution of SPECT is low and the positioning ability is poor. The PET image is called Positron Emission Tomography, which reveals the true information of blood flow and can accurately identify the location of the patient's lesion. Its principle is using positrons to generate γ photons in collision with electrons in the tissue. The purpose of PET is to detect the number of γ photons, showing a color image of brain function information, suitable for tumor detection; its sensitivity is high, but it is difficult to obtain accurate brain structure position information; soft tissue and bone boundary resolution is lacking, so the spatial resolution is very low and the spatial distortion is highly probable.

There are many fusions of imaging methods in medical image fusion, such as MRI and PET, MRI and CT, MRI and SPECT, CT and PET, CT and SPECT, SPECT and PET, and MRI-T1 and MRI-T2. Different ways of integration keep their own characteristics, such as MRI/PET fusion images, which are important for detecting liver metastasis, Alzheimer's disease and brain tumor diagnosis; MRI/SPECT fusion images are helpful for the localization of lesions and vertebral bone metastasis in tinnitus patients. CT/PET fusion image energy improves the diagnosis of lung cancer; SPECT/PET for abdominal research; and ultrasound/MRI for vascular blood flow diagnosis [56].

## III.4 Medical applications of data fusion

The medical applications of data fusion can be classified into several categories [56].

### III.4.1 Intra subject and intra modality fusion

Relates to the fusion between different datasets coming from the same modality for a subject. This category corresponds to three main clinical objectives:

#### III.4.1.1 Monitoring over time of changes in the patient's anatomy

The monitoring over time of changes in the patient's anatomy allows, for example, to follow the growth or to study the evolution of a lesional area or the effects of therapeutic treatment. In surgery or radiotherapy, this context of fusion makes it possible to compare pre- and postoperative or pre- and post-treatment images.

#### III.4.1.2 Comparison of different states

This fusion context can also be used to allow the comparison of the different states of the subject. In functional MRI, measurements of functional activations can be carried out by the statistical comparison of images acquired respectively in successive states of activity and rest [56, 57]. The comparison of two SPECTexams (single positron emission computed tomography), acquired respectively before an epileptic crisis (inter-ictal) and just after the crisis (ictal-a tracer is injected at the very beginning of the crisis), see allows to highlight areas belonging to the epileptogenic network (crisis causes epilepsy) [57].

#### II.4.1.3 Subtraction imagery

Subtraction imagery is based on the calculation of a difference between two images corresponding to two different acquisitions made with and without a tracer or contrast agent (Figure II.17).

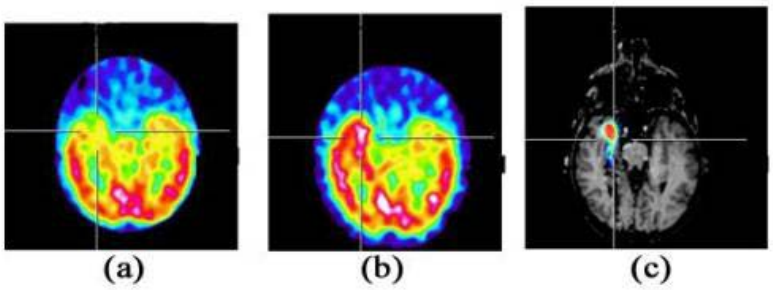


Figure II.17: Image Fusion between two PET based on subtraction technique: Images (a) (b) at $T_1$, $T_2$, and (c) substrated image.

### II.4.2 Intra-subject and intermodality Fusion

Relates to the fusion of multi-modality data from the same subject. No medical imaging modality makes it possible to explore all the anatomical structures or to provide the information at same times, anatomical and functional information at the highest spatial and temporal resolution. This second category of applications makes possible to take advantage of the complementary nature of the different imaging methods and for different anatomical areas (head, heart, chest, thorax, liver or abdomen, kidneys, spine, pelvis, fundus, etc.).

The mapping between PET and MRI data facilitates joint anatomical localization of bone structures and soft tissue (Figure II.18) [57-60].

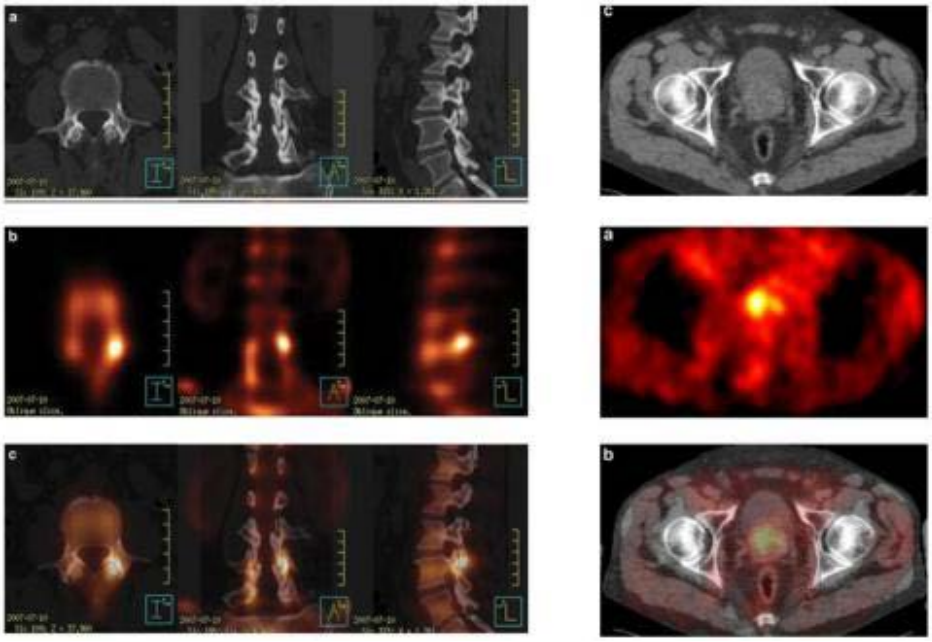

Figure II.18: MRI / PET multimodal fusion examples:

raw1: MRI-raw2: PET-raw3: Fusion

### II.4.3 Inter subject and intra or inter modality Fusion

It concerns the fusion between single or multi-modality data between different subjects. The main applications of this category are related to the study of anatomical or functional variability within a population of subjects (healthy subjects or patients). This type of registration makes possible to build average models (called Template) [59, 60], to compare the data of a subject to an atlas or to a “Template”, to compare, via a “Template” (Figure II.19), data concerning different subjects belonging to the same population or, finally, comparing two populations of subjects [60]. This category of fusion contexts provides a framework for segmentation methods

based on the use of models. The methods and applications related to this category are still, and for a large majority of them, part of the research field.

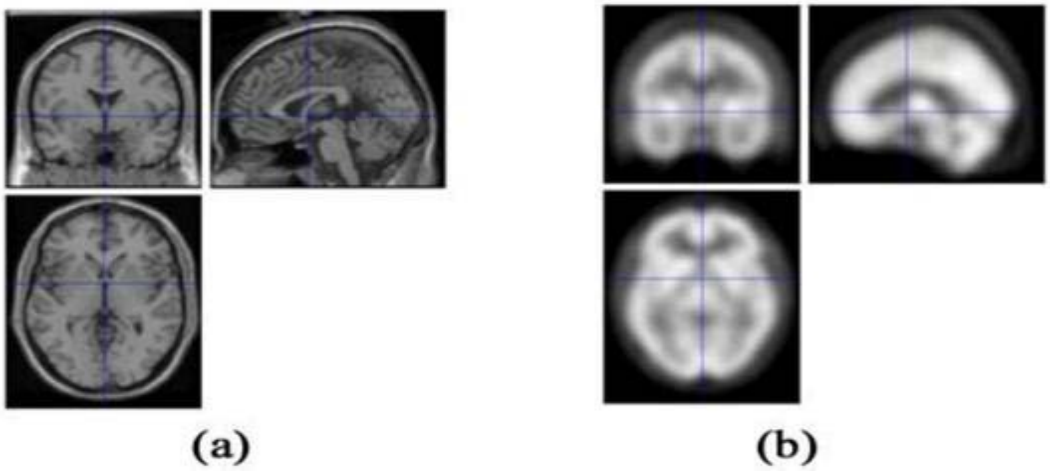


Figure II.19: Presentation of the models used (a): MRI atlas image, (b): Template SPECT.

# IV. Registration assessment

## IV.1 Qualitative evaluation (Visual assessment)

Evaluation of a registration is usally made from a visual analysis of the images (Figure II.20).

This technique is a qualitative evaluation which allows to have a first idea on the quality of registration; It is generally carried with visualization software called viewer and which allow to display the two readjusted images on the same interface and to analyze them with different tools such as colorimetry or the distance between anatomical points [61, 62].

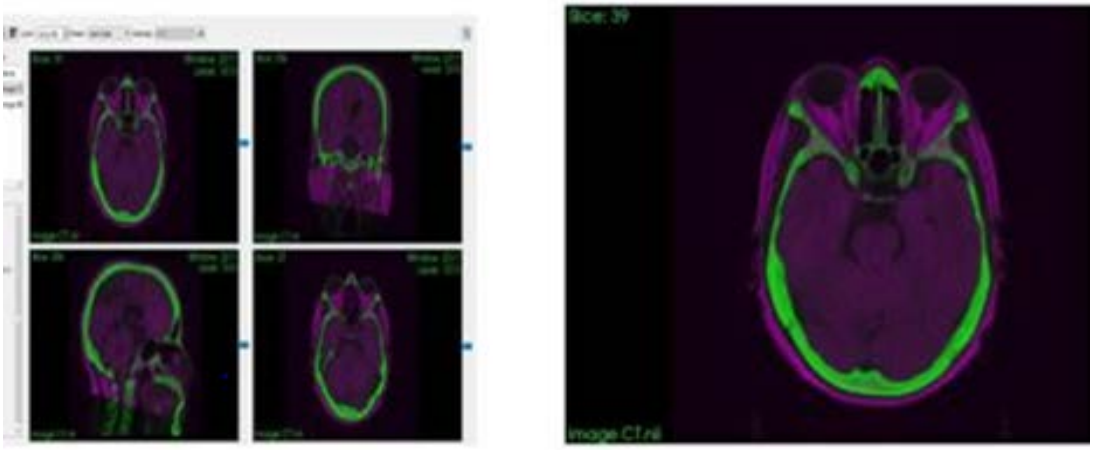

Figure II.20: Qualitative assessment of registration.

## IV.2 Quantitative evaluation

The literature available in the field of image processing uses numerous metrics for calculating the performance of algorithms for registration or fusion of medical images. These metrics make possible to quantify the errors between two models in terms of distance between surfaces or volumes. Metrics are generally symmetrical, which means that they are calculated taking into account each of the two analysis models; to highlight the local differences of each of the two models. Many metrics allow you to calculate the difference between two shapes (surfaces or volumes). These metrics are based on the analysis of sets of points (sets of pixels for surfaces or sets of voxels for volumes) defining each shape. In this chapter and for relating to our work we choose only some of them and they are shown bellow [61, 62]:

### IV.2.1 Average symmetric distance between two forms (ASD)

In imaging, it is represent the average pixel-to-pixel distance (resp. Voxels to voxels for volumes) between the two shapes. It is the most common distance metric in the evaluation literature. Are equation is as follows:

$$\mathrm{ASD(U,V)}=\frac{\mathrm{D(U,v)+D(V,u)}}{\mathrm{|S(u)|+|S(V)|}} \quad \text{(II.14)}$$

Where S(U) and S(V) indicate the set of voxels belonging to contours U and V, respectively; D(U,v) and d(V,u) indicate the shortest distances between an arbitrary voxel and the contours U and V, respectively

### IV.2.2 Root mean square distance (RMSD)

The root-mean-square deviation (RMSD) or root-mean-square error (RMSE) is a frequently used measure of the differences between values (sample or population values) predicted by a model or an estimator and the values observed. The RMSD represents the square root of the second sample moment of the differences between predicted values and observed values or the quadratic mean of these differences.

$$RMSD = \sqrt{\frac{1}{N}\sum_{i=1}^{N}\delta_i^2} \quad \text{(II.15)}$$

Where $\delta i$ is the distance between structure $i$ and either a reference structure or the mean position of the $N$ equivalent structure.

*RMSD* is always non-negative, and a value of 0 (almost never achieved in practice) would indicate a perfect fit to the data. In general, a lower RMSD is better than a higher one. However, comparisons across different types of data would be invalid because the measure is dependent on the scale of the numbers used.

### IV.2.3 Hausdorff distance (HD)

The Hausdorff distance is an estimate of the distance between two graphic surfaces. If X and Y are two surfaces and d (x, y) is the Euclidean distance between two points x and y of X and Y respectively, the HD is then given by the following equation

$$d_H(X,Y) = (\underbrace{sup}_{x\in X}\ \underbrace{inf}_{y\in Y}\ d(x,y), \underbrace{sup}_{y\in Y}\ \underbrace{inf}_{x\in X}\ d(x,y)) \quad \text{(II.16)}$$

HD is measured in mm and ranges from 0 (identical surfaces) to + ∞.

### IV.2.4 Jaccard similarity index (JDC)

The Jaccard similarity coefficient is a statistical measure of the similarity between two sets of samples (A and B). It is defined as the cardinality of their intersection divided by the cardinality of their union and given by the following equation.

$$\mathrm{JSC} = \frac{|\mathrm{A} \cap \mathrm{B}|}{|\mathrm{A} \cup \mathrm{B}|} \quad \text{(II.17)}$$

The JDC is between 0 and 1, 0 indicating that there is no overlap and 1 indicating a complete overlap.

### IV.2.5 Dice coefficient (DSC)

The Dice coefficient is based on the Sorensen-Dice similarity, which is a coefficient that measures the overlap between two binary structures (A and B). It is given by the following equation:

$$\mathrm{DSC} = \frac{2|\mathrm{A} \cap \mathrm{B}|}{|\mathrm{A}| + |\mathrm{B}|} \quad \text{(II.18)}$$

The DSC ranges from 0 to 1 where 0 indicates no overlap and 1 complete overlap.

# CHAPTER III :

## Emerging role of MRI in external radiotherapy treatment planning

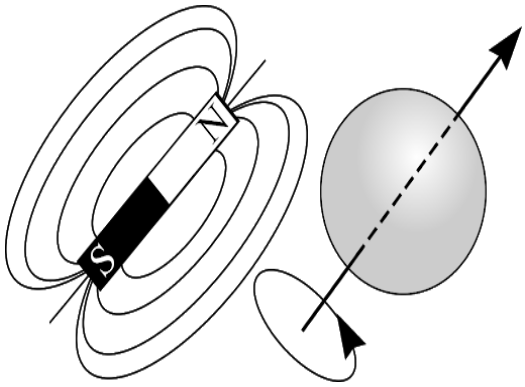


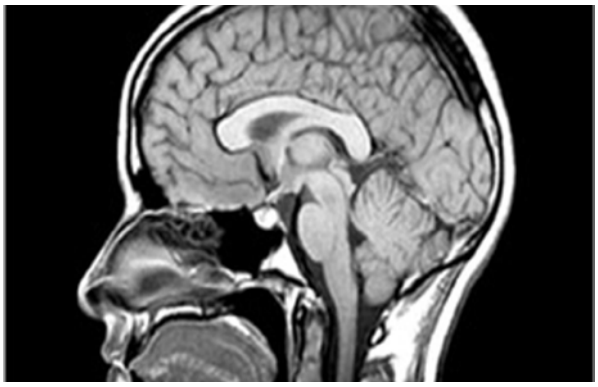

# I. MRI role in contouring the gross tumor volume and organs at risk

The mortality rate of cancer has decreased over the last century for almost all disease sites except glioblastoma and pancreatic cancer witch remain the most fast and aggressive cancer [63]. This is in part related to the advances in medical imaging, technology and treatment resulting in better outcome and survival. The most important technic witch increase the quality Traitement is the Radiotherapy, which is playing an increasing role as an important modality along with chemotherapy for the management of cancer patients in most disease sites. [64-66] More than 60% of cancer patients are treated with radiation in the management of their disease during their life span.

Advances in imaging, providing accurate information of the target volume (that is, the volume to be irradiated), and the adjacent critical structures or organs at risks (OARs), has made significant improvements in delivery of the external beam radiation dose and increased treatment precision [67].

## I.1 How MRI is involved in RT?

The increased dosimetry conformity of modern treatment techniques has generated new constraints on the accuracy of target delineation through imaging in RT. In order to deliver highly conformal treatments accurately, a precise definition of tumor and OAR is needed. This is the main reason MRI has seen increased usage in radiation oncology departments. Although in many cases CT still acts as the master reference scan, MRI provides superior soft-tissue contrast compared to CT, as well as a myriad of information on tumor characteristics that aid the delineation of both the tumor and OARs. The flexibility to acquire multiple contrasts has shown advantages for accurate tumor delineation in a large body of literature over the recent years. The American Association of Physicists in Medicine (AAPM) Task Group (TG-101) [68] on stereotactic body RT states that MRI is a gold-standard for visualization of brain tumors and “is increasingly used in SBRT applications including prostate, spinal tumors, chest, and solid abdominal tumors.”

MRI is routinely utilized in a number of malignancies (Table III.1) for treatment planning. T2-weighted imaging, for example, is able to distinguish tumor from normal tissue and fat in rectal and esophageal cancer, whereas T1-weighted imaging provides good tumor contrast in squamous cell carcinoma in head and neck cancer [69]. Besides native T1 and T2 contrast, physiological contrasts such as dynamic contrast enhanced (DCE), blood oxygen level-

dependent (BOLD), and diffusion-weighted imaging (DWI) have been shown to have added value in defining tumor boundaries. [70-73]

Physiological information from DCE, DWI, and BOLD imaging (often all referred to as functional imaging in the RT community) has been successfully used to derive tumor probability maps in prostate cancer, a major male cancer in the Western world [74]. This information was later used in a large Phase 3 trial, called the FLAME trial, [75]. in which a focal micro boost up to 95 Gy in 35 fractions was given to the tumor (ie, GTV), while the prostate gland (ie, CTV) received a standard dose of 77 Gy in 35 fractions.

Table III.1: Examples of common malignancies for which MRI is routinely used for pretreatment Planning.

| **Organ** | **Contouring and delineation** |
|---|---|
| Brain | Better delineation of brain tumors on MRI as these tumors are not conspicuous on CT exam |
| Nasopharynx | Nasopharyngeal tumor are contoured on T2 MRI due to higher contrast resolution |
| Liver and pancreas | MRI is being increasingly utilized for hepatobiliary and pancreatic malignancy |
| Spine | Spinal tumor are visualized on MRI due to higher contrast resolution on Dixon and T2W images |
| Prostate | Prostate anatomy is not well visualized on CT and it can be difficult to delineate prostate from rectum. T2W MRI is helpful for visualization of prostate anatomy and tumor. |

In a standard MRI-aided workflow, the acquired MRI data are registered to the planning CT on which the treatment plan is simulated. In order to minimize co-registration errors between the MRI and CT datasets, it is important that most imaging be performed in the treatment position. This, however, requires adaptations to the MRI workflow and the use of specialized imaging

hardware. Most major MRI vendors themselves or in partnership with third-party suppliers offer special editions of their flagship 1.5T and 3T scanners that are equipped with tailored RT hardware and software. These options include more accurate laser positioning devices, flat tabletops that match the treatment table, coil bridges to prevent deformation of the patient's body contour, and fixation devices such as thermoplastic masks and arm supports, but compatible in the magnetic field. The imaging protocols are also adapted to the specific requirements of treatment simulation. In comparison with diagnostic imaging, much more emphasis is put on the geometric accuracy of the imaging. The geometric accuracy of the preparatory scans determines the required safety margins, [76-79] and thus the amount of healthy tissue that is irradiated. Therefore, it is important to achieve the highest geometric accuracy possible. For this reason, RT scans are typically acquired at higher resolution and higher readout bandwidths, at the expense of signal-to-noise ratio (SNR). The push for 3D acquisitions is also higher than in diagnostic imaging, for two reasons: 1) the need to acquire isotropic resolution, and 2) the need to correct for gradient nonlinearity along all three dimensions. All these adaptations have to ensure that the MRI matches the planning CT as well as possible, because any misregistration would introduce a systematic error that propagates through the entire treatment.

**I.2 MRI vs. CT**

Many Studies confirm the aims of MRI on RT and shown that the advantage of MRI compared with CT scanning for radiotherapy planning is the excellent soft tissue contrast. Figure III.1 illustrates the difference between CT and MR images of the prostate, in the CT scan it is hard to identify even the boundaries of the prostate, whereas in the MR image not only the prostate boundary but also a good deal of the internal structure of peripheral zone and central gland is observed. In many cases one or more of the dominant intraprostatic lesions are seen, which raises the additional possibility of targeting a boost dose to this region [80-81]. Organs at risk (OARs), such as rectum and bladder, are also generally well delineated, and therefore help to identify the regions in which minimized doses are desired in the radiotherapy plan.

Table III.2 illustrates which modality are preferable to be used on delineation of OARs and tumor volumes in brain Cancer [82]. Figure III.1 Comparison of axial CT and T2-weighted MR images to depict prostate tumours. In the CT image (left) only the boundaries of the prostate may be estimated. In the enlarged T2- weighted MR image (right) structure within the prostate is readily apparent. PZ = Peripheral Zone, CG = central gland, TU = tumour.

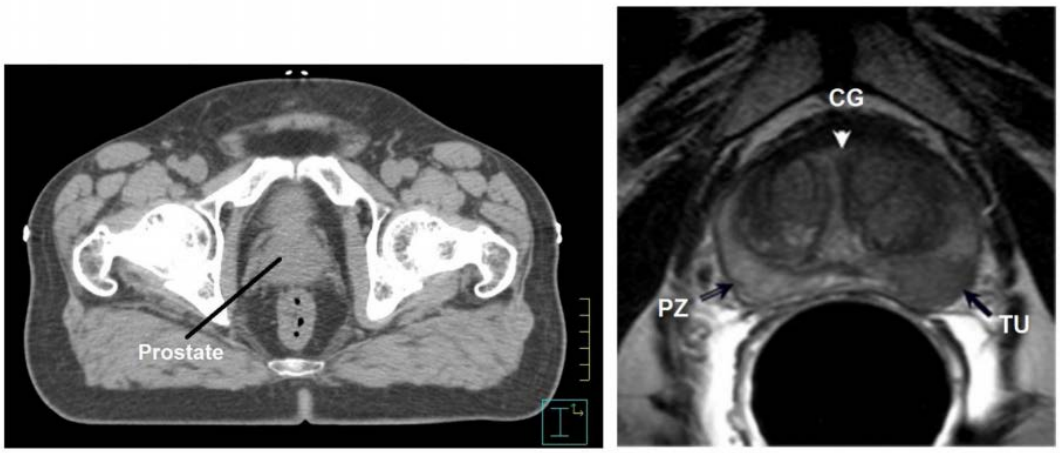


Figure III.1: Comparison of axial CT (left) and T2-weighted MR (right) images to depict

Table III.2: Which Modality are preferable to be used on delineation of OARs in RT?

| **Organ at risk** | **Modality for delineation** |
|---|---|
| GTV | MRI |
| edema | MRI |
| chiasma | MRI |
| pituitary | MRI |
| optic nerve | CT |
| brainstem | MRI |
| eyes | CT |
| BRAIN | CT |
| crystalline | CT |

Many other studies published that compare delineations performed on different modalities, often CT and MRI. For the prostate, a study by Roach et al. [83] in 1996 compared target volumes delineated on ten patients with a T1-weighted MRI and a CT, both without contrast enhancement. The images were matched using bony anatomy, and the delineated volumes where compared. They found that the average volume was 32% larger on CT as compared to

MRI, and concluded that the prostate volume is overestimated on non-contrast enhanced CT scans. Kagawa et al. [84] performed a similar study in 1997 by delineating prostate target volumes, either only prostate or prostate and seminal vesicles, on 22 patients with CT and T2-weighted MRI scans. They found a 19% reduction in target size on the MRI scan, and concluded that MRI localization of the prostate is more accurate than CT. They also suggested that MRI adds valuable information to CT by using image fusion to enable more precise target localization of the prostate. Debois et al. [85] found similar results in 1999, with a prostate volume reduction of 32% when delineating on MRI as compared to CT. They conclude that the use of MRI can substantially improve the delineation accuracy of the prostatic apex and the anterior aspect of the rectal wall, resulting in a better prostate coverage. Other groups have focused more on comparing intraobserver and interobserver differences between prostate delineations based on different modalities. Milosevic et al. [86] published a study in 1998 where three physicians defined the prostate apex on MRI, CT and urethrography. They found that the interobserver agreement was significantly improved on MRI scans as compared to CT, and concluded that MRI is superior to CT and urethrography for localization of the prostate apex. Parker et al. [87] published a study in 2003 where they found that the interobserver variation was significantly lower for delineations based on MRI as compared to CT and they concluded that this, in combination with a registration procedure based on intra-prostatic fiducial markers, could enable smaller PTV margins.

Studies that compare target delineations for other sites have also been presented. Weltens and co-workers [88] published a study in 2001 that compared target volumes in the brain for five patients delineated by nine physicians. They found that the interobserver variations was not reduced by the addition of MRI to CT data; however, the CT and MRI target volumes where complementary, i.e. the MRI study added information to the CT based target delineations as it resolved conspicuous anatomy that was not visible on CT alone. Prabhakar et al. [89] compared delineations on 25 patients with brain tumor and found that the MRI delineated volumes where 27% larger than CT based delineations and they also found a shift in the tumour centre of mass between CT and MRI based volumes. They concluded that MRI imaging is more sensitive than CT imaging when it comes to target definitions of brain tumours, and that MRI is an indispensable tool that should be compulsory for treatment planning of brain tumours. Datta et al. [90] found that CT based delineations significantly underestimated the target volume of high grade gliomas as compared to MRI. They concluded that radiotherapy treatment planning

should be based on MR imaging to avoid geographic misses, especially for high-grade tumours with peritumoral edema present.

### I.3 Additional advantages of MRI for radiotherapy planning

MRI uses low amplitude non-ionizing radio waves, unlike CT scanning which uses ionizing radiation. MRI is of particular benefit for pediatric populations in which radiation dose needs to be carefully controlled, and in cases where repeat scans are helpful during treatment both to ensure that the treatment plan is revised to follow radiation-induced tissue changes, and to monitor early response. Another feature of MRI is that owing to the method of data acquisition the slice orientation is not required to be transaxial, as it is for CT, but can be sagittal, coronal, or at any oblique angle desired. This enable images to be better aligned with anatomy. However, most radiotherapy planning software still assumes that images are acquired in the transverse plane, and it may be a while before this particular feature of MRI can be optimally utilised.

Tumor in many tissues experience movement not just between treatment fractions, but also during fractions. While breath-holding (and active breathing control) is one approach, there is some residual variation between tumor position between sub-fractions. Another potential approach is to adjust the treatment during the fraction dynamically. Radiation dose and poor soft-tissue contrast exclude CT scanning for this purpose, but both ultrasound and MRI have potential for real-time RT guidance. Real-time MR-guided RT is now under development and clinical trial [91]. MRI has been integrated with LINACs and Cobalt units in different approaches As with the MR-PET combination, it has been a huge challenge to combine the modalities together, so that both the imaging and the treatment behave as required, in particular to operate the accelerator close to the magnetic field, and to gain access for the beam into the centre of the magnet, and to avoid significant RF interference from the accelerator into the images. While not yet widely available, these developments hold great promise.

## II. MRI for treatment assessment

Advanced radiation techniques, including intensity modulated radiation therapy (IMRT), volumetric modulated arc therapy (VMAT) or high-dose stereotactic body radiotherapy (SBRT) pursue the goal of delivering high doses to the tumor, while sparing the surrounding tissues and organs at risk (OARs). To ensure a precise dose delivery, image-guided radiotherapy (IGRT) has been developed and widely introduced into clinical practice. Current IGRT techniques using on-board cone-beam CT (CBCT) are already very effective, but are limited due to the reduced soft-tissue contrast. Frequently, it remains challenging to distinguish tumor

from normal tissues, with the consequence that dose escalation strategies are not readily feasible, or generous planning target volume (PTV) margins are applied to account for uncertainties in gross tumor volume (GTV) delineation, dose delivery and target coverage.

On-board real-time Magnetic Resonance Imaging (MRI)-guided radiotherapy (MRgRT) with hybrid MRlinear accelerator (MRL) systems marks the beginning of a new era. MRI is the most versatile and suitable imaging modality for RT, as it provides direct visualization of the tumor and surrounding tissue anatomy. Moreover, it provides real-time imaging to characterize and eventually track anatomical motion. Respiratory gating by MRI is particularly advantageous in several aspects for high dose SBRT [92]. It enables motion mitigation and a reduction of PTV margins and allows for an accurate dose delivery to the PTV by reducing dose exposure of OARs. Certain anatomical sites or specific organs affected by motion from different sources (e.g. breathing, bowel displacement /bladder filling) may benefit from MR-guided gating techniques: thoracic tumors, including lung or mediastinal lesions, breast cancer, and abdominal or pelvic tumors, such as liver or pancreatic lesions and prostate cancer. Moreover, real-time plan adaptation, while the patient is on the treatment table, is a disruptive concept of the innovative MR-linear accelerator (MRL) workflow [93]. This new key feature will allow physicians to optimize dose escalation strategies, as there is a further potential for reducing dose to OARs, especially when a precise localization and real-time tracking of the tumor is ensured.

### II.1 Advantages of MRI-guided radiotherapy in treatment quality

Using MRI-guided radiotherapy into clinical practice remains challenging. To date, the initial availability of next-generation hybrid MRI-Linac systems is still limited. In summary, MRI-guided RT creates a new perspective towards an individualized patient-centric planning approach using online adaptation for treatments. Furthermore, a significant increase in knowledge is expected concerning the biological processes, which occur during radiotherapy and its effect on patient survival for brain diseases. Below some advantages of MRgRT in particular cancer.

#### II.1.1 Brain Cancer

Tumors of the central nervous system (CNS) are frequently treated with RT. Specific entities are metastases, primary brain tumors (low-grade gliomas, anaplastic astrocytomas, oligodendrogliomas, glioblastomas. A MRI-based planning workflow could potentially be both, cost- and time-saving while reducing uncertainties associated with CT-MRI registration. MRI already represents the gold-standard imaging method for brain tumor diagnosis and the

assessment of treatment response [94]. In this context, MRgRT allows for the first time to obtain both, structural and functional information during RT and to manage the adaptation of the prescribed dose during the treatment, in order to optimize outcome. To date, in daily clinical practice, a recent MRI is usually co-registered to bony structures of a simulation CT, achieving a high degree of confidence. Thus, due to these consolidated procedures, RT is already commonly delivered with a high level of precision to brain targets. Therefore, as well as hypothesized after the introduction of PET and MRI, a lot of concerns could be related to the real usefulness of MRgRT in brain RT.

However, in treatment Assessment, a crucial difference emerges, the Magnetic Resonance Linac (MRL) systems enable a rapid adaptation, immediate target volume delineation and quick tumor response assessment. An example is the treatment of a resection cavity, which can change significantly in shape and size between the simulation and the initiation of treatment [94]. Furthermore, if hypofractionated stereotactic radiosurgery (SRS) is applied, the resection cavity could also change during the treatment course of 3–5 fractions, which would be visible using MRI-guided RT.

### II.1.2 Head & Neck Cancer

MRI is increasingly used in head and neck (H&N) RT due to its superior soft tissue contrast and its versatility. MRI is utilized in treatment planning to delineate the GTV, the clinical target volume (CTV), and to estimate the necessary PTV margin and to assess the loco-regional treatment response [95-96]. Undoubtedly, the advent of MRL [93] opens the door to fully exploit the advantages of MRI over CBCT by its online adaptation capability during the treatment procedures (Figure III.2). The following significant improvements are anticipated:

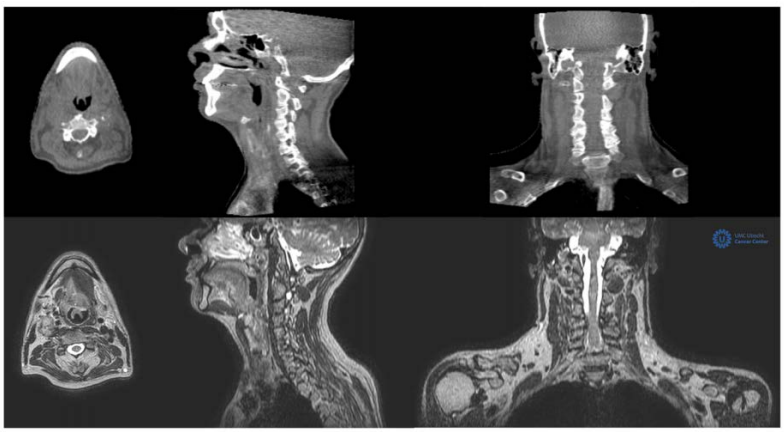

Figure III.2: Cone beam CT images of an oropharyngeal cancer patient (top) compared to the 1.5 T MR images (T1) of the same patient acquired at the MRL (bottom).

### II.1.2.1 Adaptation to anatomical changes

During the course of irradiation, H&N patients can significantly lose weight and OARs, such as the parotid glands can dramatically shrink [97]. The time scale of these changes does not require online optimization. However, the MRL and its workflow are designed to inherently manage these potential changes and online, offline or weekly adaptation can be applied for optimal OAR sparing

### II.1.2.2 Adaptation to tumor response

Tumor response varies from significant volumetric changes of large lymph nodes to more subtle MR signal changes within the GTV. When the tumor clearly shrinks and is replaced by healthy tissue, the GTV might be adapted in a straightforward manner [98]. How to adapt to MR signal intensity changes within the initial GTV must be investigated in well-designed clinical trials. For oropharyngeal cancer, a distinction should be proposed between HPV positive patients, where dose deescalation could be considered for well-responding GTVs, and HPV-negative patients that require dose escalation to poor-responding regions inside the GTV.

H&N cancer patients are treated using an immobilization mask that, in combination with the several rigid bony structures, minimize major intrafraction motion. However, considerable motion has been observed for the larynx and the tongue due to breathing, movement of the tongue and swallowing [96]. Cine-MR during radiation can be applied to guarantee minimal PTV margins. Furthermore, exception gating might be applied to interrupt irradiation in case of excessive motion.

Curative treatment schemes for H&N cancer patients usually consist of 30 to 35 fractions. Full online plan optimization including the registration, adaptation, optimization and QA steps currently takes approximately 45 min for relatively simple dose distributions. Nevertheless, thirty fractions of 45 min in a noisy, claustrophobic environment is probably too distressing for many patients. This discomfort might be reduced by developing a quick MRL workflow when minimal adaptation is needed, and apply full online adaptation only, when major changes occur. Furthermore, comfortable patient positioning methods including noise reduction will be developed. Both patient comfort and a reduced workflow are prerequisites to fully exploit the promises of MR-guidance for head-and-neck cancer patients [93].

In summary, MRI-guided RT can be considered a groundbreaking new technology that is capable of creating new perspectives towards an individualized, patient-oriented planning and treatment approach, especially due to the ability to use daily online adaptation strategies.

Furthermore, MRL systems overcome the limitations of conventional IGRT, especially in soft tissue, where target and OARs need accurate definition. Nevertheless, some concerns remain concerning the additional time needed to re-optimize dose distributions online, the reliability of the gating and tracking procedures and the interpretation of functional MR imaging markers and their potential changes during the course of treatment. Due to its continuous technological improvement and rapid clinical large-scale application in several anatomical settings, further studies may confirm the potential disruptive role of MRI-guided RT in the evolving oncological environment.

## III. Generation of synthetic CT from MRI data

To fully exploit the advantages of magnetic resonance imaging (MRI) for radiotherapy (RT) treatment planning, a method is required to overcome the problem of lacking electron density information. The generation methods of synthetic CTs **(**sCT) can be divided into two major groups: Voxel based and atlas based generation methods. However, some methods are a combination of the two major groups.

### III.1 Voxel-based methods

The idea of the voxel-based approaches is to convert individual MR voxels to their corresponding CT HU value based on a learned criterion such as a regression model or a combination of classification and bulk density assignment. Many approaches in this category use intensity as the main feature, which means that bone/air ambiguities must be solved by e.g., using specialized MR sequences such as the ultrashort echo time (UTE) sequence. Using an unconventional acquisition approach and dual echo times, this sequence is optimized to maximize the amount of signal coming from short T2 components [99-101].

Aside from assigning a bulk water-equivalent CT number to the entire patient, the simplest voxel-based approaches use manually determined thresholds and morphological operations to label voxels of UTE images according to tissue classes such as soft tissue, bone, and air. A bulk density is then assigned to the classes in order to create the sCT [101].

The main drawback of these methods is the need for manual intervention; the difficulty in tuning the relative intensity thresholds and choosing the appropriate bulk density values could place the voxel-wise and geometric accuracy of these methods in the lower end. More sophisticated methods are supervised, where model parameters are learned in a training phase from pre-acquired and co-registered MR and CT data. This automates the sCT generation, and can yield either a continuous-valued or a segmented sCT depending on the chosen model. Once

the model parameters have been determined from the training phase, these methods are fast in predicting an sCT and they generally perform better than the above-mentioned threshold-based approaches. Other Study found that regression models such as a random forest or a kernel regression model parameterized by a mixture of Gaussians are among the most promising methods in the voxel-based category when using UTE scans of the brain [102,103].

The common denominator of the above methods is the need for the non-standard UTE sequence. From a practical point of view, introducing additional MR sequences in the RT work-flow is unappealing since it prolongs the MR scan time of each patient and introduces the risk of PTV and/or OAR movement between the sCT sequence and the delineation sequence. Furthermore, a low signal-to-noise ratio and partial volume effects in the UTE scans means that sCT predictions suffer at tissue interfaces such as in the ear and nasal cavities [99-101].

Another class of voxel-based approaches uses conventional MR sequences such as T1-weighted or T2-weighted scans. This puts additional demands on the model, since the MR intensity ambiguities must be solved in some way. One way to achieve this is to train separate regression models; one for the bone region and one for the remaining regions. This approach, however, requires a segmentation of the bone region, which in the reported approaches, requires a manual delineation. Another way to solve the intensity ambiguities is to extract features from the MR images. These features can then be used in combination with the gray-scale intensity to help distinguish otherwise similar voxels. Aside from spatial features and anatomical knowledge, typical features from computer vision describing neighborhood and texture can be used for bone segmentation. A concern with voxel-based methods is that MR voxel intensities can vary between different scanners and different scans even for the same MR sequence and patient. If the methods should be generally applicable, this means that special care should be taken when choosing the input to a voxel-based model. Intensity alone, or features that directly rely on the intensity could yield an approach that is only applicable to certain data or certain scanners [103-107].

### III.2 Atlas-based methods

With conventional atlas-based methods, the sCT prediction relies on a nonlinear registration between the patient MR scan to be converted and one or multiple atlases of MR scans with known correspondence to a CT and possibly an organ label-map. The MR intensity ambiguities are thus resolved by the spatial information provided by the registration, which means that conventional MR sequences can be used. With a population-based atlas technique, the atlas consists of an average MR scan and a registered average CT. The average scans are formed by

registering and averaging a population of MR/CT atlases in a common space prior to observing the patient MR. The sCT is created by nonlinearly registering the average MR with the patient MR and applying the same transformation to the average CT, which then provides the sCT estimate [108–111].

With a multi-atlas technique, the sCT is formed by averaging (or fusing) multiple atlases after a non-linear alignment with the patient MR. Each atlas consists of an MR scan and a co-registered CT scan. The procedure is to non-linearly register each atlas MR with the patient MR, after which the same transformations are applied to each atlas CT. The atlas CTs are then fused to provide the sCT estimate. The fusion can be done in a number of ways, e.g., using a local similarity measure to create a locally weighted averaging . This gives less weight to regions in the atlases where the non-linear registration was sub-optimal. Figure III.3 shows an illustration of the multi-atlas approach [108–113].

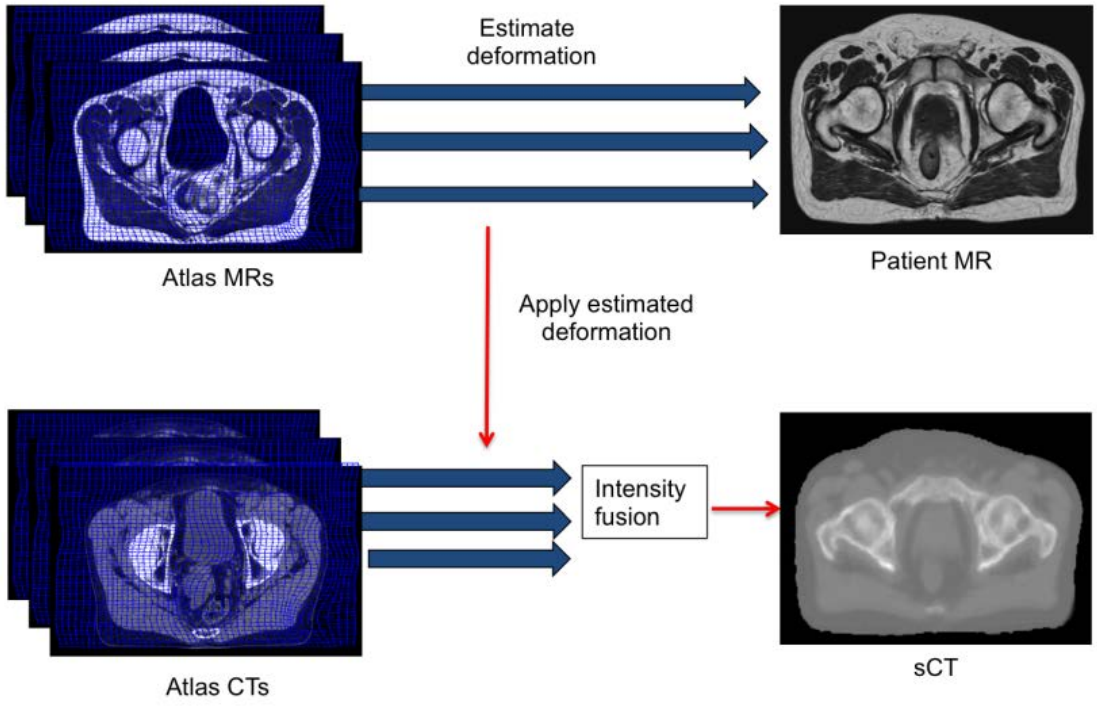


Figure III.3: Illustration of a multi-atlas

Atlas-based methods generally perform well compared to voxel-based techniques. A concern, however, is that they depend entirely on the accuracy of the registration; in cases where the patient geometry is very different from the atlas(es), this may pose a problem. The multi-atlas

technique remedies this to some degree by using multiple registrations and assuming that at least one of the atlases will be well aligned in a given region of the patient MR. This provides a better sCT estimate than the population-based atlas technique . The improved sCT quality comes at the cost of computation time due to the number of required non-linear registrations between the patient MR and the atlases. Typically between 15-38 patients are used as atlases, meaning that the same number of registrations are required [109, 111, 113].

A way that relies less on the accuracy of the non-linear registration is to perform pattern recognition after aligning the atlases with the patient MR by defining a rectangular image sub-region (a patch) around each MR voxel and extracting all such patches from the patient MR and registered atlas MRs, a Gaussian process regression model can predict an sCT value based on spatially close and similar atlas MR patches, which have a known correspondence to the atlas CTs. This improves the prediction accuracy compared to simpler multi-atlas techniques [113].

Some authors, however, point out that the added computational complexity of a pattern recognition step on top of the non-linear registrations may not make it worthwhile. Both the pattern recognition technique and most similarity measures used to create a locally weighted averaging of the atlas CTs rely on an intensity-based similarity measure between the atlas MRs and the patient MR. Similar to the voxel-based approaches, these methods are therefore affected by the relative nature of the MR voxel intensities. An intensity normalization step is usually performed to account for this.

## IV. Rational for MRI-only radiotherapy

### IV.1 Main advantages

There are many advantages put forward in the literature in favor of MR-only radiotherapy planning compared to a workflow where CT is the primary imaging modality and MR a secondary (CT-MR workflow). The advantage for MR-only most often mentioned is that the registration between CT and MR will introduce geometrical uncertainties. These errors introduced in the planning stage will affect each fraction and are systematic. In an MR-only workflow, image registration with the introduction of geometrical uncertainties is avoided. Secondly, it is hypothesized that MR-only is more efficient and cost-effective as no CT acquisition is necessary. This would be of special importance in the scenario of adaptive radiotherapy based on MR data. Finally, the unspecific exposure of ionizing radiation will be reduced with the exclusion of CT. Although this statement is correct, the dose reduction is marginal as compared to the treatment dose the patients will receive, and we will therefore not

examine this argument in depth in this review. These advantages apply to traditional linac based treatments. The introduction of combined MR and treatment units, MR-linacs, could bring further advantages in areas such as adaptive treatment, where re-planning could be executed daily on the acquired MR image set [114].

### IV.2 Existing challenges

Significant challenges remain to be addressed in regards to the development of MR for radiation therapy.

#### IV.2.1 Estimation of electron density

Image intensity in MRI is not directly related to electron density, and this limits the use of MRI-only RT planning and MRI-simulators. As MRI provide Protonic density, it is not possible to calculate the right dose planning for treatment. For this issue many solutions are provided and are mentioned above.

#### IV.2.2 Limitations of RT and MRI workstations

Radiotherapy planning systems are designed to display imaging data in 2D and 3D and to allow users to delineate 3D volumes (tumors, organs at risk) to which margins are later added, prior to treatment planning. However RT systems were originally designed for CT datasets, which are invariably transaxial. RT planning systems vary in their ability to handle MRI DICOM data; currently some handle transaxial images only, some accept either transaxial, sagittal or coronal images and fewer still handle MRI datasets acquired in oblique orientations. This can be a problem for MRI examinations, as diagnostic MRI examinations are most likely to be orientated around anatomical landmarks, and MRI-trained personnel generally make use of MRI's flexibility in choosing orientation of the volume of interest. This makes it necessary to know the restrictions of a given planning system prior to MRI data acquisition, and therefore limits the overlap of MRI examinations done for diagnostic and planning purposes. In addition RT planning systems do not necessarily handle multiple MRI series with different contrast, and do not always allow flexible transfer of image registration parameters between different series.

#### IV.2.3 Geometric accuracy of MRI images

MRI makes use of magnetic field gradients to provide a linear relationship between resonant frequency and position, and hence to assign signals to their spatial origins. Consequently, imperfections in the static magnetic field uniformity and gradient linearity may lead to geometric distortion of MR images. In addition, the patients themselves disturb the magnetic

field with their own particular spatial distribution of magnetic susceptibilities, causing a degree of patient-dependent image distortion. Both system-related and patient-related causes of geometric distortion are undesirable for RT planning, and must be quantified and minimized [115].

### IV.2.3.1 System-related geometric distortion

In ideal conditions MR images are generated by superimposing a constant and linear magnetic field gradient to a uniform static magnetic field. In practice there are design constraints on magnet size and conflicting demands for gradients of high magnitude and high slew rates. The final compromise often leads to geometrical image distortions which increase away from the magnet isocentre, reaching a few centimeters at the edges of the scanner's maximum field of view [115]. In addition to the geometric distortion in the readout and phase encoding directions, the selective RF excitation is also affected, causing warping of the excited slice (or slab) and thickness changes as a function of position. The use of high imaging gradient amplitudes makes the sequences less sensitive to the non-uniformity of the static magnetic field, but this requires an increase in bandwidth. Higher receiver bandwidth leads to reduction in SNR and higher excitation bandwidth requires more radiofrequency power to be applied to the patient. In addition, higher imaging gradients may lead to distortion of gradient waveforms, which in turn may cause further geometric distortion. Therefore a careful choice of pulse sequence parameters is required for applications which rely on geometric integrity: radiotherapy planning, stereotactic surgery and accurate geometric measurements [116].

Distortion correction for gradient imperfection can be performed on 2D images or 3D volumes. Because the distortion in itself affects all directions, the use of 3D correction on a 3D volume is likely to be more successful. However, post-processing for correction of geometric distortion can degrade image quality and change noise characteristics as the acquired voxels of the original images are either contracted or extended. The main MRI vendors have incorporated post-processing for distortion correction to their products, and this can be applied automatically with minimal increase in image reconstruction time. Once the system-based geometric distortion is known, it can be corrected by using a transformation from the real coordinate system to an undistorted one, a process akin to non-rigid image registration. The function describing this transformation is either a global mathematical description of the distortion or a localised one. Using standard vendor's distortion correction, the displacement is greatly reduced, only reaching to 2-3 millimetres on the outer edges of the clinically useful volume [117].

### IV.2.3.2 Metal Artifacts and their reduction

Many metallic implants are MR-safe, but cause severe local artifacts in MR images due to susceptibility-related magnetic field inhomogeneity and to currents induced in the implant by radiofrequency fields and by the imaging gradient fields. Common artifacts are areas of signal loss, bright areas of signal accumulation and local distortions. Previously described strategies can be used to reduce distortion in conventional techniques: the choice of spin-echoes over gradient-echoes, the use of short echo-times (TE) and imaging with high receiver and excitation bandwidth. However, the field inhomogeneity associated with common orthopaedic implants has been shown to be orders of magnitude higher than the naturally occurring field inhomogeneity in biological material. As a result conventional MRI techniques cannot eliminate completely the artifacts associated with metallic implants. This is a particular challenge for RT planning as CT images also suffer from streak artifacts in the presence of metallic implants. In extreme cases MR-CT registration can be compromised [118].

MRI machines manufacturers have responded to this problem by offering specialist MR techniques to minimise the signal loss. This is achieved in part by high imaging gradients, as previously described. In addition, through plane and in-plane distortions are compensated for with further encoding. The resulting images do minimise signal loss, but often at a cost of increasing the total acquisition time. In some cases, specialist techniques introduce some image blurring. These techniques require validation prior to further use in RT planning but merit further investigation, as they can provide a more reliable MR-CT fusion in the vicinity of metallic implants [119].

# CHAPTER IV :

## MRI Contribution in Glioblastoma radiotherapy treatment planning and delivered dose conformity

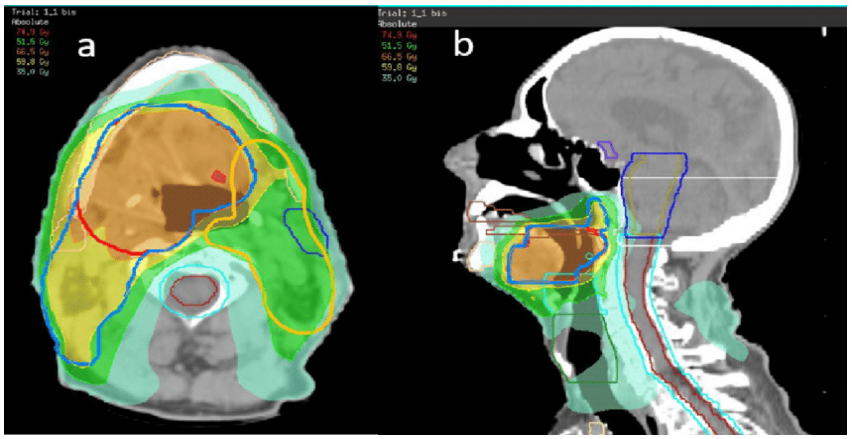

## I. Background & objectives of the thesis project

Radiotherapy plays a major role in the treatment of cancer. 3D conformal radiotherapy technique used in this work aimed to deliver the prescribed dose to the tumor volume by sparing the surrounding tissues and organs. Thus, lot of information on tumor and organs at risk (OAR) volumes are necessary to avoid any over dose or inacceptable dose uncertainty. X-ray computed tomography (CT) is the main imaging modality used for radiotherapy treatment planning and different volumes and structures delineation. Unfortunately, CT, in case of brain cancer, cannot provide information on low density tissues in comparison with magnetic resonance imaging (MRI). Indeed, MRI is able to provide high-resolution anatomical and structural image and details on the extension of the tumor and its impact on adjacent organs by using some specific MRI sequences. Glioblastoma is the most common brain cancer among adults. It is caused by an abnormal proliferation of central nervous system cells called astrocytes. With radiotherapy these cancer cells are destroyed or their development is stopped by exposing them to ionizing radiation. Radiotherapy is often prescribed after surgery. This technique is also used as the main treatment combined with chemotherapy when the tumor is not operable. In order to optimize the results of the treatment, the used beams ballistic is finely planned in order to specifically target the tumor and to avoid side effects. Thus, the contouring phase is crucial to achieve such objective. Indeed, many contouring models were proposed based on clinical tumor volume (CTV) and edema delineation. In this work, we focused on the contribution of MRI in radiotherapy treatment planning and, particularly, its role in the visualization and delineation of the gross tumor volume (GTV), the programmed target volume (PTV), and the OARs for patients suffering from Glioma. The necessary CT/MRI image registration and fusion are sometimes and for a specific case of radiotherapy treatments so difficult to be performed in respect to the recommended conditions by Khan [120] and Barett et al. [121]. The related issues of such technical limitations are studied in this work. This work concerns only rigid registration because non-rigid registration remains relatively not used in radiotherapy planning though some very interesting approaches are under development. Many registration and fusion assessment metrics are proposed in this work to help clinicians to do accurate delineation. In this study, *Eclipse* treatment planning system (TPS) and *Elastix* rigid registration methods were studied and compared for a specific case of Glioma radiotherapy treatment. The comparison was performed in terms of volume delineation and dose calculation based on external and independent metrics.

# II. Material & methods

This work is divided on two parts. The first part will focus on the parameterization and evaluation of multimodal registration techniques based on Elastix code for the registration and Plastimatch for the evaluation using different dice (Jaccard, Dice and Hausdorff). Also, and using same Evaluation codes we will compare our registration performed with Elastix to the 3 (Manuel, automatic and semi-automatic) performed with Eclipse Software from Varian System at CLCC of Setif. In the second part, we will show the importance of MRI images in delineation of tumour and OARs to improve the quality of treatment in Radiotherapy.

## II.1 Material

### II.1.1 Varian Eclipse TPS

Eclipse is a comprehensive treatment planning system that simplifies modern radiation therapy planning for all kinds of treatment, including 3D conformal, intensity-modulated radiation therapy (IMRT), electron, proton, and brachytherapy. With the rich functionality in Eclipse, dosimetrists, physicists, and physicians can efficiently create, select, and verify the best treatment plans for their patients. In addition to ensuring high standards of care and effective protocols, Eclipse provides clinicians with the flexibility to quickly tailor plans for each patient. Designed to meet the needs of modern clinics and evolving technologies, Eclipse supports advanced processes such as image-guided radiation therapy (IGRT) and Dynamic Adaptive Radiation Therapy (DART). The efficiency and cost effectiveness of Eclipse enables growing clinics to adopt advanced techniques, protecting investments while improving the quality of care. The treatment planning system used in this work is the Varian Eclipse version 11.0.31. This System offer many tools for many features, Registration, fusion, segmentation, dose calculation and treatment planning Tools. The dose calculation algorithm used within this system is the Anisotropic Analytical Algorithm (AAA).

In order to be able to carry out this work, a knowledge and a perfect mastery of the eclipse treatment planning System as well as of the workflow (Figure IV.1) of the treatment was necessary.

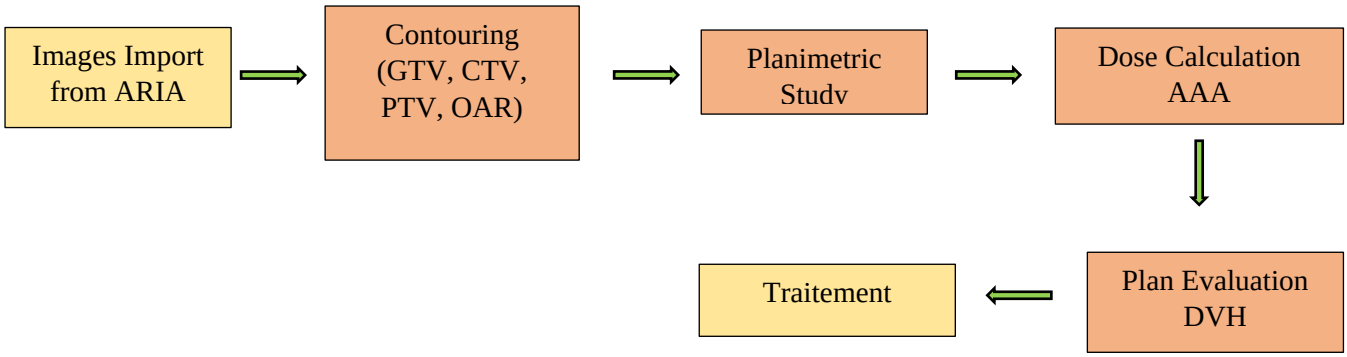


Figure IV.1: Radiotherapie Planning Treatement Work Flow on Eclipse

### II.1.1.1 Contouring

For RapidArc, IMRT, 3D conformal, and proton therapy planning, segmenting organs at risk and accurately delineating target volumes are critical (Figure IV.2). The powerful contouring tools in Eclipse reduce structure segmentation time from hours to minutes. Clinicians can accurately define targets and organs at risk on fused multimodality images with advanced drawing and editing capabilities. Enhanced templates and powerful post-processing of structures accelerate the contouring process.

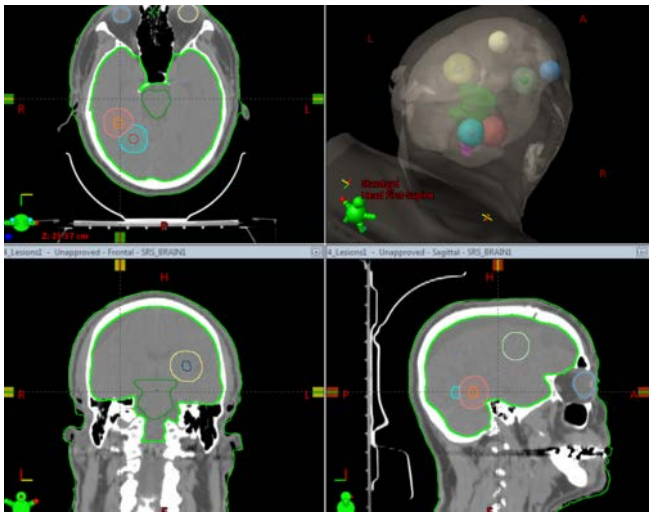

Figure IV.2: Eclipse contouring example on head Cancer

### II.1.1.2 Planimetric Study

Treatment planning with Eclipse is a complex process; physicists throughout the department of CLCC of Setif with the right experience accomplish this task. Creating a set of fields enveloping the target volumes and sparing the OARs thanks to the different angulation, direction, subfields or bolus (Figure IV.3).

Eclipse integrates virtual simulation and treatment planning in one comprehensive system. Virtual simulation and planning processes are accelerated through excellent segmentation software that includes:

- Comprehensive clinical protocol templates
- Automatic field positioning
- Hot-keys
- Automatic field aperture shaping with a flexible interactive user interface.

Eclipse can create 3D patient models from any DICOM 3.0-compliant image set, including CT, MR, and PET.

In our work, the same steps were followed for both CT and FUSION image series:

- Same number of fields
- same angulation
- optimization of the dose on target volumes
  Dose minimization on OARs

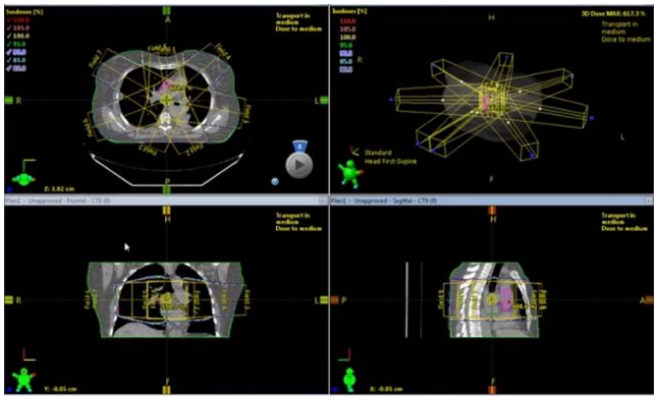

Figure IV.3: Eclipse contouring example on head Cancer

### II.1.1.3 Dose Calculation

After the treatment fields are designed with appropriate beam angles, lateral, distal, and proximal margins or beam-specific targets, customized apertures, and compensators, the next step is the dose calculations. Advanced algorithms in Eclipse accurately and quickly calculate dose distributions for photons, electrons, protons, and brachytherapy. With the combination of modular algorithms and the flexible architecture of Eclipse, clinicians can select the optimum algorithm for each treatment modality. The clinician can rapidly customize IMRT plans using the interactive dose-volume optimization. A flexible calculation framework increases efficiency in the treatment planning process, particularly in a distributed planning environment.

In this work, Dose calculation is based on Analytical Anisotropic Algorithm (AAA).

#### A. Analytical Anisotropic Algorithm

The AAA algorithm is a 3D pencil-beam convolution / superposition algorithm that uses separate Monte Carlo-derived modelling for main photons, extra-focal scattered photons, and electrons scattered from beam-limiting devices. The lateral dose deposition characteristics are modelled using six exponential curves. The functional forms of the basic physical expressions of the AAA algorithm allow analytical convolution, which significantly reduces computation times.

Significant improvements have been made to the AAA dose calculation algorithm in the field of processing machines and tissue heterogeneity modelling, as well as in the optimization of the accuracy of scattered dose calculations.

The AAA algorithm ensures anisotropic heterogeneity of tissues throughout the three-dimensional neighbourhood of an interaction site using nuclei that scatter photons in multiple lateral directions. The final dose distribution is obtained by superimposing the convolutions of photons and electrons on the calculated dose.

The clinical implementation of the AAA algorithm is subdivided into two secondary algorithms:

**A.1 Configuration algorithm:** determines basic physical parameters required to perform dose calculation.

**A.2 Dose Calculation Algorithm:** Calculates the dose deposition using fundamental physical parameters. These parameters characterize the fluences of particles and the energy spectra of the photons and electrons from which the clinical beam is formed.

### II.1.1.3 Plan Evaluation

Plan evaluation is an important step of RT treatment planning. It consists of slice-by-slice inspection of the dose coverage to the target and evaluation of dose volume metrics for OAR. Eclipse TPS provides both the DVH curves and the dose statistics for this purpose (Figure IV.4). Various tools are available to inspect the DVH curves for specific DVH metric. Eclipse TPS also allows the planner to view multiple plans using a multiplan window. Dose distribution in orthogonal planes can be visualized and compared, and DVHs of multiple plans can be displayed.

At Setif Hospital, oncology team can decide on the most effective course of treatment for each patient by comparing different plan modalities. Using Eclipse, clinicians can combine, compare, and evaluate different candidate plans and even different treatment modalities on a single integrated system. When Eclipse workstations are distributed throughout a clinic, plans can be evaluated anywhere and anytime, greatly speeding the planning process.

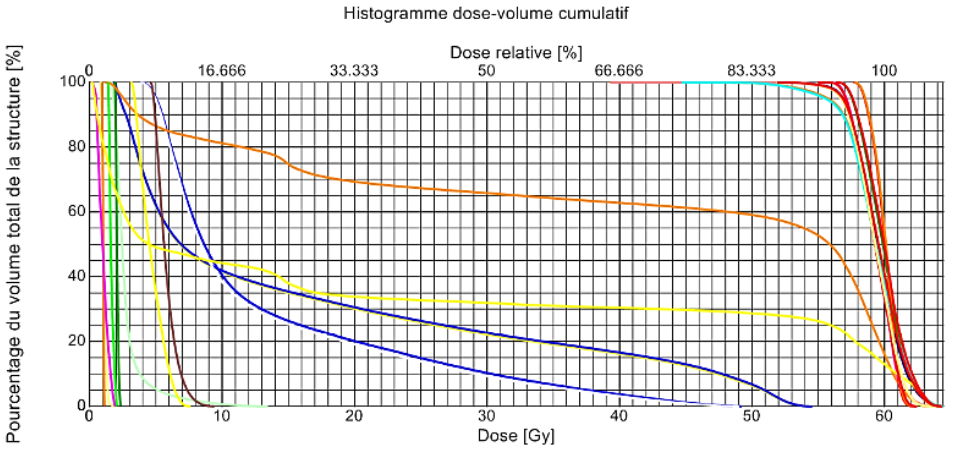


Figure IV.4: Dose Volume Histogram example for plan evaluation in eclipse TPS

**Dose Volume Histogram**

The dose-volume histogram (HDV) displays the 3D Complex dose distribution as a two-dimensional graph. HDV reveals uniformity of doses delivered to all facilities and is an ideal tool for evaluating dose distributions from various plans.

It is possible to plot multi-structure HDVs from a single Treatment planes (single-plan HDV) in the same graph. Likewise, multi-structure HDV curves can be drawn in the same graph from multiple planes (multi-plan HDV). In the Radiotherapy Planning application, it is possible to calculate a dose-area histogram for any slice.

The types of HDV available are:

- Cumulative
- Differential

### II.1.2 Image registration software and tools

#### A. Eclipse TPS software

In this work, several codes and software were used to perform and to assess different registrations. Four patient cases were considered in this study covering a wide variety of Glioblastoma localisation. For each image registration, a new dose calculation was performed using Varian Eclipse TPS. Comparisons between registrations were then performed in terms of treatment plans (doses), and tumour and structures volumes.

#### A.1 Image registration in Varian Eclipse TPS

The Varian TPS (11.0.31) offers several possibilities for clinicians to perform image registration, allowing them to achieve good registration and processing. Registration applications meet clinical requirements for multimodal image alignment for treatment planning and are used daily at Hospital of Setif.

In the field of radiotherapy, registration from a clinical point of view remains complex and time-consuming tasks. In addition, in many cases, data from different imaging modalities must be considered and verified to allow proper alignment. The Registration module provides tools for conveniently viewing and aligning multimodal images to enhance treatment-planning support. This offers the possibility of evaluating the changes that occur, during treatment, in the position of the organs and the patient's anatomy.

### A.2 Image registration methods and tools of Varian Eclipse TPS

Varian Eclipse TPS (11.0.31) used the following rigid registration methods.

#### A.2.1 Automatic Registration

One of the methods of image registration is to let the application calculate the registration using data from the DICOM coordinate system and the UID FOR DICOM attribute, found in the image sets. The registration is carried out by aligning the origins of the DICOM coordinate system saved at the level of the images by the imaging system. This type of registration is easy to perform and does not take much time.

#### A.2.2 Manual Registration

Eclipse's Registration applications provide tools for manually adjusting a rigid registration between volumetric images. Alignment tools can be used to translate and rotate a source image to align structures in the source image with visual features in the target image. A manual comparison can be used to perform a coarse alignment before the automatic registration of images or to refine an existing registration.

#### A.2.3 Hybrid Registration

The Point Match feature aligns two 3D images of similar or different modalities (CT, PET, and MRI) of a patient. It uses registration markers placed manually at specific anatomical landmarks to define the transformation between the two image coordinate systems. The

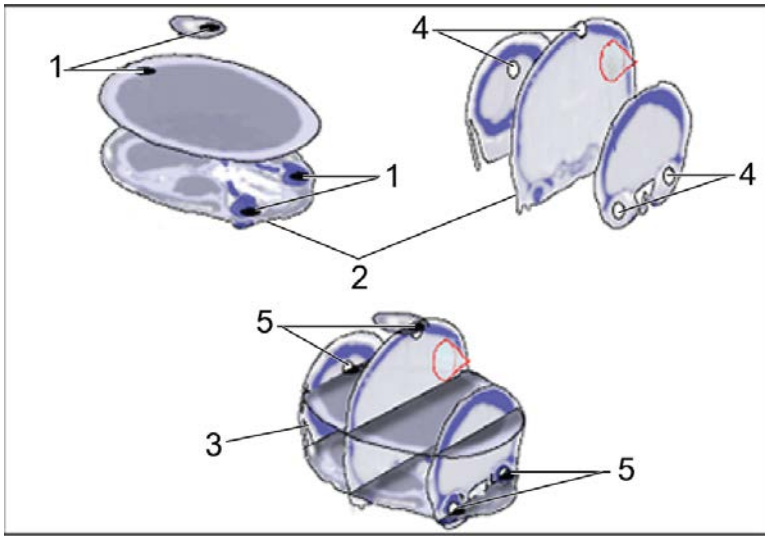


Figure IV.5 : Hybride Registration Principe

Following Figure IV.5 illustrates how user-defined registration points are used to align two 3D images.

1. Registration markers placed manually on the set of CT images

2. Original images (CT)

3. Moved images (MRI)

4. Registration markers placed manually on the set of MRI images

5. Aligned registration markers for CT and MRI images

Registration markers are arranged on specific anatomical landmarks or on user-defined "artificial" landmarks on the source and target images. When starting the point comparison, the default number of pairs of registration markers is automatically displayed on the two images. To perform the point comparison, a minimum of three pairs of markers must be positioned on both images. A maximum of 20 markers can be defined.

The accuracy of the registration depends on the accuracy of the positioning of the individual markers. Therefore, positioning multiple markers provides adequate registration for all image content and reduces any operator-caused error due to an individual marker positioning error. Markers should be positioned tri-dimensionally (top, bottom, left and right) on each image by dragging and dropping each marker over the marks chosen in multiple views of the source image and to the corresponding positions of the target image. Bone, organ or implant markers can be used as benchmarks for registration markers. The choice of a benchmark can influence the precision of the comparison.

**A.3 Architecture of the registration algorithm**

In Registration Tools, a common Varian application architecture is used for rigid registration. The user can flexibly configure the modular design of this tool. Rigid registration is essentially an optimization problem where the alignment of two 3D images must be optimized. The most important modules are the similarity measure, which compares the two volumes in the current alignment and the optimization system, which tests a multitude of different adjacent alignments to finally select the one offering the best result in terms of similarity.

The components and modules of the rigid registration architecture and their interconnections are displayed in Figure IV.6.

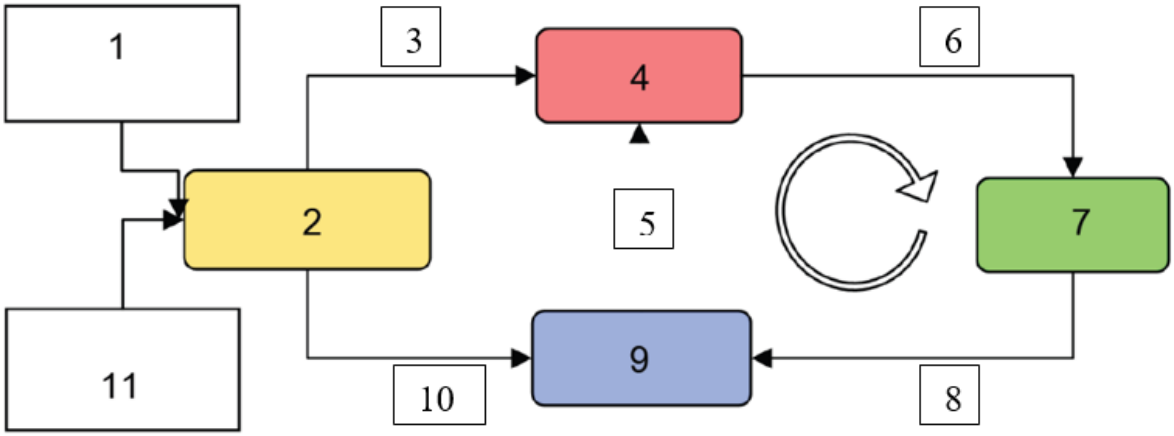


Figure IV.6: Rigid registration architecture in Varian TPS

1. Target image pixels
2. Pretreatment (optional)
3. Pixel preprocessing of the target image
4. Similarity
5. Preprocessing of the pixels of the source image, interpolated
6. Similarity value
7. Optimizer
8. Transformation parameters
9. Interpolator
10. Source image pixel preprocessing
11. Pixels of the source image

The basic idea of this architecture is to allow the user to apply different types of optimization systems, similarity measures, pre-processing tools and interpolators. Several sets of parameters can be saved and loaded. All available sets have been preconfigured. However, the user can modify and save settings for later use. Default settings can be restored, allowing the user to change settings without losing the default sets.

Each configuration (set of parameters) comprises a series of distinct adjustment steps, each capable of using a different combination of certain parameters (modules, internal resolutions and tolerance values). During registration, the displacement resulting from each step is automatically supplied as input to the next step. The internal resolution generally increases for the following steps, which corresponds to a multi-resolution approach. It is often used for resetting in order to increase the speed and reduce the risk of the optimization system jamming

on local minima. The following sections briefly describe the modules available in the Eclipse systems registration architecture:

### A.3.1 Similarity measures

The similarity component is used to assess how well the source and target images match the specified region of interest. The following similarity measures are available:

Mutual Information

Pattern Intensity

Cross Correlation

### A.3.2 Optimization systems

The optimization system is used to find the maximum (or minimum) of the similarity cost function. The optimization algorithms available are as follows:

- ✓ Downhill Simplex (Nelder-Mead Method),
- ✓ Direction Set,
- ✓ Gradient Descent,
- ✓ Exhaustive Search.

### A.3.3 Interpolator

The interpolator is used to sample the superimposed points of the input images, which are available in the form of multi-resolution pyramids in order to guarantee an anti-aliasing quality. Linear interpolation is the interpolation used by default.

### A.3.4 Pre-treatment program

You can use image pre-processing to modify the characteristics of the N-dimensional function whose minimum (or maximum) must be found. The available pre-treatment filter cores are:

- ✓ Gaussian (Gaussian),
- ✓ Laplacian or Gaussian (Laplacian or Gaussian).

### B. Elastix software

### B.1 Presentation

Elastix is image registration software. The authors use it in their research on medical image data alignment, but it can be used for all types of images. It is composed of numerous registration methods, composed of different transformation models (rigid, affine, non-rigid), of similarity measures (for example mutual information), of optimization methods (gradient descent), of methods of interpolation (nearest neighbor, linear, cubic). Components can be implemented to allow the user to configure their own registration methods.

Elastix is used through command lines, but also through a library interface. Most configuration parameters are defined in a parameter file. This makes it possible to use scripts that perform resets with different parameters, on large image databases, in a fully automatic manner. In this way, the effect of each parameter can be studied in depth and different methods can be compared systematically. Since 2015 bindings are available in the most popular scripting languages, so as to provide user friendly access to many common image recording algorithms, making elastix available in languages such as C ++, Python, Java , R, Ruby, Octave, C # and Lua. Example of command line is showed on Figure IV.7.

```
F:\test et presentation\elastix>elastix -f "image CT .nii.gz" -m "Image IRM .nii.gz" -p "fiche de parametre.txt" -out "out image apres recalage"

elastix is started at Tue May 08 11:47:57 2018.

which elastix:   elastix
elastix runs at: DESKTOP-9LHPR32
  Windows  Professional (x64),  (Build 9200)
  with 8084 MB memory, and 0 cores @ 2591 MHz.
------------------------------------------------------------------------

Running elastix with parameter file 0: "fiche de parametre.txt".

Current time: Tue May 08 11:47:57 2018.
Reading the elastix parameters from file ...

Installing all components.
InstallingComponents was successful.

ELASTIX version: 4.800
Command line options from ElastixBase:
-f        image CT .nii.gz
-m        Image IRM .nii.gz
-fMask    unspecified, so no fixed mask used
-mMask    unspecified, so no moving mask used
-out      out image apres recalage\
-p        fiche de parametre.txt
-priority unspecified, so NORMAL process priority
-threads  unspecified, so all available threads are used
Command line options from TransformBase:
-t0       unspecified, so no initial transform used
```

Figure IV.7: Example of command line and input for Elastix

### B.2 Elastix structure and workflow

Large parts of the Elastix code are based on ITK (Insight Segmentation and Registration Toolkit). This open source C ++ library defines a framework into which almost any registration method can be incorporated. Elastix is a kind of "wrapper" around ITK components. He ensures that the right parameters are defined at the right time and ensures that the results are saved. Like ITK, Elastix also uses CMake to manage the build process. In addition, some ITK-type components have been written to add registration techniques not implemented in ITK.

ITK's modular structure was adopted. The Elastix source code is structured according to the components that can be distinguished in a registration structure, such as metrics, optimizers, transformation models and interpolators. The components are made known by elastix-core, which takes care of initiating the components and connecting them correctly. Each component itself knows the parameters that it must read in the parameter file and the elements to be displayed on the screen and / or recorded on the disk. This implies that if new components are added, the core of Elastix is unchanged. Thus, new ITK components can be easily integrated Elastix.

### B.3 Registration parameterization in Elastix

The registration on Elastix must be correctly configured; it is based on the use of a parameter sheet, which groups together all the components necessary for an alignment of two images, Table IV.1 shows a list of the most important components to be specified in the parameter sheet. Workflow architecture for ELASTIX registration is showed in figure IV.8.

Table IV.1: List of the most important registration parameters of the ELASTIX.

| Component | Role of the component |
|---|---|
| Registration | Connect all the components and implement the multi-resolution aspect of the registration |
| Image Pyramid | preprocessing of target and source images before registration (smoothing or sub-sampling) |
| Metric | measure the statistical dependence of the two images |
| Sampler | samples some or all pixels of the image |
| Interpolator | evaluation of the intensity at non-pixel position of the motion image (necessary for optimization) |
| Transform | Type of Transformation Rigid/Elastic |
| Optimizer | Optimization Parameter for the Minimum Cost |
| Re-sampler | Generates the distorted image after registration |

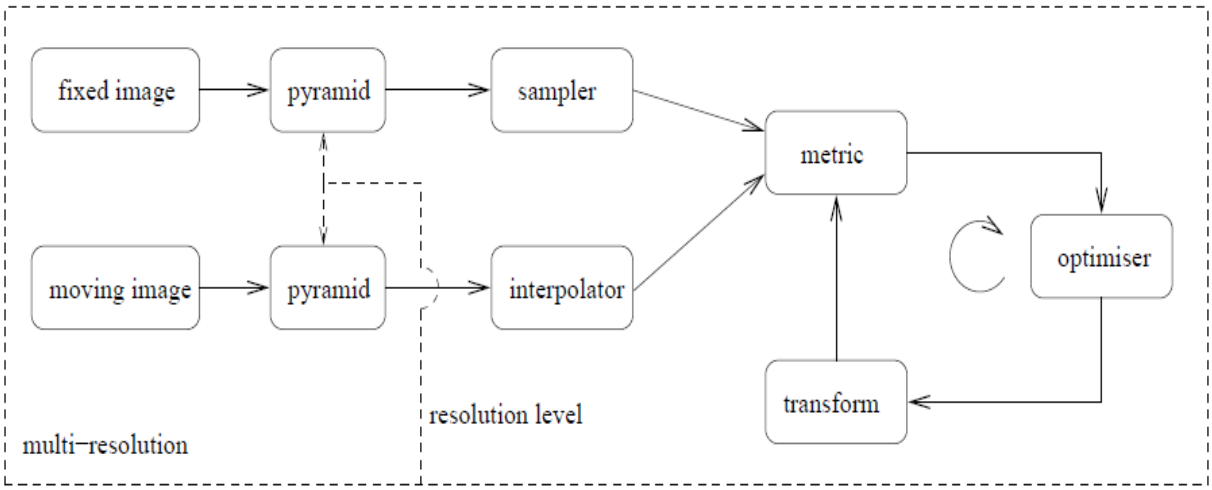


Figure IV.8: Workflow architecture for ELASTIX registration

### II.1.3 Registration evaluation tools

In this work, the registration results were evaluated qualitatively and quantitatively. For qualitative evaluation, Visual Tools were used and in our case ITK-SNAP, for the quantitative comparison three metrics were considered: the Dice score coefficient (DSC), the Jaccard similarity coefficient (JSC), and the Hausdorff distance (HD).

#### II.1.3.1 Qualitative registration assessment tools

ITK-SNAP is a software application used to segment and evaluate registered structures in 3D medical images (Figure IV.9).

ITK-SNAP provides semi-automatic segmentation using active contour methods, as well as manual delineation and image navigation. In addition to these core functions, ITK-SNAP offers many supporting utilities. Some of the core advantages of ITK-SNAP include:

- Linked cursor for seamless 3D navigation,
- Manual segmentation in three orthogonal planes at once,
- Support for many different 3D image formats, including NIfTI and DICOM,
- Support for concurrent, linked viewing, and segmentation of multiple images,
- Support for color, multi-channel, and time-variant images,
- 3D cut-plane tool for fast post-processing of segmentation results,

- Extensive tutorial and video documentation.

Compared to other, larger open-source image analysis tools, ITK-SNAP design focuses specifically on the problem of image segmentation, and extraneous or unrelated features are kept to a minimum. The design also emphasizes interaction and ease of use, with the bulk of the development effort dedicated to the user interface.

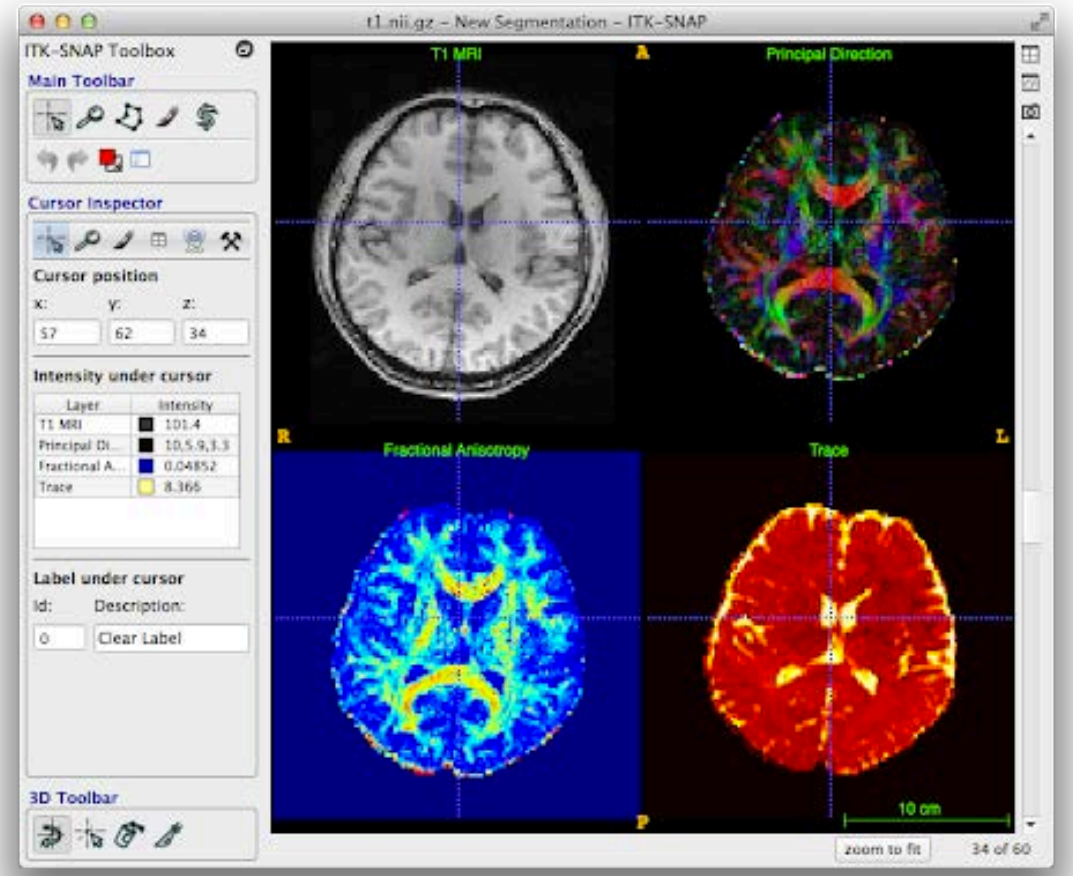


Figure IV.9 : ITK-SNAP interface

### II.1.3.2 Quantitative registration assessment tools

The Dice score coefficient is based on the Sorensen-Dice similarity coefficient that measure the overlapping between two binary structures (A and B) with the following equation:

$$DSC = \frac{2|A \cap B|}{|A| + |B|} \quad \text{(IV. 1)}$$

The DSC ranges from 0 to 1 where 0 indicate no overlapping, and 1 full overlapping.

The Jaccard similarity coefficient is a statistical measurement of the similarity between two sample sets (A and B). It is defined as the cardinality of their intersection divided by the cardinality of their union and given by the following equation:

$$JSC = \frac{|A \cap B|}{|A \cup B|} \quad \text{(IV.2)}$$

The JCD ranges from 0 to 1 where 0 means no overlapping, and1indicates a full overlapping.

The Hausdorff distance is an evaluation of the distance between two graphic surfaces. If *X* and *Y* are two surfaces and $d(x, y)$ is the Euclidean distance between two points *x* and *y* from X and *Y* respectively, the HD is then given by the following equation:

$$d_H(X,Y) = (\underbrace{sup}_{x\in X}\ \underbrace{inf}_{y\in Y}\ d(x,y), \underbrace{sup}_{y\in Y}\ \underbrace{inf}_{x\in X}\ d(x,y) \quad \text{(IV.3)}$$

The HD is measured in mm and ranges from 0 (identical surfaces) to $+\infty$.

For this evaluation several code are used and combined on Plastimatch code.

Plastimatch is a computer software application, which has been designed for volumetric (usually medical) image processing and radiation therapy applications. It can be used for the following purposes:

1) Deformable registration
2) Atlas-based segmentation
3) Image conversion and manipulation
4) Vector field conversion and manipulation
5) Gamma analysis
6) Dose calculation
7) Registration analysis (Jacobian)
8) Segmentation analysis (Dice, Hausdorff)
9) Many other things

In this study, Plastimatch will be used for the evaluation of the various adjustments carried out with specific metric. It is performed using a command line where it is necessary to enter the name of the software, the type of function applied and on which file to perform it, an example is showed on Figure IV.10.

```
F:\test et presentation\plastimatch>plastimatch dice --hausdorff "image CT.nii.gz" "Image IRM .nii.gz"
Hausdorff distance = 857.320801
Avg average Hausdorff distance = 716.680542
Max average Hausdorff distance = 726.953552
Percent (0.95) Hausdorff distance = 807.700256
Hausdorff distance (boundary) = 857.320801
Avg average Hausdorff distance (boundary) = 686.645264
Max average Hausdorff distance (boundary) = 728.073975
Percent (0.95) Hausdorff distance (boundary) = 807.080933
```

Figure IV.10: Example of command line and input for Plastimatch

### II.1.4 Used registered imaging modalities

This study was performed on four patients. The CT and MRI data were collected around Siemens SOMATOM AS high definition CT-scanner and 1.5T GE Optima MR450W MRI machine respectively. According to the protocol usually used for cerebral acquisition with a reconstruction resolution and a voxel spacing as indicated on Table IV.2.

Table IV.2: Imaging modalities and reconstructed image sampling.

| | | Mode | Patient 1 | Patient 2 | Patient 3 | Patient 4 |
|---|---|---|---|---|---|---|
| **CT** | **Dimension** | Cerebral | 512X512X71 | 512X512X74 | 512X512X74 | 512X512X74 |
| | **Voxel Spacing (mm)** | | 0,48X0,48X3 | 0,48X0,48X3 | 0,48X0,48X3 | 0,48X0,48X3 |
| **MRI** | **Dimension** | T1 Gd | 512X512X296 | 512X512X250 | 512X512X264 | 512X512X37 |
| | | T2 Flair | 512X512X45 | 512X512X34 | 512X512X49 | 512X512X37 |
| | **Voxel Spacing (mm)** | T1 Gd | 0,46X0,46X0,7 | 0,46X0,46X1 | 0,46X0,46X1 | 0,46X0,46X5 |
| | | T2 Flair | 0,46X0,46X5 | 0,46X0,46X5 | 0,46X0,46X5 | 0,46X0,46X5 |

## II.2 Methods and procedures

### II.2.1 Patients selection, imaging data collection and treatment planning

This study was carried out on four patients admitted for Glioma brain tumor (Table IV.3). The CT and MRI data were collected around Siemens SOMATOM AS high definition CT-scanner and 1.5T GE Optima MR450W MRI machine respectively. The radiotherapy TPS used is the Varian *Eclipse* 11.0.31. The dose calculation algorithm used is the anisotropic analytical algorithm (AAA). The MRI sequences used are the T2-weighted flair sequence for the visualization of Edema and the T1 sequence with Gadolinium contrast agent injection for the visualization of the tumor.

Table IV.3: Studied cases.

| | **Patient 1** | **Patient 2** | **Patient 3** | **Patient 4** |
|---|---|---|---|---|
| **PTV CT ($cm^3$)** | 448,3 | 519,8 | 328,5 | 297,9 |
| **PTV MRI ($cm^3$)** | 620,4 | 696,6 | 408,7 | 466,5 |
| **Tumor localization (x, y)** | Right posterior parietal (189,409) | Left parietal (273,303) | Right posterior parietal (171,338) | Right anterior (198,181) |

The accuracy of dose delivery and radiotoxicity optimization depends on the well different treatment volumes delineation. Although, dose calculation is based on electron density directly related to Hounsfield units (HU) measured on CT-slice, the CT cannot ensure in all cases the correct delineation of the treated volume and OARs. This can affect seriously the quality and the accuracy of the treatment plan. The used TPS allows the structures and principles volumes delineation on the basis other imaging modalities such as MRI in addition to CT described below. Thus, radiation tolerance of organs at risk is the main factor limiting the dose prescribed by the clinician. The OARs are, generally, divided into 3 categories: 1- very radiosensitive organs (eye, ovary, and testicle), 2- moderately radiosensitive (small intestine, heart, and lung) and 3) not very radiosensitive (bone, muscle, large vessels). On basis of their very important vital functions, some organs have to be protected first, while others are protected to just to maintain the quality of life after treatment (salivary glands, intestine, eye, bone). On Table IV.4 are indicated some dose constraints of some organs that must be respected during radiotherapy planning and treatment of brain tumors.

Table IV.4: Dose constraints for some organs in radiotherapy treatment of brain tumors

| Organ | Dose Constraint (Gy) |
|---|---|
| Optic chiasm | $D_{max}$ = 54 |
| Pituitary | $D_{max}$ = 45–50 |
| Larynx | $D_{max}$< 63–66 |
| Spinal cord | $D_{max} \leq 50$ |
| Optic nerve | $D_{max} \leq 54$ |
| Eyes-crystalline | $D_{max}$< 10–15 |
| Eyes-retina | $D_{average} \leq 45$ |
| Brain | $V_{60Gy}$< 33 % |

### II.2.2 CT/MRI Image registration and fusion

As defined in chapter II, multimodalities image registration is a geometrical process used in medical imaging to align two different images in order to bring together complementary information that are necessary to perform correct diagnosis and accurate volumes and structures delineation. The image registration consists of a set of spatial transformations (translation, rotation, scaling, sampling ...) to be applied to a targeted image in order to make it spatially aligned to a reference image. In this work, the necessary CT/MRI image registration and fusion was performed within the Eclipse TPS by using three tools: automatic, manual and hybrid (semi-automatic) registrations. These three registration tools used different similarity metrics, linear interpolators, registration optimizers, and three-dimensional image translation and rotation. Within the Eclipse TPS and for most cases, the CLCC's clinicians uses the rigid automatic registration based on mutual information similarity metric and Downhill simplex optimizer.Unfortunately, these image registration tools do not give same results within the same execution time. Therefore, depending on the considered treatment case, one Eclipse registration method might be more appropriate than another. In this work, the automatic registration is considered as a reference registration. In addition to the Eclipse registration tools and methods, the TPS independent Elastix image registration was also studied. Elastix registration is also used to evaluate the Eclipse image registration methods. Elastix registration uses the mutual information as similarity metric and the gradient decent as optimizer. After image registration with Elastix, Eclipse fuse the information of two images into a single one by selecting the suitable transparency and opacity parameters that give satisfaction to the radiotherapy clinician.

### II.2.3 Volumes and structures delineation

In this work guess and check method is used. Thus, the cyclic work is achieved through a close collaboration between radiotherapy clinician that performs CT/MRI image registration and fusion as well as different volumes and structures delineations and the medical physics that performs dose calculation. The procedure is repeated for each new CT/MRI image registration and fusion. The delineation of the tumor and the OARs was done first on CT-slices and then corrected on fused CT/MRI images according to the protocol of Glioma treatment described in chapter 3. The imaging modalities used for the delineation of the different volumes and structures of the studied cases are presented in Table IV.5.

Table IV.5: Reference delineation modalities for Glioma radiotherapy treatment.

| **Tumor's volumes and Organ at Risk** | **Modality of Delineation** |
|---|---|
| GTV | MRI |
| PTV | MRI |
| Edema | MRI |
| Chiasma | MRI |
| Pituitary | MRI |
| Optic nerve | MRI |
| Brainstem | MRI |
| Eyes | CT |
| Brain | CT |
| Crystalline | CT |

### II.2.4 CT/MRI Image registration and evaluation

In this study, Varian *Eclipse* TPS (11.0.31) and *Elastix* rigid registration methods described above were studied and compared for specific cases of Glioma radiotherapy treatment. The comparison was performed in terms of volume delineation and dose calculation based on external and independent metrics that were described in material section. Thus, for each CT/MRI registration a new treatment plans were recalculated.

### II.2.5 Planimetric Study

In this study, we followed the same steps Used by Setif hospital in normal conformational 3D RT treatment. The prescribed dose as well as the number and angulation of the arm and the accelerator table were the same for the same patients. Optimization of the treatment plan to deliver the maximum dose to the target volumes and the protection of OARs was carried out with the utmost care and precision than for real treatment. the ballistics used are shown in the Table from 6 to 9 and Figure From 11 to 14

Table IV.6: Field parameter Information for patient 1

| Field Name | Field Weighting | Arm Rotation | Collimator Rotation | Table Rotation |
|---|---|---|---|---|
| **Field 1** | 1.112 | 300 | 0 | 0 |
| **Field 2** | 1.267 | 125 | 0 | 0 |
| **Filed3** | 0.392 | 340 | 45 | 90 |
| **Sub-Field 1** | 0.147 | 300 | 0 | 0 |
| **Sub-Field 3** | 0.082 | 340 | 45 | 90 |

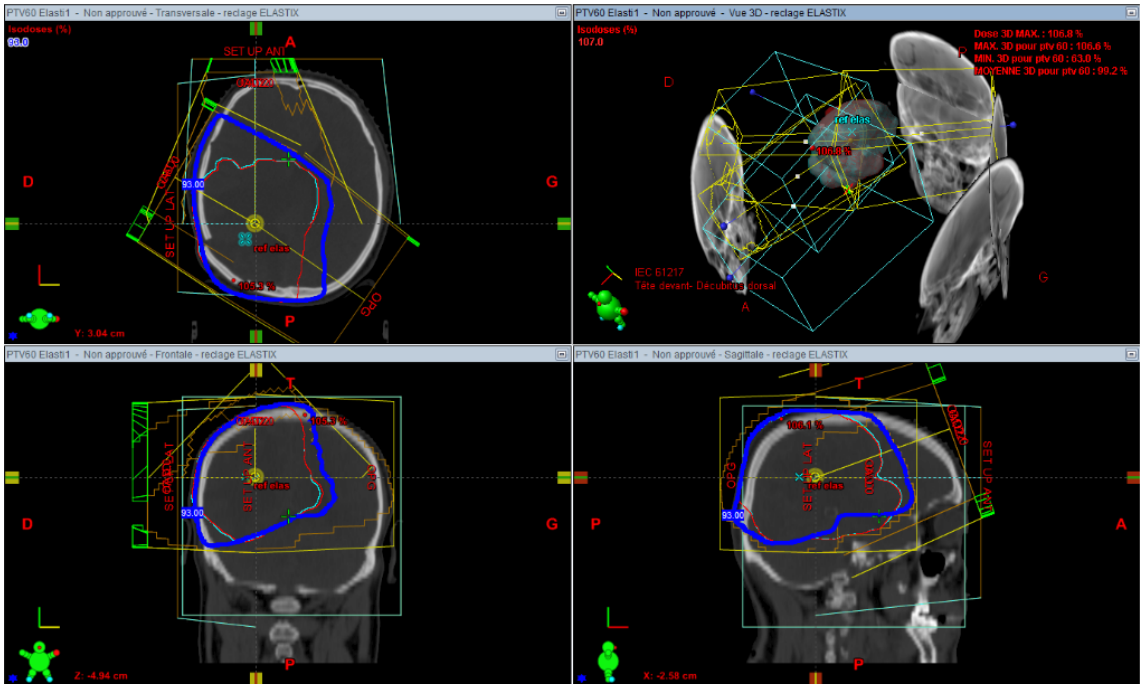


Figure IV.11: 2D and 3D field parametrisation for patient1

Table IV.7: Field parameter Information for patient 2

| Field Name | Field Weighting | Arm Rotation | Collimator Rotation | Table Rotation |
|---|---|---|---|---|
| **Field 1** | 0.189 | 40 | 0 | 270 |
| **Field 2** | 1.004 | 270 | 0 | 0 |
| **Filed3** | 1.250 | 90 | 0 | 0 |
| **Sub-Field 1** | 0.062 | 40 | 0 | 270 |
| **Sub-Field 3** | 0.094 | 90 | 0 | 0 |

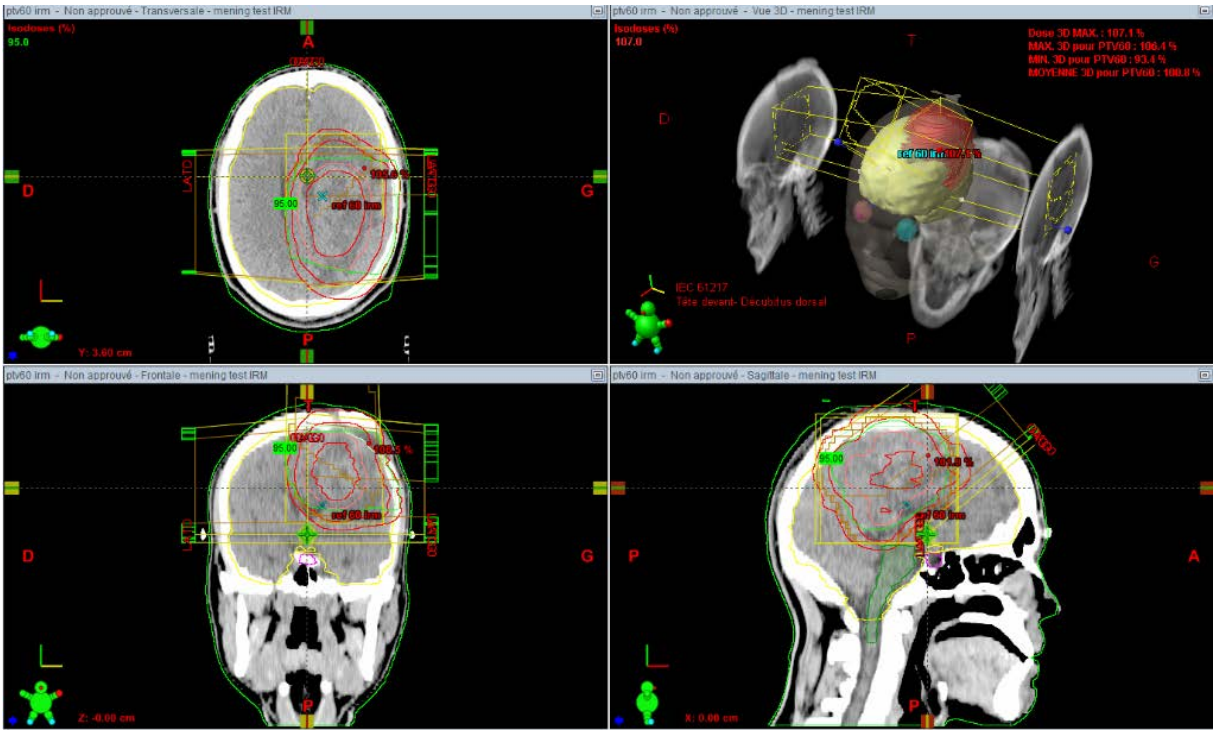


Figure IV.12: 2D and 3D field parametrisation for patient 2

Table IV.8: Field parameter Information for patient 3

| Field Name | Field Weighting | Arm Rotation | Collimator Rotation | Table Rotation |
|---|---|---|---|---|
| **Field 1** | 1.081 | 340 | 0 | 0 |
| **Field 2** | 0.403 | 40 | 0 | 270 |
| **Filed3** | 0.989 | 160 | 0 | 0 |
| **Sub-Field 1** | 0.084 | 340 | 0 | 0 |
| **Sub-Field 2** | 0.080 | 40 | 0 | 270 |
| **Sub-Field 3** | 0.062 | 160 | 0 | 0 |
| **Sub-Field 1.1** | 0.092 | 340 | 0 | 0 |
| **Sub-Field 3.1** | 0.072 | 160 | 0 | 0 |
| **Sub-Field 3.2** | 0.066 | 160 | 0 | 0 |

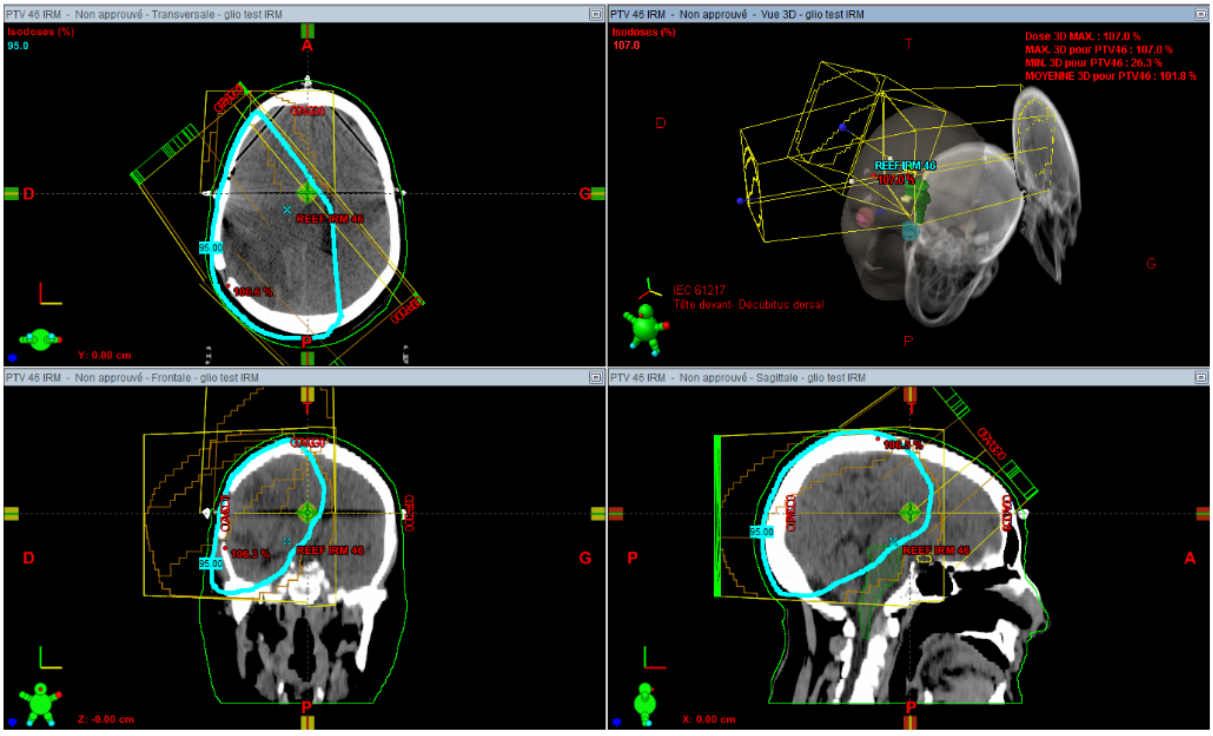


Figure IV.13: 2D and 3D field parametrisation for patient 3

Table IV.9: Field parameter Information for patient 4

| Field Name | Field Weighting | Arm Rotation | Collimator Rotation | Table Rotation |
|---|---|---|---|---|
| **Field 1** | 1 | 270 | 0 | 270 |
| **Field 2** | 1 | 90 | 0 | 0 |
| **Filed3** | 0.882 | 45 | 339.1 | 330 |
| **Filed4** | 1 | 215 | 30 | 330 |
| **Sub-Field 3** | 0.118 | 45 | 339.1 | 330 |

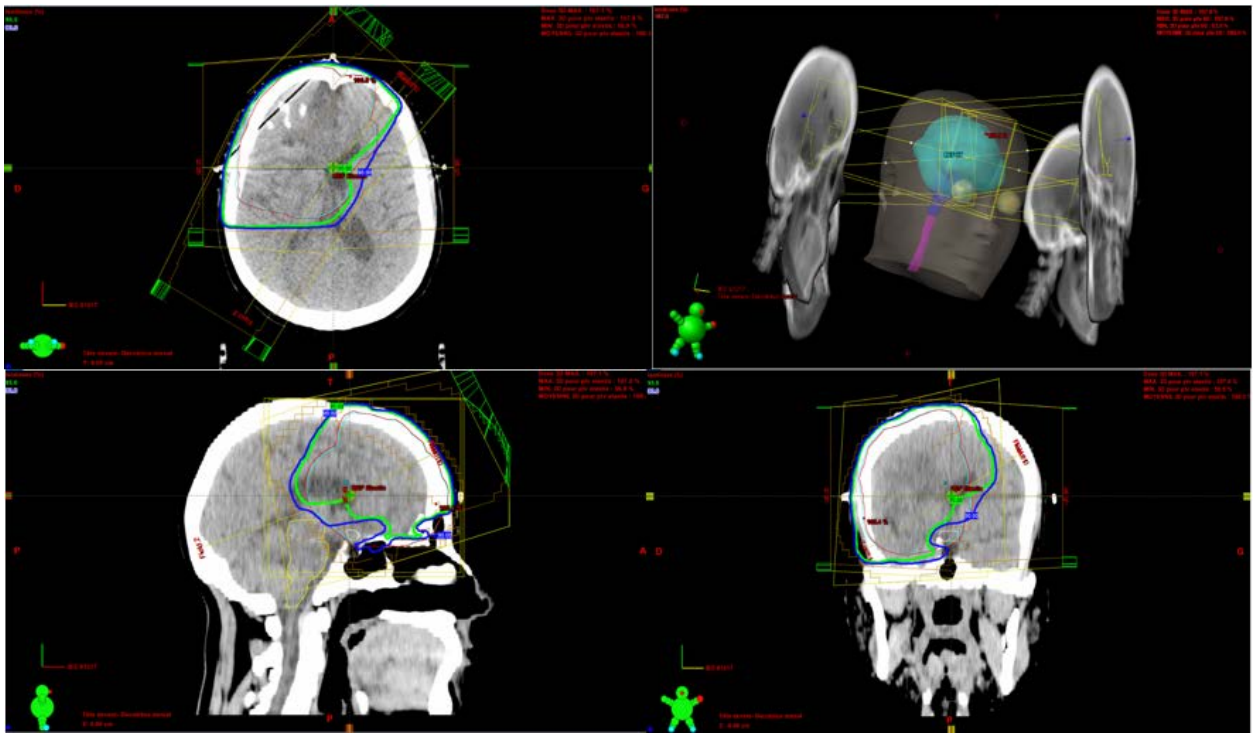

Figure IV.14: 2D and 3D field parametrisation for patient 4

### II.2.6 Parametrization of Elastic Registration

In this part, we are interested in the evaluation of the components included in an elastix registration sheet and in the best possible configuration. During this step we produced a specific parameter sheet for multimodal registration between MRI and CT. in order to evaluate the best parameter to carry out the registration, we proceed to several tests and changed all the components of the parameter file one by one until we conclude with the best possible Result. The components of the final configuration file are presented in Table IV.10.

Table IV.10: Final configuration parameter used on Elastix registration parameter file

| Component | Elastix Parameter |
|---|---|
| Image Pyramid | Smoothing Image Pyramid |
| Interpolator | B Spline Interpolator |
| Metric | Advanced Mattes Mutual Information |
| Optimizer | Adaptive Stochastic Gradient Descent |
| Transform 1 | Euler Transform |
| Image Sampler | Random Coordinate |

By taking into account the attributes of each image, we carried out a series of adjustments by changing the parameters of the two most important components, namely the number of iterations for the optimizer, which we varied between 100-1000 iterations and t between 100 and 6000 for samples number. More than 500 parameters sheet were performed to Conclude for the best one. The comparison of the resulting registrations was carried out using visual evaluation (Figure IV.15 and Figure IV.16) and two comparison indexes (Dice, Hausdorff). The best result was performed with 6000 sampler Number and 500 iteration as its shown on Table IV.11.

Table IV.11: Qualitative & Quantitative result for Elastix parameter file

| Iteration | Sampler | Dice Score | HD Distance | Visual evaluation |
|---|---|---|---|---|
| 100 | 100 | 0.900295 | 13.571147 | Really bad |
| 100 | 500 | 0.938431 | 17.737652 | Really bad |
| 100 | 1000 | 0.935822 | 19.461752 | Really bad |
| 100 | 2000 | 0.925831 | 23.911646 | Really bad |
| 100 | 3000 | 0.924984 | 24.48064 | Really bad |
| 100 | 4500 | 0.929519 | 29.702734 | Really bad |

| | | | | |
|---|---|---|---|---|
| 100 | 6000 | 0.926473 | 32.083912 | bad |
| 300 | 6000 | 0.910218 | 44.813877 | Good |
| **500** | **6000** | **0.960019** | **44.813877** | **Really good** |
| 600 | 6000 | 0.910035 | 44.775852 | good |
| 1000 | 6000 | 0.910095 | 44.726048 | good |
| 500 | 5000 | 0.910258 | 44.681435 | good |
| 500 | 3000 | 0.909990 | 44.842663 | good |
| 500 | 2000 | 0.910155 | 44.813877 | good |
| 500 | 1000 | 0.910855 | 44.169159 | good |

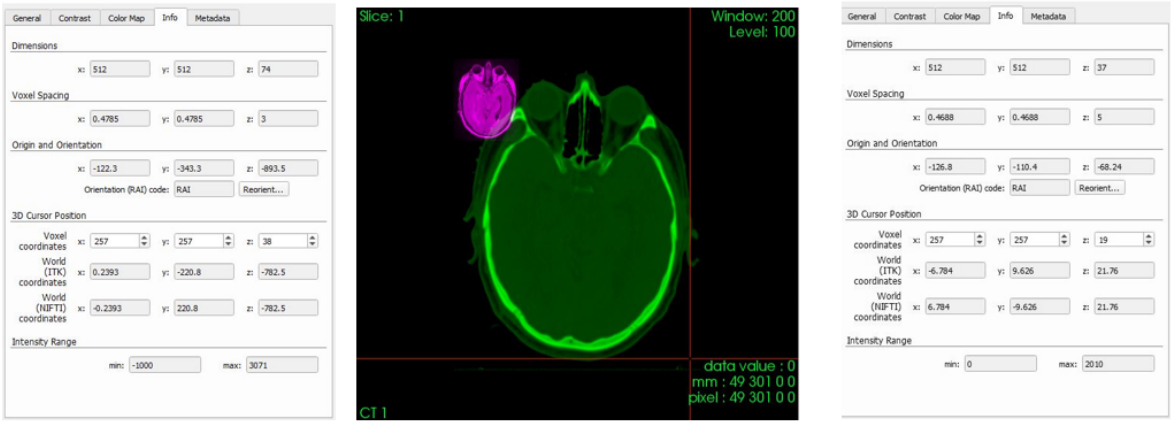


CT Informations Before Registration

Visual Evaluation of CT&MRI before Registration

MRI Informations Before Registration

Figure IV.15: Visual Evaluation of MRI and CT images Before Registration, where the two images are not on same plan and are not sharing any spatial Information


Figure IV.16: Visual Evaluation of MRI and CT images After Registration, where the two images on same plan, sharing same spatial Information and perfectly

# III. Results

## III.1 Evaluation and comparison between registration methods

The PTV's localization and shape of the image registration studied methods were compared to the TPS automatic registration results. The results on PTVs comparison are shown in Figure IV.17 For the visual assessment, clinician uses contrast and colour tools to evaluate the registration. Clinician's self-appreciations are presented on Table IV.12. It can be easily verified that a poor overlapping was observed for the case of hybrid registration, acceptable one for the manual registration and almost good overlapping for the *Elastix* registration.

Table IV.12: clinician visual evaluation for Manual Hybrid and Elastix Registration.

| Registration method | Evaluation | Recommendation for the studied case |
|---|---|---|
| Manual registration | Good | Suitable for experienced clinician |
| Hybrid registration | Bad | Not suitable |
| ELASTIX registration | Very good | Suitable for confirmation purpose |

The comparison between registrations methods on the basis of used metrics are presented in Figure 17 to 22. The PTV of the automatic registration is taken each time as a reference. The metrics comparison demonstrates clearly that the hybrid registration is the poor one in terms of exact volume and structure overlapping, a mean divergence is observed for the manual registration and almost a good registration similarity for the *Elastix* method. Comparison between re-calculated doses, based on these three registrations and new treatment planning, was also performed. According to the obtained results (Figure 17 to 22), the re-calculated doses of the *Elastix* registration were in good agreement with those of the automatic registration (reference). Thus, the *Elastix* registration was the best method followed by the manual registration which is better than the hybrid registration.

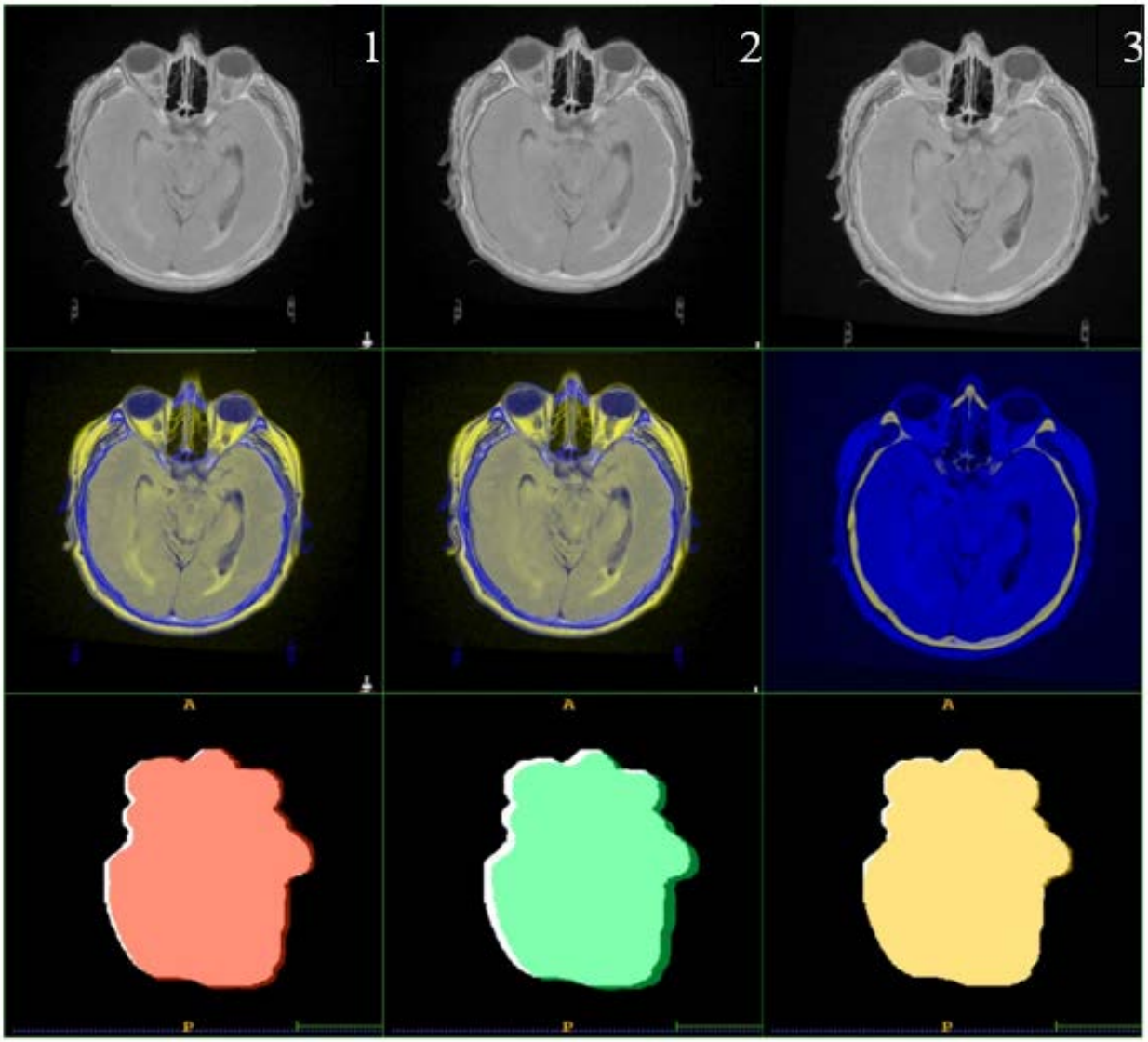


Figure IV.17: Qualitative registration evaluation (First and Second row). PTV's volumes overlapping of the three tested registration methods in comparison with the reference automatic registration (Third row) -Overlapping difference is in white color: 1. Manual, 2. Hybrid and, 3. *Elastix*-.

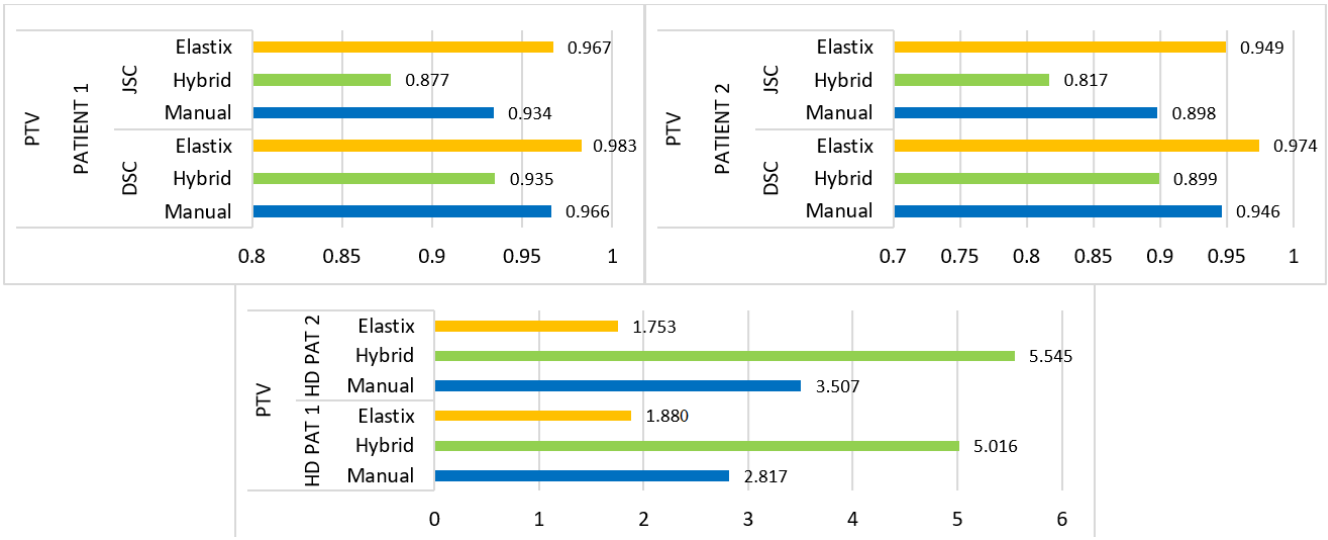


Figure IV.18: PTVs Comparison on fused images after manual, hybrid and elastix registrations suing DSC, JSC and HD metrics. The automatic registration is taken as reference.

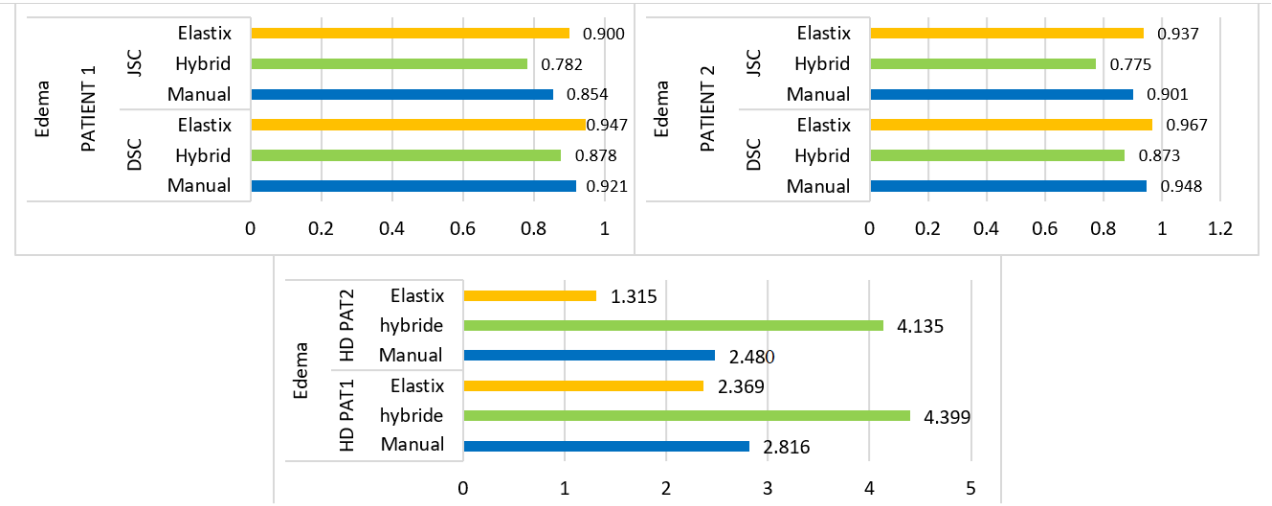


Figure IV.19**:** Edema Comparison on fused images after manual, hybrid and Elastix registrations suing DSC, JSC and HD metrics. The automatic registration is taken as reference.

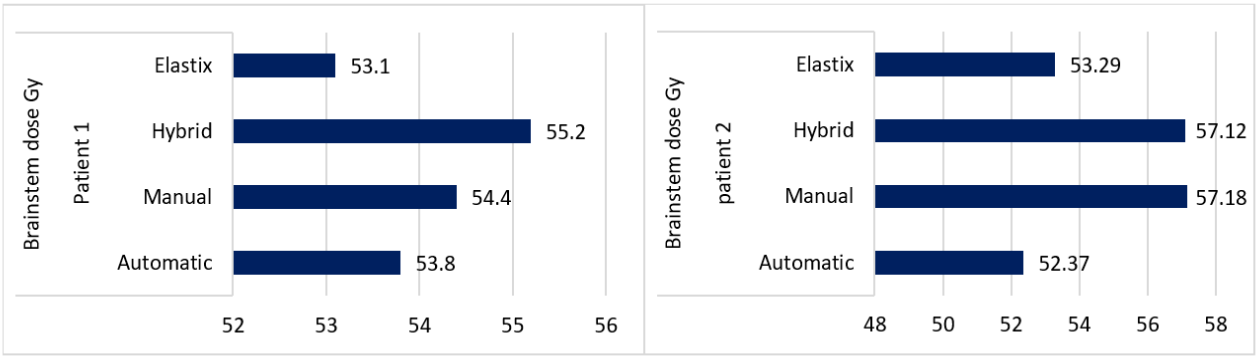


Figure IV.20: Recalculated doses to be delivered to brainstem for different registrations

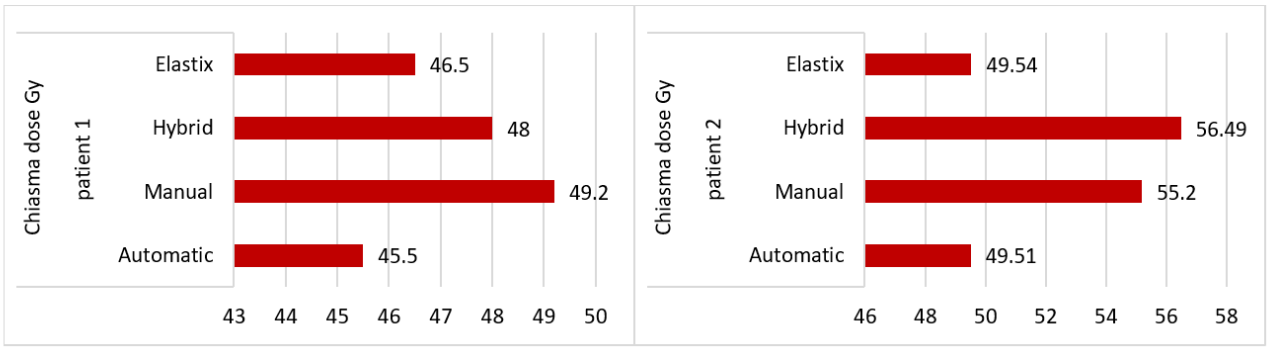


Figure IV.21: Recalculated doses to be delivered to Chiasma for different registrations.

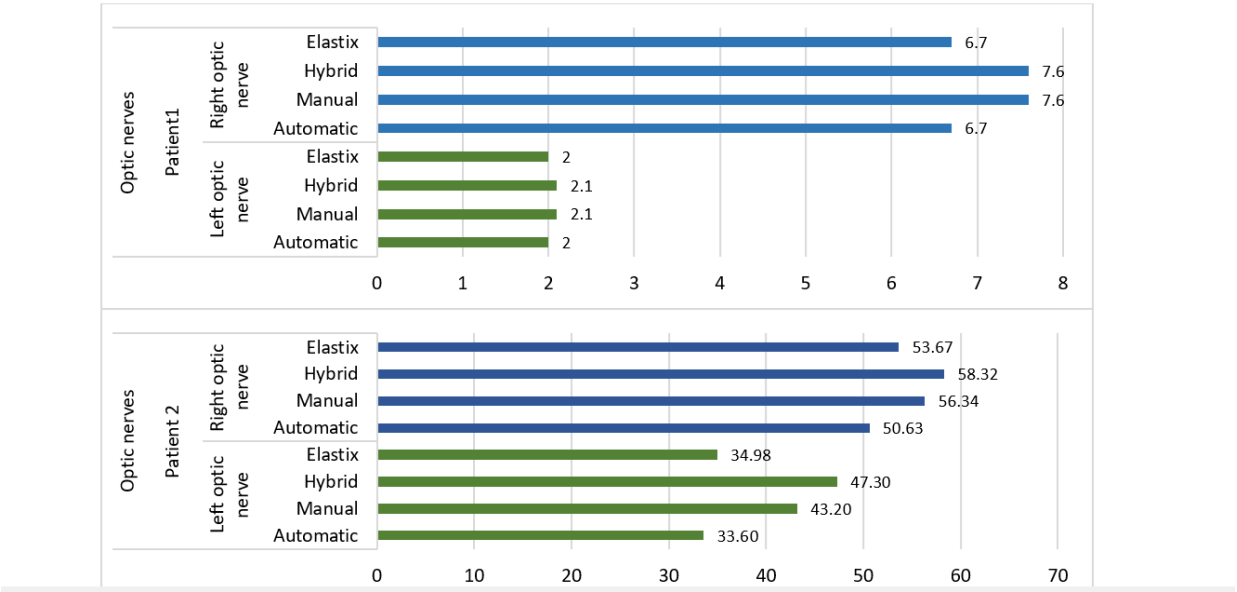


Figure IV.22: Recalculated doses to be delivered to optic nerve for different registrations.

### III.2 Comparison between delineation and calculated dose on CT and CT/MRI fusion

In this work, the PTVs and OARs delineated on CT images and CT/MRI fused images (Figure IV.23) are compared in terms of volumes and re-calculated doses. On the basis of the obtained results, the PTVs delineated on the CTs were ~1.38 times smaller than the PTVs delineated on CT/MRI fused image. Otherwise, large differences between delineated volumes by CT and MRI were observed for edema and brainstem as showed in Figure IV.24. The observed differences are due to the non-accurate localization and incorrect delineation of the PTV and the OARs on CT that can induce the irradiation omission of some tumor parts or the overdosing of the surrounding OARs (see Figure IV.25 and Figure IV.26). Figure IV.27 shows the dose levels to be delivered to the sensitive organs at risk (optic nerve and brainstem) when delineation is performed on CT-slices only or on CT/MRI fused images. It is well verified that MRI optimizes considerably the dose to be delivered to the optic nerve and brainstem. Dose optimization is between -5.71% and -19.27% for the right optic nerve, between -4.76% and -57.69 % for the left optic nerve except for patient 3 where dose increased by 10.34%, and between -2.53% and -14.13 % for the brainstem except for patient 1 where dose increased by 18.32%. The exceptional observed dose augmentation is a normal effect of considered case complexity. From these results it can be concluded that the tumor's localization (Table IV.3) has a great

impact on the optic nerve and the brainstem dose optimization. By referring to the constraints on doses (Table IV.4), the deviations on calculated doses with respect to these constraints are all within the admissible limits.

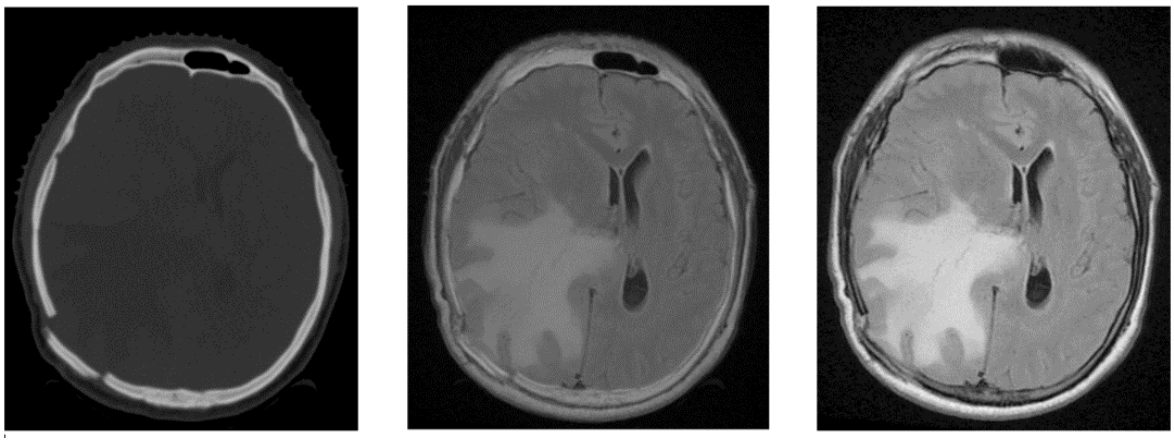

Figure IV.23 : CT image (left), Fused Image (Center), T2 Flair MRI Image (right)

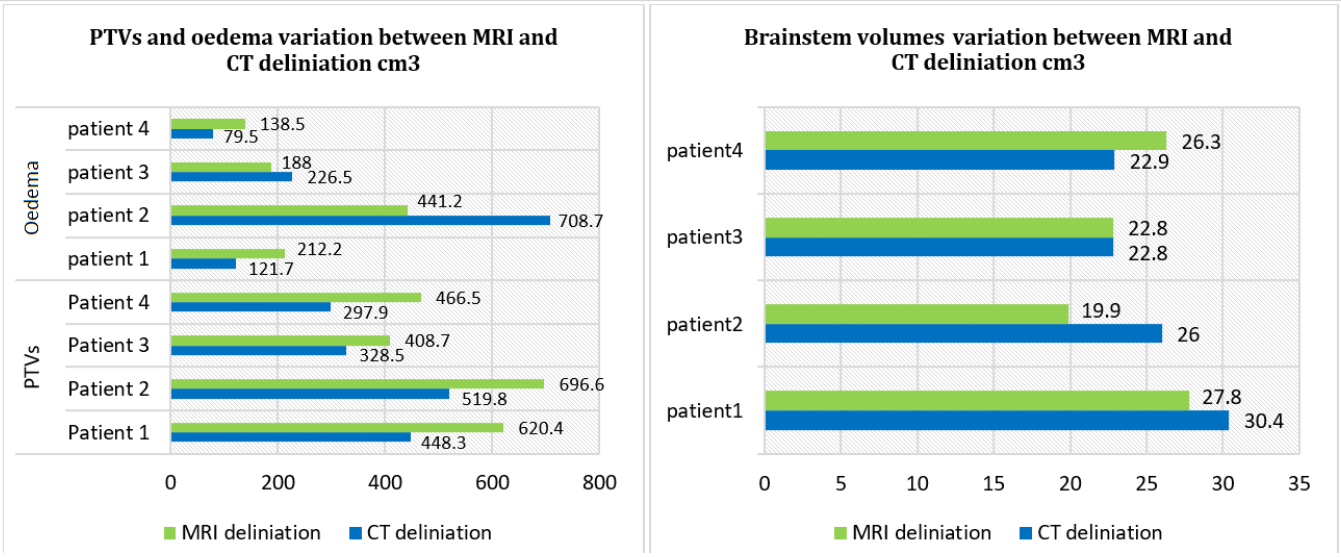


Figure IV.24: PTVs, Oedema and Brainstem delineation by CT and MRI in $cm^3$.

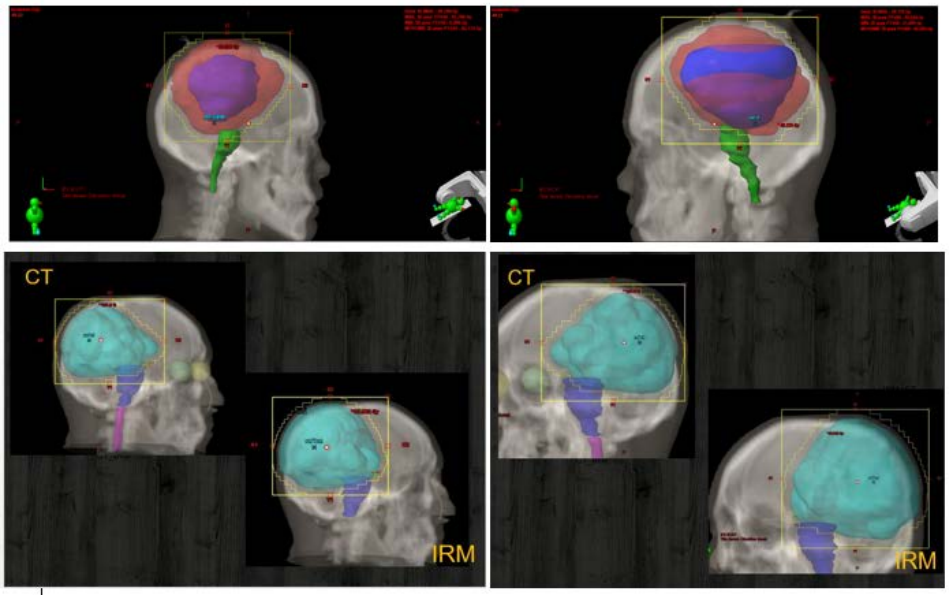


Figure IV.25: 3D images showing difference between Glioma's PTV delineated on CT and on MRI images.

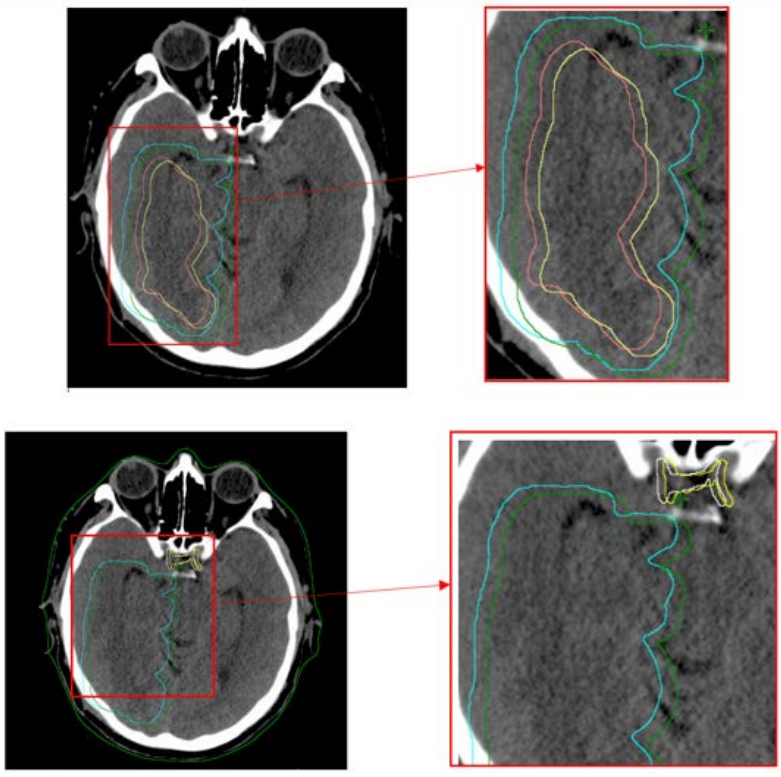

Figure IV.26: 2D images showing difference between Glioma's (PTVs and Oedema in 1st row) (PTV's and Chiasma in 2nd row) delineated on CT and on MRI images.

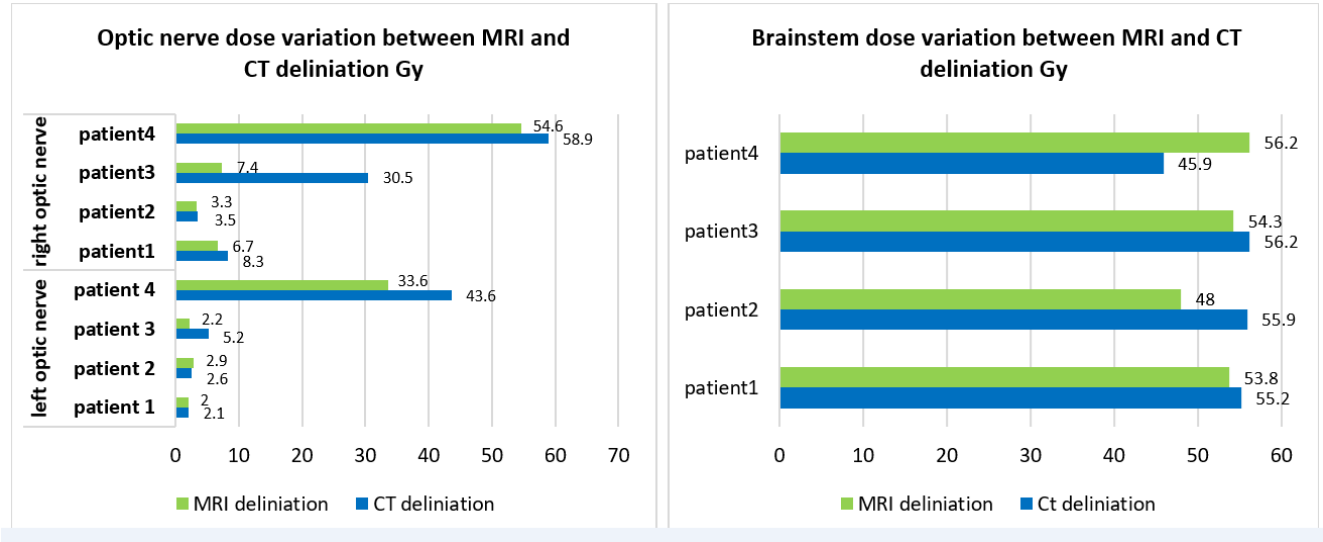


Figure IV.27: Calculated dose (Gy) to be delivered to the optic nerve and the brainstem on the basis of CT and MRI delineations.

## IV. Discussion

Several studies have evaluated the importance of image fusion and the use of MRI Images in the delineation and planning of therapeutic radiotherapy. They have demonstrated the contribution of these images in the delineation of target volumes and organs at risk as well as the dosimetry consequences. The study performed at the level of the CLCC of Setif was based on the contribution of magnetic resonance imaging in the delineation of the volumes of interest in cerebral tumors.

In the various cases studied at the Sétif hospital, the course of radiotherapy is based on teamwork between manipulators, a medical physicist and a radiotherapist in order to optimize and maximize the patients' chances of recovery.

Before the treatment itself, radiotherapy comprises two important steps, the first of identifying and delimiting the Target Volume and OAR and the second a step of calculating the distribution of the dose (dosimetry).

For the delineation of PTV and OAR the doctor must do an important step which is the registration, using the tools provided by Eclipse TPS from Varian and for the studied tumor, the radiotherapy clinician uses first the rigid automatic registration, which based on mutual information similarity metric and *Downhill* simplex optimizer, for CT/MRI image registration

and fusion. This automatic registration is fast, simple and gives generally good results. However, the other manual and hybrid *Eclipse'* registrations are used instead the automatic registration particularly when this last one fails due to MRI images that were not carried out in the right condition or in a positioning other than that of the simulation scanner or even delivered by another institute . The manual registration is more difficult and time consuming because the radiotherapy clinician is generally asked to perfectly use the TPS translation and rotation tools in order to perform correct 3D registration in the sagittal, coronal and axial plans. In hybrid registration, the task is based on manual selection of a set of points by the clinician on CT and MRI images at specific anatomical landmarks. Here, the registration consists in matching between defined points; task which is also so difficult and time consuming.

In this study, the advantages and the limitations of the CT/MRI image registration and fusion were well demonstrated in case of Glioblastoma radiotherapy treatment with 3D conformal radiotherapy technique. The great contribution of MRI in the delineation of the Edema and PTV, which cannot be correctly achieved by CT, was sufficiently demonstrated. The difference in terms of PTV localization and delineation between CT and MRI was found very large to reject completely the treatment planning based on CT data only. This difference is principally due to the excellent MRI soft tissues contrast and to its multitude robust imaging sequences (T1, T2, T2-Flair, T1-Gd.) that can be used for excellent brain examination. It was also demonstrated that *Elastix* registration could be used to judge the accuracy of the TPS automatic registration, which is generally first used. The registration performance was evaluated by the comparison of PTV and Edema delineation on the basis of DSC, JSC and HD metrics and also by comparing the re-calculated doses after each registration. The results showed that an almost good reproduction of the automatic registration results was obtained by the *Elastix* registration within an average of 0.98 (98%) for DSC and less than 1 mm for HD.

# CONCLUSIONS

## Conclusions

In this thesis work, the effective of the magnetic resonance imaging (MRI) in radiotherapy treatment planning was investigated. Special interests were focused on the contribution of MRI in treatment optimization and delivered dose conformity in case of Glioblastoma cancer. This disease was selected because diagnosis and most surrounding organs delineation must, essentially, be performed by MRI instead computed tomography (CT). Indeed, CT/MRI image registration and fusion in Glioblastoma 3D conformal radiotherapy treatment planning was used overcome some specific dose delivery and organs at risks (OARs) sparing issues. This because good CT/MRI image registration and fusion made great impact on dose calculation and treatment planning accuracy. Thus, the uncertainties associated with the registration and fusion used methods were verified dose recalculation. The registration and fusion used methods were also compared on the basis suitable metrics. The main objective of this study was, thus, the assessment of the effective contribution of MRI in Glioma radiotherapy treatment by improving the localization of target volumes and OARs. It was also question to provide clinicians with some suitable metrics to evaluate the CT/MRI image registration and fusion results. The CT/MRI image registration and fusion studied in the framework of this project were those of Eclipse Varian TPS (11.0) and Elastix open source software. The quantitative evaluation of CT/MRI image registration fusion were evaluated is performed using Dice score coefficient (DSC), Jaccard similarity coefficient (JSC), and Hausdorff distance (HD) which were found to be very suitable metrics.

Results shows that the programmed tumor's volumes (PTV) delineated on CT slices were approximately 1.38 times smaller than those delineated on CT/MRI fused images. Large differences were observed for the edema and the brainstem. It was also found that MRI optimizes considerably the dose to be delivered to the optic nerve and brainstem. Among the studied registration methods, Elastix registration was demonstrated to perform the best registration and therefore the most accurate radiotherapy planning according to the considered intensity and anatomical landmarks metrics. The manually and hybrid TPS methods were found to be less efficient than the Elastix method and time consuming. I terms of registration comparison metrics, Elastix method gives the most closet results to the TPS automatic registration method (reference). Special care must be taken when applying TPS automatic registration because it doesn't give suitable results for each considered tumor's case. In summary, we have shown that CT/MRI image registration in radiotherapy treatment planning can effectively be evaluated and improved by the clinician through the combination between

TPS automatic registration and Elastix registration. Furthermore, we have demonstrated the importance of employing suitable evaluation metrics when assessing the accuracy of the registration used. It was, then, well demonstrated that the used registration could seriously affect the accuracy dose calculation if not well assessed and optimized.

Finally, it was well demonstrated that image registration and fusion is a fundamental step for suitable and efficient Glioma treatment planning in 3D conformal radiotherapy that ensure accurate dose delivery and unnecessary organs at risk irradiation. MRI has the ability to provide accurate localization of targeted volumes leading to better irradiation control of Glioma tumour.

## References

[1] J.R Marbach, M.R. Sontag, J. Van Dyk and A.B. Wolbarst, Management of Radiation Oncology Patients, AAPM Report n°45, Med Phys 21(1) p85-90 (1994).

[2] V. Martin, E Moyal, et al. Radiothérapie des tumeurs cérébrales : quelles marges ? Cancer Radiothérapie, 2013.

[3] M. Yang. Optimisation des plans de traitement en radiothérapie grâce aux dernières techniques de calcul de dose rapide. Thèse doctorat. Université Paris Sud - Paris XI, 2014.

[4] C. De Conto. Evaluation dosimétrique des algorithmes implémentés dans les systèmes de planification de traitement en présence d'hétérogénéités de forte densité : cas de la sphère ORL en radiothérapie externe. Imageries medical. University de Franche-Comté, 2014.

[5] S. David. Basic Radiotherapy Physics and Biology, Springer Science&Business Media. New York. 2014.

[6] P. Mayles, A. Nahum. Handbook of Radiotherapy physics: theory and practice. Taylor & Francis Group, LLC 2007.

[7] A. Heath. Radiation Therapy Study Guide. Springer Science, Business Media New York 2016.

[8] P. Hoskin. Radiotherapy in Practice. Oxford University Press, 2010.

[9] H. Levitt. Technical Basis of Radiation Therapy. FIFTH EDITION .Springer Verlag Berlin Heidelberg 2012.

[10] T. Landberg, J. Chavaudra, J. Dobbs, G. Hanks, K.A. Johansson. Report 28: Prescribing, Recording and Reporting Photon Beam Therapy. Journal of the International Commission on Radiation Units and Measurements (ICRU), 26 (1), 1978.

[11] T. Landberg, J. Chavaudra, J. Dobbs, G. Hanks, K.A. Johansson. Report 50: Prescribing, Recording and Reporting Photon Beam Therapy. Journal of the International Commission on Radiation Units and Measurements (ICRU), 26 (1), 1993.

[12] T. Landberg, J. Chavaudra, J. Dobbs, J.P. Gerard, G. Hanks, J.G. Horiot, K.A. Johansson, T.Mölle, J. Purdy, N. Suntharalingam, H. Svensson. Report 62: Prescribing, Recording and Reporting Photon Beam Therapy (Supplement to ICRU report 50).Journal of the International Commission on Radiation Units and Measurements (ICRU), 32 (1), 1999.

[13] G. Huang et al., Error in the delivery of radiation therapy Results of a quality assurance review, International Journal of Radiation Oncology Biology Physics 61 (5), 1590 (2005).

[14] E. E. Klein, R. E. Drzymala, et al., Errors in radiation oncology : a study in pathways and dosimetric impact., Journal of applied clinical medical physics / American College of Medical Physics 6 (3), 81 (2005).

[15] L. Cohen, A radiation overdose incident: Initial data, International Journal of Radiation Oncology, Biology, Physics 33 (1), 217 (1995).

[16] G. G. Eichholz, Accidental Overexposure of Radiotherapy Patients in Bialystok, Health Physics, 2004.

[17] N. Smith, A Webb .Introduction to Medical Imaging. Published in the United States of America by Cambridge University Press, New York 2011.

[18] T. JERROLD. The Essential Physics of Medical Imaging. Second Edition. Lippincott Williams & Wilkins, 2002.

[19] R. William. Physics and applications of medical imaging. Reviews of Modern Physics, The American Physical Society, vol 71, 2000.

[20] G. William. History of Medical Imaging. The American Philosophical Society, Vol. 152, 2008.

[21] A. Haidekker. Medical imaging technology. Springer, 2013.

[22] B. Kastler. Comprendre l'IRM. 7ème Edition. Elsevier, 2011.

[23] F.H. Attix. Introduction to radiological physics and radiation dosimetry, WILEY, 2004.

[24] P. Bellaïche, Les secrets de l'image vidéo, Eyrolles, 2013.

[25] M. Bergougnoux, Introduction au traitement mathématique des images, Springer, 2015.

[26] P. Jannin, Fusion des données en imagerie médicale : revue méthodologique basée sue le contexte clinique, 2001.

[27] K. Friston, Holmes AP, Worsley KJ, Poline JB, Frith CD, Frackowiak RSJ. Statistical parametric maps in functional imaging: A general linear approach. Human Brain Mapping, 2: 189-210, 1995.

[28] R. William. Imaging processing in Radiation Therapy, Taylor & Francis Group, 2013.

[29] R. William. Informatics in Radiation Oncology. Taylor & Francis Group, 2014.

[30] P. Shamonin et al. Fast parallel image registration on CPU and GPU for diagnostic classification of Alzheimer's disease, 2014.

[31] S. Klein et al. Elastix: A Toolbox for Intensity-Based Medical Image Registration. IEEE Transactions on Medical Imaging, 2010.

[32] F Commandeur et al. MRI to CT Prostate Registration for Improved Targeting in Cancer External Beam Radiotherapy. IEEE Journal of Biomedical and Health Informatics, Vol. 21, No. 4, July 2017.

[33] B. Meher. A survey on region based image fusion methods," Information Fusion, vol. 48, pp. 119–132, 2019.

[34] A. James and B. Dasarathy. Medical image fusion: a survey of the state of the art, Information Fusion, vol. 19, pp. 4– 19, 2014

[35] C. Chen. Fusion of PET and MR brain images based on IHS and Log-Gabor transforms, 2017.

[36] M. Haddadpour, S. Daneshvar, and H. Seyedarabi, "PET and MRI image fusion based on combination of 2-D Hilbert transform and IHS method," Biomedical Journal, vol. 40, no. 4, pp. 219–225, 2017.

[37] M. Dilmaghani, et al. "A new MRI and PET image fusion algorithm based on BEMD and IHS methods" in 2017 Iranian Conference on Electrical Engineering (ICEE), Tehran, Iran, May 2017.

[38] M. Do and M. Vetterli, "The contourlet transform: an efficient directional multiresolution image representation," IEEE Transactions on Image Processing, vol. 14, no. 12, pp. 2091–2106, 2005.

[39] A. L. da Cunha, J. Zhou, and M. N. Do, "The nonsubsampled contourlet transform: theory, design, and applications," IEEE Transactions on Image Processing, vol. 15, no. 10, pp. 3089–3101, 2006.

[40] D. Labate, W.-Q. Lim, G. Kutyniok, and G. Weiss, "Sparse multidimensional representation using shearlets," in Wavelets XI, pp. 254–262, San Diego, California, USA, August 2005.

[41] G. Easley, D. Labate, and W. Q. Lim, “Sparse directional image representations using the discrete shearlet transform,” Applied and Computational Harmonic Analysis, vol. 25, no. 1, pp. 25– 46, 2008.

[42] S. Singh, D. Gupta, R. S. Anand, and V. Kumar, “Nonsubsampled shearlet based CT and MR medical image fusion using biologically inspired spiking neural network,” Biomedical Signal Processing and Control, vol. 18, pp. 91–101, 2015.

[43] V. Bhavana and H. Krishnappa, “Multi-modality medical image fusion using discrete wavelet transform,” Procedia Computer Science, vol. 70, pp. 625–631, 2015.

[44] M. Haribabu, C. Bindu, and K. S. Prasad, “Multimodal medical image fusion of MRI-PET using wavelet transform,” in 2012 International Conference on Advances in Mobile Network, Communication and Its Applications, Bangalore, India, August 2012.

[45] A. Wang, H. Sun, and Y. Guan, “The application of wavelet transform to multi-modality medical image fusion,” in 2006 IEEE International Conference on Networking, Sensing and Control, pp. 270–274, Ft. Lauderdale, FL, USA, April 2006.

[46] H. El-Hoseny er al. “Medical image fusion techniques based on combined discrete transform domains,” 34th National Radio Science Conference (NRSC), Alexandria, Egypt, March 2017.

[47] A. Krizhevsky, I. Sutskever, and G. Hinton, “Image net classification with deep convolutional neural networks,” International Conference on Neural Information Processing Systems, vol. 25, pp. 1097–1105, 2012.

[48] G. Balakrishnan, A. Zhao et al. a learning framework for deformable medical image registration,” IEEE Transactions on Medical Imaging, vol. 38, no. 8, pp. 1788–1800, 2019.

[49] Y. Hu, M. Modat, E. Gibson et al., “Weakly-supervised convolutional neural networks for multimodal image registration,” Medical Image Analysis, vol. 49, pp. 1–13, 2018.

[50] X. Yang, R. Kwitt, M. Styner, and M. Niethammer, “Quicksilver: Fast predictive image registration – A deep learning approach,” Neuroimage, vol. 158, pp. 378–396, 2017.

[51] Y. Liu, X. Chen, H. Peng, and Z. Wang, “Multi-focus image fusion with a deep convolutional neural network,”Information Fusion, vol. 36, pp. 191–207, 2017.

[52] L. Yu, C. Xun, J. Cheng, and P. Hu, “A medical image fusion method based on convolutional neural networks,” in 2017 20th International Conference on Information Fusion (Fusion), Xi'an, China, July 2017.

[53] S. Zagoruyko and N. Komodakis, “Learning to compare image patches via convolutional neural networks,” in 2015 IEEE Conference on Computer Vision and Pattern Recognition (CVPR), Boston, MA, USA, June 2015.

[54] F. Fan, Y et al., “A semantic-based medical image fusion approach,” 2019.

[55] X. Xia and B. Kulis, a deep model for fully unsupervised image segmentation, 2017.

[56] P Jannin., Fusion des données en imagerie médicale : revue méthodologique basée sue le contexte clinique, 2001.

[57] A. Holmes, K Worsley, J Poline., Statistical parametric maps in functional imaging: A general linear approach. Human Brain Mapping, 1995.

[58] R. Duncan, SPECT Imaging in Focal Epilepsy, London: Kluwer Academic Publishers, 1997.

[59] A. Evans, D. Collins., S. Mills et al, 3d statistical neuroanatomical models from 305 MRI volumes, Proc. Of IEEE Conference Record, Nuclear Science Symposium and Medical Imaging Conference, 1993.

[60] J. Ashburner and K. Friston. Multimodal image coregistration and partitioning - a unified framework, NeuroImage, 1997.

[61] A.Ribeiro, J. Nutt, and J. McGonigle. Which Metrics Should Be Used in Non-linear Registration Evaluation, Springer International Publishing Switzerland 2015.

[62] B Rigaud, A Simon, J. Castelli, M. Gobeli, et al. Evaluation of Deformable Image Registration Methods for Dose Monitoring in Head and Neck Radiotherapy. Hindawi Publishing Corporation BioMed Research International Volume 2015.

[63] ACS. American Cancer Society. Cancer Facts and Figures 2015; http://www.cancer.org/acs/groups/content/@editorial/documents/document/ acspc-044552.pdf. 2015

[64] F. Hamdy, J. Donovan et al. 10-Year outcomes after monitoring, surgery, or radiotherapy for localized prostate cancer. N Engl J Med 2016.

[65] B. Fisher, S. Anderson, J. Bryant, et al. Twenty-year follow-up of a randomized trial comparing total mastectomy, lumpectomy, and lumpectomy plus irradiation for the treatment of invasive breast cancer. N Engl J Med 2002;347:1233–1241.

[66] U. Veronesi, Cascinelli N, Mariani L, et al. Twenty-year follow-up of a randomized study comparing breast-conserving surgery with radical mastectomy for early breast cancer. N Engl J Med 2002;347:1227–1232.

[67] D Citrin. Recent developments in radiotherapy. N Engl J Med 2017; 377:2200–2201.

[68] H. Chandarana et al. Emerging role of MRI in radiation therapy. J Magn Reson Imaging. 2018.

[69] S. Benedict et al. Stereotactic body radiation therapy: the report of AAPM Task Group 101. Med Phys 2010.

[70] P Metcalfe et al. The potential for an enhanced role for MRI in radiation-therapy treatment planning. Technol Cancer Res Treat 2013.

[71] van der Heide UA, Houweling AC, Groenendaal G, et al. Functional MRI for radiotherapy dose painting. Magn Reson Imaging 2012.

[72] J. Lagendijk. The magnetic resonance imaging-linac system. Semin Radiat Oncol 2014.

[73] J. Lagendijk et al. MR guidance in radiotherapy. Phys Med Biol 2014.

[74] G. Groenendaal et al. Pathologic validation of a model based on diffusion-weighted imaging and dynamic contrast-enhanced magnetic resonance imaging for tumor delineation in the prostate peripheral zone. Int J Radiat Oncol Biol Phys 2012.

[75] I. Lips, van der Heide UA, Haustermans K, et al. Single blind randomized phase III trial to investigate the benefit of a focal lesion ablative microboost in prostate cancer (FLAME-trial): study protocol for a randomized controlled trial. Trials 2011.

[76] M Moerland et al. Analysis and correction of geometric distortions in 1.5 T magnetic resonance images for use in radiotherapy treatment planning. Phys Med Biol 1995.

[77] E. Paulson, S Crijns, B Keller, et al. Consensus opinion on MRI simulation for external beam radiation treatment planning. Radiother Oncol 2016.

[78] T Stanescu, D. Jaffray. Investigation of the 4D composite MR image distortion field associated with tumor motion for MR-guided radiotherapy. Med Phys 2016.

[79] T. Stanescu, K Wachowicz. Characterization of tissue magnetic susceptibility-induced distortions for MRIgRT. Med Phys 2012.

[80] S. Riches et al. Effect on therapeutic ratio of planning a boosted radiotherapy dose to the dominant intraprostatic tumour lesion within the prostate based on multifunctional MR parameters. Br J Radiol. 2014.

[81] J. Pouliot et al. Inverse planning for HDR prostate brachytherapy used to boost dominant intraprostatic lesions defined by magnetic resonance spectroscopy imaging. Int J Radiat Oncol Biol Phys. 2004.

[82] L.Feuvert, D.Antoni, J.Biau, G.Truc, G.Noël, J.-J.Mazeron. Guidelines for the radiotherapy of gliomas. Cancer/Radiotherapy Journal 2016.

[83] M. Roach et al. Prostate volumes defined by magnetic resonance imaging and computerized tomographic scans for three-dimensional conformal radiotherapy. International journal of radiation oncology, biology, physics.

[84] K. Kagawa et al. Initial clinical assessment of CT-MRI image fusion software in localization of the prostate for 3D conformal radiation therapy. International journal of radiation oncology, biology, physics. 1997.

[85] M. Debois et al. The contribution of magnetic resonance imaging to the three-dimensional treatment planning of localized prostate cancer. International journal of radiation oncology, biology, physics, 1999.

[86] M. Milosevic et al. Magnetic resonance imaging (MRI) for localization of the prostatic apex: comparison to computed tomography (CT) and urethrographic. Radiotherapy and oncology journal, 2000.

[87] C. Parker et al. Magnetic resonance imaging in the radiation treatment planning of localized prostate cancer using intra-prostatic fiducial markers for computed tomography coregistration. Radiotherapy and oncology : journal of the European Society for Therapeutic Radiology and Oncology. 2003.

[88] C. Weltens et al. Interobserver variations in gross tumor volume delineation of brain tumors on computed tomography and impact of magnetic resonance imaging. Radiotherapy and oncology : journal of the European Society for Therapeutic Radiology and Oncology, 2001.

[89] R. Prabhakar et al. Comparison of computed tomography and magnetic resonance based target volume in brain tumors. Journal of cancer research and therapeutics. 2007.

[90] N. Datta et al. Implications of contrast-enhanced CT-based and MRI-based target volume delineations in radiotherapy treatment planning for brain tumors. Journal of cancer research and therapeutics. 2008.

[91] J. Lagendijk et al. van der Heide UA. MRI/linac integration. Radiother Oncol. 2008.

[92] V. Sörnsen. MR-guided Gated Stereotactic Radiation Therapy Delivery for Lung, Adrenal, and Pancreatic Tumors: A Geometric Analysis. International Journal of Radiation and Oncology, 2018.

[93] B. Raaymakers et al. First patients treated with a 1.5 T MRI-Linac: clinical proof of concept of a high precision, high-field MRI guided radiotherapy treatment. Phys Med Biol. 2017.

[94] E. Hessen et al. Significant tumor shift in patients treated with stereotactic radiosurgery for brain metastasis. Clin Transl Radiat Oncol. 2017.

[95] E. Jager et al. Validated guidelines for tumor delineation on magnetic resonance imaging for laryngeal and hypopharyngeal cancer. Acta Oncol (Madr). 2016

[96] H. Ligtenberg et al. Modality-specific target definition for laryngeal and hypopharyngeal cancer on FDG-PET, CT and MRI. Radiother Oncol. 2017

[97] S. Marzi et al. Radiation-induced parotid changes in oropharyngeal cancer patients: the role of early functional imaging and patient−/treatment-related factors. Radiat Oncol. 2018

[98] H. Bahig et al. Clinical and Translational Radiation Oncology Magnetic Resonance-based Response Assessment and Dose Adaptation in Human Papilloma Virus Positive Tumors of the Oropharynx treated with, 2018.

[99] J. Edmund and T. Nyholm. A review of substitute CT generation for MRI-only radiation therapy. Radiation oncology, 2017.

[100] J. Dowling et al. “Automatic substitute CT generation and contouring for MRI-alone external beam radiation therapy from standard MRI sequences,” International Journal of Radiation Oncology, Biology, Physics 2015.

[101] V. Keereman et al. “Mri-based attenuation correction for pet/mri using ultrashort echo time sequences.” Journal of nuclear medicine: official publication, Society of Nuclear Medicine, 2010.

[102] C. Siversson et al. “Technical note: Mri only prostate radiotherapy planning using the statistical decomposition algorithm,” Medical Physics, 2015.

[103] D. Andreasen, K. Van Leemput, R.H. Hansen, J.A. Andersen, and J.M. Edmund. Patch-based generation of a pseudo CT from conventional MRI sequences for MRI-only radiotherapy of the brain, Medical physics, 2015.

[104] A. Jog et al. “Random forest flair reconstruction from T1, T2, and pd-weighted MRI, in: 2014 IEEE 11th International Symposium on Biomedical Imaging (ISBI), 2014.

[105] C. Qian, L. Wang,.“In vivo mri based prostate cancer identification with random forests and auto-context model,” in [Machine Learning in Medical Imaging], Wu, G., Zhang, D., and Zhou, L., eds., Lecture Notes in Computer Science 8679, 314–322, Springer International Publishing (2014).

[106] V. Zografos. “Hierarchical multi-organ segmentation without registration in 3d abdominal ct images,” MCV workshop (MICCAI 2015).

[107] Z. Tu. “Auto-context and its application to high-level vision tasks,” in [Computer Vision and Pattern Recognition, 2008. CVPR 2008. IEEE Conference on], 1–8, IEEE (2008).

[108] N. Tustison, et al., “N4itk: improved n3 bias correction,” Medical Imaging, IEEE Transactions on medical Imaging, 2010.

[109] L.Nyul, J.Udupa and X. Zhang. “New variants of a method of MRI scale standardization,” Medical Imaging, IEEE Transactions on medical Imaging, 2000.

[110] S. Klein. “elastix: a toolbox for intensity-based medical image registration,” IEEE Transactions on Medical Imaging, 2010.

[111] T. Ojala. “Multiresolution gray-scale and rotation invariant texture classification with local binary patterns,” Pattern Analysis and Machine Intelligence, IEEE Transactions on medical Imaging, 2002.

[112] C. Rank et al. “Mri-based simulation of treatment plans for ion radiotherapy in the brain region.” Radiotherapy and Oncology, 2013.

[113] T.Huynh, et al. “Estimating ct image from MRI data using structured random forest and auto-context model,” IEEE Transactions on Medical Imaging, 2015.

[114] H. Chandarana. Emerging role of MRI in radiation therapy. Journal of Magnetic Resonance Imaging, 2018.

[115] S. Doran, L. Charles-Edwards. A complete distortion correction for MR images: I. Gradient warp correction. Phys Med Biol, 2005.

[116] J. Jovicich, et al. Reliability in multi-site structural MRI studies: effects of gradient non-linearity correction on phantom and human data. Neuroimage, 2006.

[117] A. Janke. Use of spherical harmonic deconvolution methods to compensate for nonlinear gradient effects on MRI images. Magn Reson Med, 2004.

[118] B. Hargreaves et al. Metal-induced artifacts in MRI. AJR Am J Roentgenol. 2011.

[119] K. Koch. A multispectral three-dimensional acquisition technique for imaging near metal implants. Magn Reson Med, 2009.

[120] F. Khan. Treatment planning in radiation oncology. Second ed. Philadelphia PA: Lippincot, Williams & Wilkins, 2009.

[121] A. Barett et al. Practical radiotherapy planning. Fourth ed. London: Hodder Arnold, 2009.

# Article

Int J Cancer Manag. 2020 September; 13(9):e102160. doi: 10.5812/ijcm.102160.
Published online 2020 September 10. Research Article

## Computed Tomography/Magnetic Resonance Imaging (CT/MRI) Image Registration and Fusion Assessment for Accurate Glioblastoma Radiotherapy Treatment Planning

Khalil Mohamed Mokhtar Touabti [1,2], Faycal Kharfi [2,3,*], Karim Benkahila [1,2,3] and Sid-Ali Merouane [3]

[1] Department of Physics, Ferhat Abbas Setif University, Setif, Algeria
[2] Laboratory of Dosing, Analysis and Characterization in High Resolution (DAC), Ferhat Abbas Setif University, Setif, Algeria
[3] Department of Radiotherapy, Fighting against Cancer Medical Centre (CLCC), Setif, Algeria

*Corresponding author: Department of Physics, Ferhat Abbas Setif University, Setif, Algeria. Email: kharfifaycal@yahoo.com

Received 2020 March 30; Revised 2020 June 02; Accepted 2020 July 11.

**Abstract**

**Background:** In this study, computed tomography/magnetic resonance imaging (CT/MRI) image registration and fusion in the 3D conformal radiotherapy treatment planning of Glioblastoma brain tumor was investigated. Good CT/MRI image registration and fusion made a great impact on dose calculation and treatment planning accuracy. Indeed, the uncertainty associated with the registration and fusion methods must be well verified and communicated. Unfortunately, there is no standard procedure or mathematical formalism to perform this verification due to noise, distortion, and complicated anatomical situations.

**Objectives:** This study aimed at assessing the effective contribution of MRI in Glioma radiotherapy treatment by improving the localization of target volumes and organs at risk (OARs). It is also a question to provide clinicians with some suitable metrics to evaluate the CT/MRI image registration and fusion results.

**Methods:** Quantitative image registration and fusion evaluation were used in this study to compare Eclipse TPS tools and Elastix CT/MRI image registration fusion. Thus, Dice score coefficient (DSC), Jaccard similarity coefficient (JSC), and Hausdorff distance (HD) were found to be suitable metrics for the evaluation and comparison of the image registration and fusion methods of Eclipse TPS and Elastix.

**Results:** The programmed tumor's volumes (PTV) delineated on CT slices were approximately 1.38 times smaller than those delineated on CT/MRI fused images. Large differences were observed for the edema and the brainstem. It was also found that MRI considerably optimized the dose to be delivered to the optic nerve and brainstem.

**Conclusions:** Image registration and fusion is a fundamental step for suitable and efficient Glioma treatment planning in 3D conformal radiotherapy that ensure accurate dose delivery and unnecessary OAR irradiation. MRI can provide accurate localization of targeted volumes leading to better irradiation control of Glioma tumor.

*Keywords:* X-Ray Computed Tomography, Magnetic Resonance Imaging, Conformal Radiotherapy, Glioma, Radiotherapy

### 1. Background

Radiotherapy plays a major role in the treatment of cancer (1). 3D conformal radiotherapy technique used in this study aimed at delivering the prescribed dose to the tumor volume by sparing the surrounding tissues and organs (2). Thus, a large amount of information on tumor and organs at risk (OAR) volumes is necessary to avoid any overdose or unacceptable dose uncertainty (3-5). X-ray computed tomography (CT) is the main imaging modality used for radiotherapy treatment planning and different volumes and structures delineation. Unfortunately, CT, in the case of brain cancer, cannot provide information on low-density tissues in comparison with magnetic resonance imaging (MRI). Indeed, MRI can provide high-resolution anatomical and structural images and details on the extension of the tumor and its impact on adjacent organs by using some specific MRI sequences (4, 5). Glioblastoma is the most common brain cancer among adults. It is caused by an abnormal proliferation of central nervous system cells called astrocytes. With radiotherapy, these cancer cells are destroyed or their development is stopped by exposing them to ionizing radiation. Radiotherapy is often prescribed after surgery. This tech-

Int J Cancer Manag. 2020 September; 13(9):e103160. doi: 10.5812/ijcm.103160.

Published online 2020 September 19. **Research Article**

# Computed Tomography/Magnetic Resonance Imaging (CT/MRI) Image Registration and Fusion Assessment for Accurate Glioblastoma Radiotherapy Treatment Planning

Khalil Mohamed Mokhtar Touabti [1, 2], Faycal Kharfi [1, 2, *], Karim Benkahila [1, 2, 3] and Sid-Ali Merouane [3]

[1] Department of Physics, Ferhat Abbas Setifi University, Setif, Algeria
[2] Laboratory of Dosing, Analysis and Characterization in High Resolution (DAC), Ferhat Abbas Setifi University, Setif, Algeria
[3] Department of Radiotherapy, Fighting against Cancer Medical Centre (CLCC), Setif, Algeria

[*] *Corresponding author*: Department of Physics, Ferhat Abbas Setifi University, Setif, Algeria. Email: kharfifaycal@yahoo.com

**Received** 2020 March 30; **Revised** 2020 June 02; **Accepted** 2020 July 11.

## Abstract

**Background:** In this study, computed tomography/magnetic resonance imaging (CT/MRI) image registration and fusion in the 3D conformal radiotherapy treatment planning of Glioblastoma brain tumor was investigated. Good CT/MRI image registration and fusion made a great impact on dose calculation and treatment planning accuracy. Indeed, the uncertainly associated with the registration and fusion methods must be well verified and communicated. Unfortunately, there is no standard procedure or mathematical formalism to perform this verification due to noise, distortion, and complicated anatomical situations.
**Objectives:** This study aimed at assessing the effective contribution of MRI in Glioma radiotherapy treatment by improving the localization of target volumes and organs at risk (OARs). It is also a question to provide clinicians with some suitable metrics to evaluate the CT/MRI image registration and fusion results.
**Methods:** Quantitative image registration and fusion evaluation were used in this study to compare *Eclipse* TPS tools and *Elastix* CT/MRI image registration fusion. Thus, Dice score coefficient (DSC), Jaccard similarity coefficient (JSC), and Hausdorff distance (HD) were found to be suitable metrics for the evaluation and comparison of the image registration and fusion methods of *Eclipse* TPS and *Elastix*.
**Results:** The programmed tumor's volumes (PTV) delineated on CT slices were approximately 1.38 times smaller than those delineated on CT/MRI fused images. Large differences were observed for the edema and the brainstem. It was also found that MRI considerably optimized the dose to be delivered to the optic nerve and brainstem.
**Conclusions:** Image registration and fusion is a fundamental step for suitable and efficient Glioma treatment planning in 3D conformal radiotherapy that ensure accurate dose delivery and unnecessary OAR irradiation. MRI can provide accurate localization of targeted volumes leading to better irradiation control of Glioma tumor.

*Keywords:* X-Ray Computed Tomography, Magnetic Resonance Imaging, Conformal Radiotherapy, Glioma, Radiotherapy

## 1. Background

Radiotherapy plays a major role in the treatment of cancer (1). 3D conformal radiotherapy technique used in this study aimed at delivering the prescribed dose to the tumor volume by sparing the surrounding tissues and organs (2). Thus, a large amount of information on tumor and organs at risk (OAR) volumes is necessary to avoid any overdose or unacceptable dose uncertainty (1-3). X-ray computed tomography (CT) is the main imaging modality used for radiotherapy treatment planning and different volumes and structures delineation. Unfortunately, CT, in the case of brain cancer, cannot provide information on low-density tissues in comparison with magnetic resonance imaging (MRI). Indeed, MRI can provide high-resolution anatomical and structural images and details on the extension of the tumor and its impact on adjacent organs by using some specific MRI sequences (4, 5). Glioblastoma is the most common brain cancer among adults. It is caused by an abnormal proliferation of central nervous system cells called astrocytes. With radiotherapy, these cancer cells are destroyed or their development is stopped by exposing them to ionizing radiation. Radiotherapy is often prescribed after surgery. This tech-

nique is also used as the main treatment combined with chemotherapy when the tumor is not operable. To optimize the results of the treatment, the used beams ballistic is finely planned to specifically target the tumor and to avoid side effects. Thus, the contouring phase is crucial to achieving such an objective. Indeed, many contouring models were proposed based on clinical tumor volume (CTV) and edema delineation. In this research, we focused on the contribution of MRI in radiotherapy treatment planning and, particularly, its role in the visualization and delineation of the gross tumor volume (GTV), the programmed target volume (PTV), and the OARs for patients suffering from Glioma. The necessary CT/MRI image registration and fusion are sometimes and for a specific case of radiotherapy treatments so difficult to be performed concerning the recommended conditions by Khan (6) and Barett et al. (7). The related issues of such technical limitations are studied in this study. The present study concerns only rigid registration because non-rigid registration remains relatively not used in radiotherapy planning though some interesting approaches are under development (8, 9). Many registrations and fusion assessment metrics are proposed in this work to help clinicians to do accurate delineation (10, 11).

## 2. Objectives

In this study, the *Eclipse* treatment planning system (TPS) and *Elastix* rigid registration methods were studied and compared for a specific case of Glioma radiotherapy treatment. The comparison was performed in terms of volume delineation and dose calculation based on external and independent metrics.

## 3. Methods

### 3.1. Imaging Data and Treatment Planning

This study was carried out on 4 patients admitted for Glioma brain tumor (Table 1). The CT and MRI data were collected around Siemens SOMATOM AS high definition CT-scanner and 1.5T GE Optima MR450W MRI machine, respectively. The radiotherapy TPS used is the Varian *Eclipse* 11.0.31. The dose calculation algorithm used is the anisotropic analytical algorithm (AAA). The MRI sequences used are the T2-weighted flair sequence for the visualization of edema and the T1 sequence with Gadolinium contrast agent injection for the visualization of the tumor. The dose constraints on OARs that must be respected during radiotherapy planning and treatment of brain tumors are indicated in Table 2 (12).

### 3.2. CT/MRI Image Registration and Fusion

In radiotherapy, multimodalities image registration is a geometrical process used in medical imaging to align two different images to bring together complementary information that is necessary to perform correct diagnosis and accurate volumes and structures delineation (13, 14). The image registration consists of a set of spatial transformations (translation, rotation, scaling, sampling, etc.) to be applied to a targeted image in order to make it spatially aligned to a reference image. In this research, the necessary CT/MRI image registration and fusion was performed within the *Eclipse* TPS by using automatic, manual, and hybrid (semi-automatic) registrations. These 3 registration tools used different similarity metrics, linear interpolators, registration optimizers, and 3D image translation and rotation. Unfortunately, these image registration tools do not give the same results within the same execution time. Therefore, depending on the considered treatment case, one *Eclipse* registration method might be more appropriate than another (15, 16). In the current study, automatic registration is considered a reference registration. In addition to the *Eclipse* registration tools and methods, the TPS independent *Elastix* image registration was also studied (10, 11). *Elastix* is an open-source software based on the insight segmentation and registration toolkit (ITK). *Elastix* registration is also used to evaluate the *Eclipse* image registration methods. *Elastix* registration uses mutual information as a similarity metric and the gradient descent as an optimizer. After the image registration with *Elastix*, *Eclipse* fuses the information of two images into a single one by selecting the suitable transparency and opacity parameters that give satisfaction to the radiotherapy clinician (17, 18).

### 3.3. Volumes and Structures Delineation

In the present study, the guess and check method was used. Thus, the cyclic work is achieved through a close collaboration between radiotherapy clinician that performs CT/MRI image registration and fusion as well as different volumes and structures delineations and the medical physics that performs dose calculation. The procedure is repeated for each new CT/MRI image registration and fusion. The delineation of the tumor and the OARs was done first on CT-slices and, then, corrected on fused CT/MRI images according to the protocol of Glioma treatment described by Feuvert et al. (19). The imaging modalities used for the delineation of the different volumes and structures of the studied cases are presented in Table 3 (19).

**Table 1**. Studied Cases

| | Patient 1 | Patient 2 | Patient 3 | Patient 4 |
|---|---|---|---|---|
| **PTV CT, $cm^3$** | 448,3 | 519,8 | 328,5 | 297,9 |
| **PTV MRI, $cm^3$** | 620,4 | 696,6 | 408,7 | 466,5 |
| **Tumor localization (x, y)** | Right posterior parietal (189, 409) | Left parietal (273, 303) | Right posterior parietal (171, 338) | Right anterior (198, 181) |

Abbreviation: CT, computed tomography; MRI, magnetic resonance imaging; PTV, programmed tumor's volumes.

**Table 2.** Dose Constraints for Some Organs in Radiotherapy Treatment of Brain Tumors

| Organ | Dose Constraint, Gy |
|---|---|
| **Optic chiasm** | $D_{max} = 54$ |
| **Pituitary** | $D_{max} = 45 - 50$ |
| **Larynx** | $D_{max} < 63 - 66$ |
| **Spinal cord** | $D_{max} \leq 50$ |
| **Optic nerve** | $D_{max} \leq 54$ |
| **Eyes-crystalline** | $D_{max} < 10 - 15$ |
| **Eyes-retina** | $D_{average} \leq 45$ |
| **Brain** | $V_{60\,Gy} < 33\,\%$ |

**Table 3.** Reference Delineation Modalities for Glioma Radiotherapy Treatment

| Tumor's Volumes and Organ at Risk | Modality of Delineation |
|---|---|
| **GTV** | MRI |
| **PTV** | MRI |
| **Edema** | MRI |
| **Chiasma** | MRI |
| **Pituitary** | MRI |
| **Optic nerve** | MRI |
| **Brainstem** | MRI |
| **Eyes** | CT |
| **Brain** | CT |
| **Crystalline** | CT |

Abbreviations: CT, computed tomography, GTV, gross tumor volume; MRI, magnetic resonance imaging; PTV, programmed tumor's volumes.

### 3.4. Registration Evaluation and Comparison Metrics

The CT and MRI images were used with reconstruction resolution and voxel spacing as indicated in Table 4. In this work, suitable metrics are proposed to clinicians to assess their CT/MRI image registration and fusion work. Hence, the registration results were evaluated qualitatively and quantitatively regarding the automatic registration of *Eclipse*. The proposed metrics are the Dice score coefficient (DSC), the Jaccard similarity coefficient (JSC), and the Hausdorff distance (HD) (20-22). The DSC ranges from 0 to 1, where 0 indicates no overlapping and 1 indicates full overlapping between fused images. The JSC ranges also from 0 to 1, where 0 means no overlapping and 1 indicates a full overlapping. The HD is measured in mm and ranges from 0 (identical surfaces) to $+\infty$.

## 4. Results

### 4.1. Comparison Between Delineation and Calculated Dose on CT and CT/MRI Fusion

In this study, the PTVs and OARs delineated on CT images and CT/MRI fused images are compared in terms of volumes and re-calculated doses. The PTVs delineated on the CTs were ~1.38 times smaller than the PTVs delineated on CT/MRI fused image. Otherwise, large differences between delineated volumes by CT and MRI were observed for edema and brainstem (Figure 1). The observed differences are due to the non-accurate localization and incorrect delineation of the PTV and the OARs on CT that can induce the irradiation omission of some tumor parts or the overdosing of the surrounding OARs (Figure 2). Figure 3 shows the dose levels to be delivered to the sensitive OAR (optic nerve and brainstem) when delineation is performed on CT-slices only or CT/MRI fused images. It is well verified that MRI optimizes considerably the dose to be delivered to the optic nerve and brainstem. Dose optimization is between -5.71% and -19.27% for the right optic nerve, between -4.76% and -57.69% for the left optic nerve except for patient 3, where dose increased by 10.34%, and between -2.53% and -14.13% for the brainstem except for patient 1, where dose increased by 18.32%. The exceptional observed dose augmentation is a normal effect of considered case complexity. It can be concluded that the tumor's localization (Table 1) has a great impact on the optic nerve and brainstem dose optimization. By referring to the constraints on doses (Table 2), the deviations on calculated doses concerning these constraints are all within the admissible limits.

### 4.2. Evaluation and Comparison Between Registration Methods

The PTV's localization and shape of the image registration methods were compared to the TPS automatic registration results. The results of the PTVs comparison are

**Table 4.** Used Imaging Modalities and Reconstructed Image Sampling

| | Mode | Patient 1 | Patient 2 | Patient 3 | Patient 4 |
|---|---|---|---|---|---|
| **CT dimension** | Cerebral | 512 × 512 × 71 | 512 × 512 × 74 | 512 × 512 × 74 | 512 × 512 × 74 |
| **CT Voxel spacing, mm** | | 0.48 × 0.48 × 3 | 0.48 × 0.48 × 3 | 0.48 × 0.48 × 3 | 0.48 × 0.48 × 3 |
| **MRI dimension** | T1-Gd | 512 × 512 × 296 | 512 × 512 × 250 | 512 × 512 × 264 | 512 × 512 × 37 |
| | T2-flair | 512 × 512 × 45 | 512 × 512 × 34 | 512 × 512 × 49 | 512 × 512 × 37 |
| **MRI Voxel spacing, mm** | T1-Gd | 0.46 × 0.46 × 0.7 | 0.46 × 0.46 × 1 | 0.46 × 0.46 × 1 | 0.46 × 0.46 × 5 |
| | T2-flair | 0.46 × 0.46 × 5 | 0.46 × 0.46 × 5 | 0.46 × 0.46 × 5 | 0.46 × 0.46 × 5 |

Abbreviations: CT, computed tomography; MRI, magnetic resonance imaging.

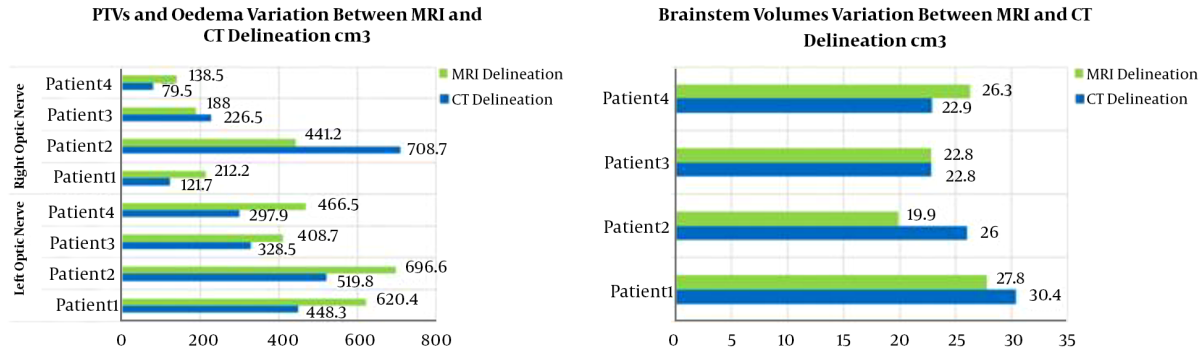


**Figure 1.** PTVs, edema, and Brainstem delineation by CT and MRI in $cm^3$

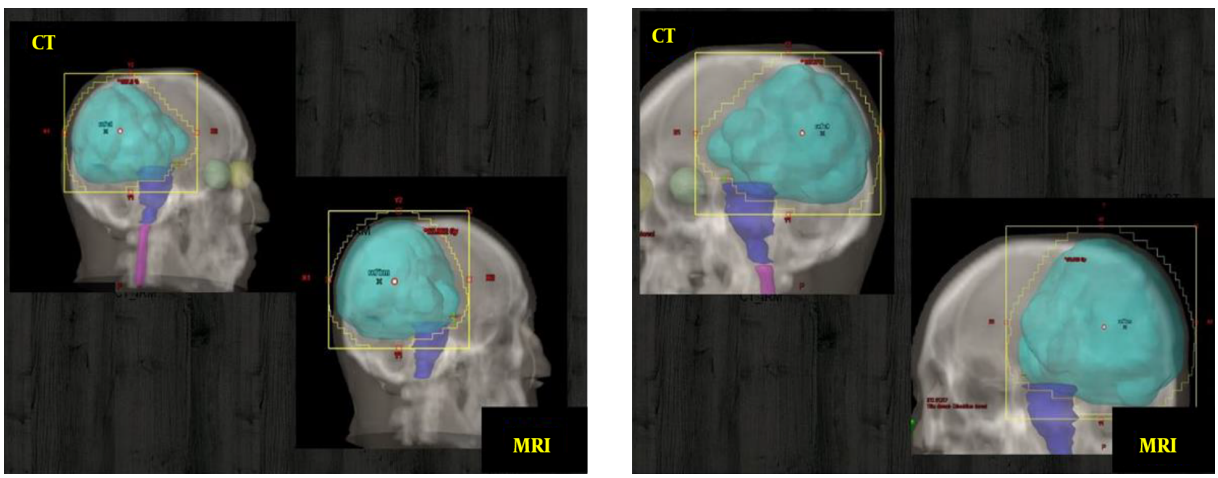


**Figure 2.** 3D images showing the difference between Glioma's PTV delineated on CT and MRI images

shown in Figure 4. It can be easily verified that poor overlapping was observed for the hybrid registration, acceptable one for the manual registration, and almost good overlapping for the *Elastix* registration.

The comparison between registration methods based on the used metrics is presented in Table 5. The PTV of the automatic registration is taken each time as a reference. The metrics comparison demonstrates that the hybrid registration is the poor one in terms of exact volume and structure overlapping, a mean divergence is observed

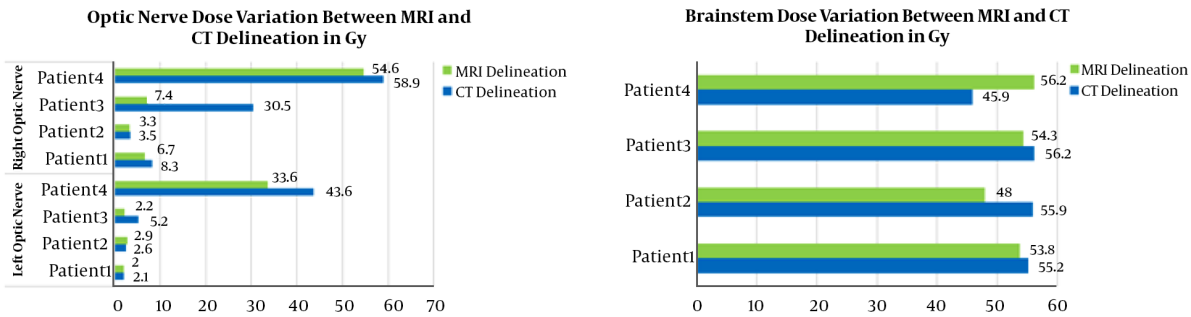


**Figure 3.** Calculated dose (Gy) to be delivered to the optic nerve and the brainstem based on the CT and MRI delineations

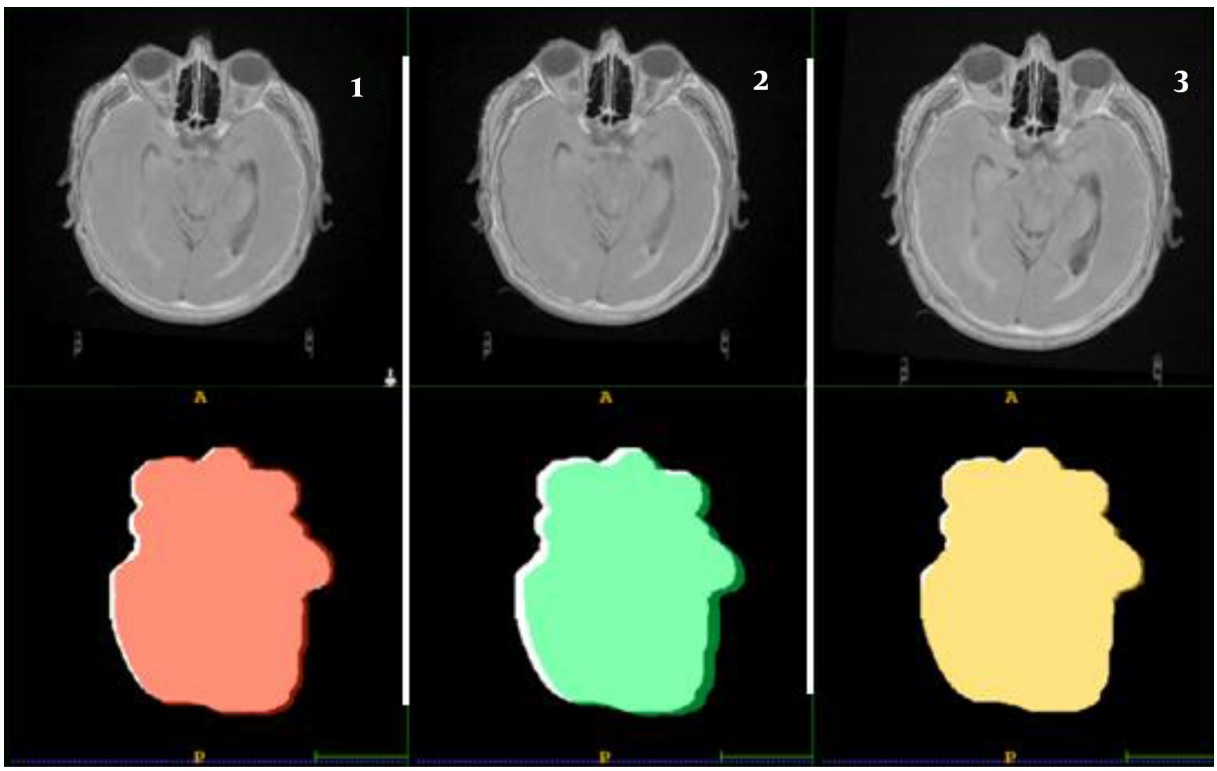


**Figure 4.** Qualitative registration evaluation (top) and PTV's volumes overlapping of the three tested registration methods in comparison to the reference automatic registration (bottom)-Overlapping difference is in white: 1, manual; 2, Hybrid; and 3, *Elastix*.

for the manual registration and almost a good registration similarity for the *Elastix* method. A comparison between re-calculated doses, based on these registrations and new treatment planning, was also performed. According to the obtained results (Table 5), the re-calculated doses of the *Elastix* registration were in good agreement with those of the automatic registration (reference). Thus, the *Elastix* registration was the best method followed by manual registration, which is better than the hybrid registration.

## 5. Discussion

For the studied tumor, the radiotherapy clinician firstly uses the rigid automatic registration, based on mutual information similarity metric and Downhill simplex optimizer, for CT/MRI image registration and fusion. This

**Table 5.** Registration Metrics and Re-Calculated Dose Comparison

| | Patient 1 | | | Patient 2 | | |
|---|---|---|---|---|---|---|
| | JSD | DSC | HD | JSD | DSC | HD |
| **Registration metrics comparison** | | | | | | |
| **PTV** | | | | | | |
| Elastix | 0.967 | 0.983 | 1.880 | 0.949 | 0.974 | 1.753 |
| Hybrid | 0.877 | 0.635 | 5.016 | 0.817 | 0.899 | 5.545 |
| Manual | 0.934 | 0.966 | 2.817 | 0.898 | 0.946 | 3.507 |
| **Edema** | | | | | | |
| Elastix | 0.900 | 0.947 | 2.369 | 0.937 | 0.967 | 1.315 |
| Hybrid | 0.782 | 0.878 | 4.399 | 0.775 | 0.873 | 4.135 |
| Manual | 0.854 | 0.921 | 2.816 | 0.901 | 0.948 | 2.480 |
| **Re-Calculated Dose, Gy for Each Registration Method** | | | | | | |
| **Brainstem** | | | | | | |
| Elastix/automatic | 53.1/53.1 | 53.29/52.37 | | | | |
| Hybrid/automatic | 55.2/53.1 | 57.12/52.37 | | | | |
| Manual/automatic | 54.4/53.1 | 57.18/52.37 | | | | |
| **Chiasma** | | | | | | |
| Elastix/automatic | 46.5/45.5 | 49.54/49.51 | | | | |
| Hybrid/automatic | 48/45.5 | 56.49/49.51 | | | | |
| Manual/automatic | 49.2/45.5 | 55.20/49.51 | | | | |
| **Optic nerve (right)** | | | | | | |
| Elastix/automatic | 6.7/6.7 | 53.67/50.63 | | | | |
| Hybrid/automatic | 7.6/6.7 | 58.32/50.63 | | | | |
| Manual/automatic | 7.6/6.7 | 56.34/50.63 | | | | |
| **Optic nerve (left)** | | | | | | |
| Elastix/automatic | 2/2 | 34.98/33.60 | | | | |
| Hybrid/automatic | 2.1/2 | 47.30/33.60 | | | | |
| Manual/automatic | 2.1/2 | 43.20/33.60 | | | | |

Abbreviation: DSC, Dice score coefficient; HD, Hausdorff distance; PTV, programmed tumor's volumes.

automatic registration is fast and simple and gives generally good results. However, the other manual and hybrid *Eclipse*' registrations are used instead of the automatic registration, particularly when the last one fails. The manual registration is more difficult and time-consuming because the radiotherapy clinician is generally asked to perfectly use the TPS translation and rotation tools to perform correct 3D registration in the sagittal, coronal, and axial plans. In hybrid registration, the task is based on the manual selection of a set of points by the clinician on CT and MRI images at specific anatomical landmarks. Here, the registration consists of matching between defined points and task which is also so difficult and time-consuming.

In this study, the advantages and limitations of the CT/MRI image registration and fusion were well demonstrated in the case of Glioblastoma radiotherapy treatment with 3D conformal radiotherapy technique. The great contribution of MRI in the delineation of the edema and PTV, which cannot be correctly achieved by CT, was sufficiently demonstrated. The difference in terms of PTV localization and delineation between CT and MRI was found so large to completely reject the treatment planning based on CT data only. This difference is principally due to the excellent MRI soft tissue contrast and to its multitude of robust imaging sequences (T1, T2, T2-Flair, and T1-Gd.) that can be used for excellent brain examination. It was also demon-

strated that *Elastix* registration can be used to judge the accuracy of the TPS automatic registration, which is generally first used. The registration performance was evaluated by the comparison of PTV and edema delineation based on DSC, JSC, and HD metrics and also by comparing the re-calculated doses after each registration. The results showed that an almost good reproduction of the automatic registration results was obtained by the *Elastix* registration within an average of 0.98 (98%) for DSC and less than 1 mm for HD.

### 5.1. Conclusions

In this research, among the studied registration methods, *Elastix* registration was demonstrated to perform the best registration and, therefore, the most accurate radiotherapy planning according to the considered intensity and anatomical landmarks metrics. The manually and hybrid TPS methods were found to be less efficient than the *Elastix* method and time-consuming. In terms of registration comparison metrics, the *Elastix* method gives the most closet results to the TPS automatic registration method (reference). Special care must be taken when applying TPS automatic registration because it does not give suitable results for each considered tumor's case. In summary, we have shown that CT/MRI image registration in radiotherapy treatment planning can effectively be evaluated and improved by the clinician through the combination of TPS automatic registration and *Elastix* registration. Furthermore, we have demonstrated the importance of employing suitable evaluation metrics when assessing the accuracy of the registration used. It was, then, well demonstrated that the used registration can seriously affect the accuracy of dose calculation if not well assessed and optimized.

## Acknowledgments

This research was supported by the General Direction of Scientific Research and Technological Development (DGRSDT) of the Algerian Higher Education and Scientific Research Ministry. The principle investigator and his research team would like to thank the DGRSDT for its support in the achievement of this work.

## Footnotes

**Authors' Contribution:** Study concept and design: KMMT, FK, KB, and SAM. Analysis and interpretation of data: FK, and KMMT. Drafting of the manuscript: KMMT. Calculation and treatment planning: KB and SAM. Final revision of the manuscript: FK.

**Conflict of Interests:** The authors declare that there is no conflict of interests.

**Funding/Support:** This research was supported by the General Direction of Scientific Research and Technological Development (DGRSDT) of the Algerian Higher Education and Scientific Research Ministry.

## References

1. Ortholan C, Estivalet S, Barillot I, Costa A, Gerard JP; Sfro. [Guide for external beam radiotherapy. Procedures 2007]. *Cancer Radiother*. 2007;**11**(6-7):329–30. French. doi: 10.1016/j.canrad.2007.09.005. [PubMed: 17962059].
2. SLosarek K, GrzĄDziel A, Szlag M, Bystrzycka J. Radiation planning index for dose distribution evaluation in stereotactic radiotherapy. *Rep Pract Oncol Radiother*. 2008;**13**(4):182–6. doi: 10.1016/s1507-1367(10)60007-7.
3. Thor M, Petersen JB, Bentzen L, Hoyer M, Muren LP. Deformable image registration for contour propagation from CT to cone-beam CT scans in radiotherapy of prostate cancer. *Acta Oncol*. 2011;**50**(6):918–25. doi: 10.3109/0284186X.2011.577806. [PubMed: 21767192].
4. Auberdiac P, Chargari C, Negrier F, Boutinaud C, Zioueche A, Cartier L, et al. [Magnetic resonance imaging for delineation of prostate in radiotherapy: monocentric experience and review of literature]. *Prog Urol*. 2012;**22**(3):159–65. French. doi: 10.1016/j.purol.2011.09.008. [PubMed: 22364626].
5. Dowling JA, Lambert J, Parker J, Salvado O, Fripp J, Capp A, et al. An atlas-based electron density mapping method for magnetic resonance imaging (MRI)-alone treatment planning and adaptive MRI-based prostate radiation therapy. *Int J Radiat Oncol Biol Phys*. 2012;**83**(1):e5–11. doi: 10.1016/j.ijrobp.2011.11.056. [PubMed: 22330995].
6. Khan FM. *Treatment planning in radiation oncology*. 2nd ed. Philadelphia PA: Lippincot, Williams & Wilkins; 2009.
7. Barrett A, Morris S, Dobbs J, Roques T. *Practical radiotherapy planning*. **Hodder Arnold**. 4th ed. London; 2009. doi: 10.1201/b13373.
8. Brunt JN. Computed tomography-magnetic resonance image registration in radiotherapy treatment planning. *Clin Oncol (R Coll Radiol)*. 2010;**22**(8):688–97. doi: 10.1016/j.clon.2010.06.016. [PubMed: 20674300].
9. El-Gamal FEZA, Elmogy M, Atwan A. Current trends in medical image registration and fusion. *Egypt Inf J*. 2016;**17**(1):99–124. doi: 10.1016/j.eij.2015.09.002.
10. Shamonin DP, Bron EE, Lelieveldt BP, Smits M, Klein S, Staring M, et al. Fast parallel image registration on CPU and GPU for diagnostic classification of Alzheimer's disease. *Front Neuroinform*. 2013;**7**:50. doi: 10.3389/fninf.2013.00050. [PubMed: 24474917]. [PubMed Central: PMC3893567].
11. Klein S, Staring M, Murphy K, Viergever MA, Pluim JP. Elastix: A toolbox for intensity-based medical image registration. *IEEE Trans Med Imaging*. 2010;**29**(1):196–205. doi: 10.1109/TMI.2009.2035616. [PubMed: 19923044].
12. Noel G, Antoni D, Barillot I, Chauvet B. [Delineation of organs at risk and dose constraints]. *Cancer Radiother*. 2016;**20 Suppl**:S36–60. French. doi: 10.1016/j.canrad.2016.07.032. [PubMed: 27516050].
13. Razlighi QR, Kehtarnavaz N, Yousefi S. Evaluating similarity measures for brain image registration. *J Vis Commun Image Represent*.

2013;**24**(7):977–87. doi: 10.1016/j.jvcir.2013.06.010. [PubMed: 24039378]. [PubMed Central: PMC3771653].
14. Manjeet Singh AD. CT and MRI brain images registration for clinical applications. *J Cancer Sci Ther*. 2013;**6**(1). doi: 10.4172/1948-5956.1000243.
15. Varian Medical Systems. *Reference manual registration. SmartA dapt and contouring*. 2013. Report No.: P1000947A.
16. Varian Medical Systems. *Reference manual registration. Smart adapt and contouring*. 2013. Report No.: P1000946A.
17. Sivagami R, Vaithiyanathan V, Sangeetha V, Ifjaz Ahmed M, Joseph Abraham Sundar K, Divya Lakshmi K. Review of image fusion techniques and evaluation metrics for remote sensing applications. *Indian J Sci Technol*. 2015;**8**(35). doi: 10.17485/ijst/2015/v8i35/86677.
18. *Anatomically constrained image reconstruction applied to emission computed tomography and magnetic impedance tomography*. University of Sheffield; 2002.
19. Feuvret L, Antoni D, Biau J, Truc G, Noel G, Mazeron JJ. [Guidelines for the radiotherapy of gliomas]. *Cancer Radiother*. 2016;**20 Suppl**:S69–79. doi: 10.1016/j.canrad.2016.07.008. [PubMed: 27521036].
20. Rigaud B, Simon A, Castelli J, Gobeli M, Ospina Arango JD, Cazoulat G, et al. Evaluation of deformable image registration methods for dose monitoring in head and neck radiotherapy. *Biomed Res Int*. 2015;**2015**:726268. doi: 10.1155/2015/726268. [PubMed: 25759821]. [PubMed Central: PMC4339705].
21. Commandeur F, Simon A, Mathieu R, Nassef M, Arango JDO, Rolland Y, et al. MRI to CT prostate registration for improved targeting in cancer external beam radiotherapy. *IEEE J Biomed Health Inform*. 2017;**21**(4):1015–26. doi: 10.1109/JBHI.2016.2581881. [PubMed: 27333613].
22. Ribeiro AS, Nutt DJ, McGonigle J. Which metrics should be used in non-linear registration evaluation? In: Navab N, Hornegger J, Wells W, Frangi A, editors. *Medical image computing and computer-assisted intervention – MICCAI 2015*. Germany: Springer International Publishing; 2015. p. 388–95. doi: 10.1007/978-3-319-24571-3_47.

**Abstract**: The contribution of nuclear magnetic resonance imaging (MRI) to radiotherapy continues to gain ground, both in treatment planning and in diagnosis and monitoring of the disease. Nowadays, MRI is mainly used for the localization of tumors and the contouring of various organs and structures that are difficult to operate with X-ray computed tomography (CT). Indeed, CT/MRI image registration and fusion contributes enormously to the improvement of radiotherapy treatment planning. In this thesis project, it was a question of establishing a synthesis on the contribution of MRI in radiotherapy on the different stages of diagnosis and treatment. As a specific objective, we were interested in the study and quantification of the contribution of MRI in radiotherapy for treatment planning of Glioblastoma. The analysis focused on optimizing the dose to be delivered to the tumour by sparing the organs at risk (OARs). The results of this thesis clearly showed how the optimal execution of the registration and fusion of CT/MRI images could help to ensure better optimization of treatment and better conformity of dose distribution according to the cases considered. Indeed, several patient cases were considered and appropriate metrics were used for the evaluation of registration and fusion of CT/MRI images.
**Keywords**: Radiotherapy; Treatment plannig; MRI; CT/MRI registration; Dosimetric control in radiotherapy.

**Résumé** : L'apport de l'imagerie par résonnance magnétique nucléaire (IRM) en radiothérapie ne cesse de se faire valoir et ce, que ce soit en planification de traitement que dans le diagnostic et le suivi de la maladie. De nos jours, l'IRM est principalement utilisée pour la localisation des tumeurs et le contourage des différents organes et structures difficiles à opérer avec la tomodensitométrie à rayons X (TDM). En effet, le recalage et la fusion d'image TDM/IRM contribue énormément à l'amélioration de la planification de traitement en radiothérapie. Dans ce projet de thèse, il a été question d'établir une synthèse sur l'apport de l'IRM en radiothérapie sur les différentes étapes de de diagnostic et de traitement. Comme objectif spécifique, nous nous sommes intéressés à l'étude et la quantification de l'apport de l'IRM en radiothérapie pour la planification du traitement du Glioblastoma. L'analyse a surtout porté sur l'optimisation de la dose à délivrer à la tumeur et l'épargne des organes à risques (OARs). Les résultats de cette thèse montraient clairement comment l'exécution optimale du recalage et de la fusion d'images TDM/IRM pourrait contribuer à garantir une meilleure optimisation du traitement et une meilleure conformité de la distribution de la dose en fonction de cas considérés. En effet, plusieurs cas de patients ont été considérés et des métriques appropriées ont été utilisé pour l'évaluation du recalage et fusion d'images TDM/IRM.
**Mots-clés :** Radiothérapie ; Planification de traitement ; IRM ; Recalage d'images TDM/ IRM; Contrôle dosimétrique en radiothérapie.

**ملخص:** تستمر مساهمة التصوير بالرنين المغناطيسي النووي (MRI) في العلاج الإشعاعي في التزايد، سواء في تخطيط العلاج أو في تشخيص المرض ومراقبته. في الوقت الحاضر، يستخدم التصوير بالرنين المغناطيسي بشكل أساسي في كشف الأورام وتحديد الأعضاء المختلفة والمناطق التي يصعب رؤيتها باستخدام التصوير المقطعي المحوسب بالأشعة السينية (CT). في الواقع، تسجيل ودمج الصور المقطعية مع صور التصوير بالرنين المغناطيسي يساهم بشكل كبير في تحسين تخطيط العلاج الإشعاعي. في مشروع الأطروحة هذا، يتعلق الأمر بإنشاء توليفة حول مساهمة التصوير بالرنين المغناطيسي في العلاج الإشعاعي في مراحله المختلفة من التشخيص والعلاج. كهدف محدد، كنا مهتمين بدراسة وتقدير مساهمة التصوير بالرنين المغناطيسي لتخطيط العلاج الإشعاعي للورم الأرومي الدبقي. ركز التحليل على تحسين الجرعة التي سيتم تسليمها إلى الورم وتجنب الأعضاء المعرضة للخطر (OARs). أظهرت نتائج هذه الرسالة بوضوح كيف أن التنفيذ الأمثل لتسجيل ودمج صور التصوير المقطعي المحوسب مع صور التصوير بالرنين المغناطيسي يمكن أن يساعد في ضمان تحسين أفضل للعلاج وامتثال أفضل لتوزيع الجرعة وفقًا للحالات التي تم النظر فيها. في الواقع، تم النظر في العديد من حالات المرضى واستخدمت المقاييس المناسبة لتقييم تسجيل ودمج صور التصوير المقطعي المحوسب مع صور التصوير بالرنين المغناطيسي.
**كلمات مفتاحيه:** العلاج الإشعاعي؛ تخطيط العلاج؛ التصوير بالرنين المغناطيسي؛ تسجيل الصور المقطعية مع صور التصوير بالرنين المغناطيسي؛ التحكم في قياس الجرعات في العلاج الإشعاعي